Biochemical and Biophysical Characterization of the Centrosomal Protein TACC3

Inaugural-Dissertation

zur

Erlangung des Doktorgrades der

Mathematisch-Naturwissenschaftlichen Fakultät

der Heinrich-Heine-Universität Düsseldorf

vorgelegt von

Harish Chandra Thakur

aus Indien

Düsseldorf, November 2012

Aus dem Institut für Biochemie und Molekularbiologie II
der Heinrich-Heine-Universität Düsseldorf

Gedruckt mit der Genehmigung der
Mathematisch-Naturwissenschaftlichen Fakultät der
Heinrich-Heine-Universität Düsseldorf

Referent: Priv. Doz. Dr. Reza Ahmadian
Koreferent: Prof. Dr. Lutz Schmitt

Tag der mündlichen Prüfung:

Dedicated to Maa and Babu Ji

उत्तिष्ठत जाग्रत प्राप्य वरान्निबोधत

(Uttishthata jagrata prapya varan nibodhata)

Arise! Awake! and Stop not till the goal is reached

Katha- Upanishad

Table of contents

Table of contents

Table of contents

Table of contents

Abbreviations

APC	Anaphase promoting complex
ARNT	Aryl hydrocarbon receptor nuclear translocator
APS	Ammonium persulfate $(NH_4)_2S_2O_8$
ATP	Adenosine-5'-triphosphate
AF4	Asymmetric Flow Field-Flow Fractionation
AGFC	Analytical gel filtration chromatography
ARM repeat	Armadillo repeat
AUC	Analytical ultracentrifugation
AUC-SV	Analytical ultracentrifugation sedimentation velocity
BSA	Bovine serum albumin
CBB	Coomassie brilliant blue
CHC	Clathrin heavy chain
CDK	Cell division kinase
chTOG	Colonic and hepatic tumor over-expressed gene
CC	Coiled coil
CD	Circular dichroism
CV	Column volume
cLSM	Confocal laser scanning microscopy
DNA	Deoxyribonucleic acid
DTT	Dithiothreitol
dNTP	Deoxyribonucleotide tri-phosphate
ddH_2O	Double distilled water
D-TACC	*Drosophila melanogaster* Transforming acidic coiled coil
EDTA	Ethylenediaminetetraacetic acid
EGTA	Ethylene glycol tetraacetic acid
EtBr	Ethidium bromide
EGFP	Enhanced green fluorescent protein
EM	Electron microscopy
FOG	Friend of GATA protein
FGFR	Fibroblast growth factor receptors
G_1-phase	First gap phase of the cell cycle
G_2-phase	Second gap phase of the cell cycle
GBM	Glioblastoma multiforme
GFP	Green fluorescent protein
GST	Glutathione S-transferase
GSH	Glutathione
HeLa	Henrietta Lacks tumor cells
HEAT	Huntingtin, elongation factor 3, protein phosphatase 2A, and the yeast kinase TOR1
HRP	Horseradish peroxidase
HMW	High molecular weight
Hs-TACC3	*Homo sapiens* Transforming acidic coiled coil 3
IPTG	Isopropyl β-D-1-thiogalactopyranoside
ITC	Isothermal titration calorimetry
IMAC	Immobilized metal ion affinity chromatography

Abbreviations

iTOL	Interactive tree of life
LB-medium	Luria-Bertani medium
LS	Light scattering
LMW	Low molecular weight
M-phase	Mitotic phase of the cell cycle
MT	Microtubule
MTOC	Microtubule organization center
MAP	Microtubule associated proteins
MALDI-TOF	Matrix-assisted laser desorption/ionization - time of flight
MALS	Multi angle light scattering
Mm-TACC3	*Mus musculus* Transforming acidic coiled coil 3
mAb	Monoclonal antibody
Ni^{2+}-NTA	Ni^{2+}-nitrilotriacetic acid
OD	Optical density
PCM	Pericentriolar matrix
pCAF	p300/CBP-associated factor
PAGE	Polyacrylamide gel electrophoresis
PCR	Polymerase chain reaction
PBS	Phosphate buffered saline
PMSF	Phenylmethylsulfonyl fluoride
PP1	Protein phosphatase 1
RNA	Ribonucleic acid
S-phase	Synthesis phase of the cell cycle
SPD-repeat	Serine (S) prolin (P) aspartate (D) rich repeat
SPE-repeat	Serine (S) prolin (P) glutamate (E) rich repeat
SP-rich	Serine (S) prolin (P) rich
SDS	Sodium dodecyl sulfate
SEC	Size exclusion chromatography
TACC	Transforming acidic coiled coil
γTURC	Gamma tubulin ring complex
TSC2	Tuberous sclerosis 2
TB-medium	Terrific broth medium
TEMED	Tetramethylethylenediamine
TCEP	tris(2-carboxyethyl)phosphine
TEV	Tobacco etch virus
TBST	Tris buffered saline and tween 20
TAE	Tris-acetate-EDTA
TBS	Tris buffered saline
UV	Ultraviolet
XMAP	*Xenopus* microtubule associated protein
Xl-TACC3	*Xenopus laevis* Transforming acidic coiled coil 3

List of Tables

List of Figures

List of Figures

1 Introduction

1.1 Proliferation and the mitotic cell cycle

Cell proliferation (cell growth and cell division) is a basic process essential for growth and development of all life forms. This facilitates the population growth of unicellular life forms while in multicellular organisms contributes to embryonic development, body growth and repair, and renovation of organs and body structure. All eukaryotes proliferate through two different division mechanisms, mitosis (somatic cells) and meiosis (reproductive cells). During the proliferation process, a series of cyclic cellular and molecular changes occur in a given orderly sequence known as the four distinct phases (G_1, S, G_2, and division phase) of the cell cycle, of which both mitosis and meiosis are the final stages (Fig. 1). The G_1-phase is the first growth phase where decision for cell division is made. The S-phase is characterized by replication or duplication of the centrosome and chromosomes and is followed by second growth phase (G_2) where preparations are made for final division. The cell cycle has three checkpoints (G_1-, G_2-, and M-checkpoints) which verify the readiness of cells before undergoing division. During the division phase, two centrosomes move to opposite poles, replicated chromosomes segregate and finally the cell divides into two identical daughter cells. Each daughter cell receives one centrosome and a set of chromosomes. The division phase is subdivided into two phases, mitotic or M-phase and cytokinesis. According to molecular changes, the mitotic phase is further divided into four different subphases called prophase, metaphase, anaphase, and telophase (Fig. 2).

Cell proliferation and cell cycle progression are tightly regulated events which determine correct duplication and segregation of each chromosome and ensure equal distribution of the complete genome at the end of cell division (1). Any escape from this regulatory mechanism leads to alterations in the genetic makeup of daughter cells, which subsequently can result in many abnormalities (including aneuploidy and cancer) and genetic disorders (2). Cyclic ON/OFF setting of different Cyclin-CDK complex activity is the core regulatory mechanism of the cell division cycle (Fig. 1). Cyclins are the regulatory units and CDKs represent the catalytic units of these regulatory complexes. In 2001, the Nobel Prize in Physiology and Medicine was awarded to three scientists (Leland H. Hartwell, Tim Hunt, and

Sir Paul Nurse) for the discovery of these cell cycle regulatory genes (3). So far several functional homologues and orthologs of cyclins and CDKs (Cell Division Kinase) have been identified (4). In parallel to Cyclin-CDK complexes, several other enzymatic and structural proteins and their complexes are involved in the regulation of proliferation whose expression and function is switched ON and OFF in order to regulate cell cycle progression and cell proliferation (5,6).

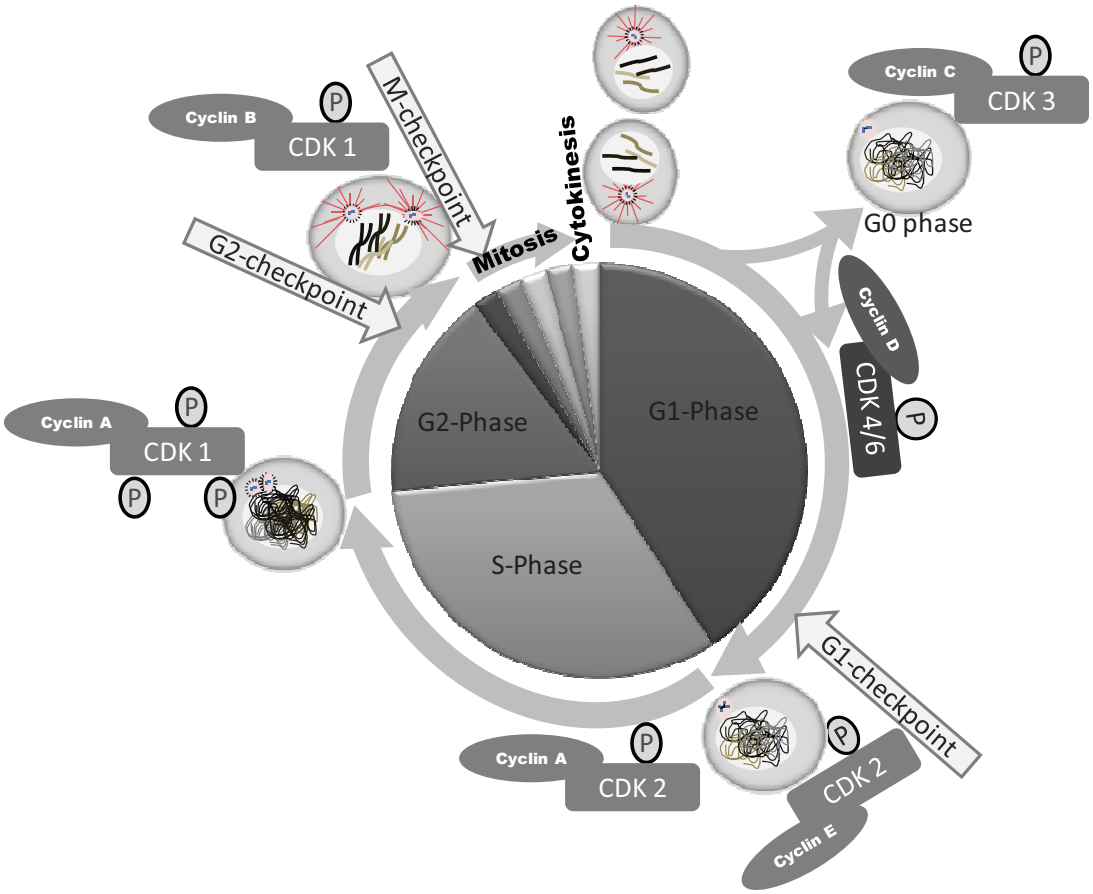

Fig. 1: The cell division cycle (mitosis).
The mitotic cell cycle proceeds through four phases: G_1 (gap 1), S (synthesis), G_2 (gap 2) and M (mitosis). Cytokinesis is the end step of mitosis after which two identical daughter cells form. Switching 'ON' and 'OFF' of different Cyclin-CDK complex regulates cell progression through different phases and different checkpoints verify the readiness of cell to go into next phase. The G_1-, G_2-, and M-checkpoints confirm the readiness of the cell for division.

Among such proteins, the Transforming Acidic Coiled Coil (TACC) protein family is one of the important classes which are expressed in a cyclic manner and displays a cell cycle regulatory function during mitosis. Members of this family are essential structural

components of the mitotic spindle apparatus and regulate centrosome-dependent assembly of spindle microtubules and their dynamics and stability (7-10). TACC3 is a vertebrate ortholog of this family that is known to be involved in cell cycle regulation by controlling spindle pole organization during mitosis. TACC3 depletion in NIH3T3 cells results into p53-$p21^{WAF}$-mediated cell cycle arrest in the G_1 and G_2 phase (11). TACC3 gene expression has been found to be upregulated in different highly proliferative cells types including cancer cells (12). RNA expression profiling indicates that TACC3 gene expression commences with the start of S-phase, reaches to peak level during the G_2/M phase, and subsequently decreased to a very low level at the end of mitosis (13).

1.2 Centrosomes and the mitotic spindle apparatus

The mitotic spindle apparatus is comprised of centrosomes, spindle microtubules, and associated protein complexes. The centrosome evolved in the metazoan lineage of eukaryotic development and is well characterized as primary microtubule organizing centre (MTOC). The normal function of the MTOC is necessary for chromosome alignment, segregation and cytokinesis during the cell cycle (14). The centrosome is comprised mainly of a perpendicularly aligned pair of centrioles surrounded by pericentriolar matrix (PCM) components. Centrosomes also duplicate and divide in a cyclic manner called “centrosome cycle” and function as spindle poles during cell division (15). Therefore the centrosome cycle is tightly linked to the cell cycle and is regulated by cell cycle regulatory proteins (16). Centrosome duplication or centriole replication is a semi-conservative process that begins immediately after the cell crosses the G_1-checkpoint. The centrosome passes through a maturation process during early G_2-phase where it augments the extent of PCM components. The maturation process stops via separation of orthogonally arranged pair of two centrioles with its own PCM components thereby generating two centrosomes at the end of G_2-phase. During mitosis, the centrosomes move away from each other to form the bipolar spindle and at the end of cytokinesis each daughter cell receives one centrosome. Following cytokinesis, centrosomes have to pass through a centrosome disorientation process to resume the next “centrosome cycle” at the beginning of a new cell division cycle (15).

Introduction

In the G_2/M transition phase, prophase and metaphase cells pass through a massive microtubule rearrangement process and two centrosomes move opposite to each other and form the bipolar spindle apparatus (Fig. 2) (17). Upon entry into the G_2/M phase and during mitosis, centrosomes dramatically boost up their microtubule nucleation capacity by recruiting the γ-tubulin ring complex (γTURC). The γTURC along with additional accessory and essential protein complex enables microtubules to grow out of the centrosome. Microtubule nucleation and its elongation is a dynamic process that depends on microtubule polymerization (rescue) and depolymerization (catastrophe) rates and the presence of various microtubule stabilizing and destabilizing factors (18,19). The XMAP215 (*Xenopus* microtubule associated protein) family members, also called processive microtubule polymerases, polymerize microtubules and boost up the elongation steps (20). Other accessory and essential microtubule associated proteins (MAPs) helps in spindle microtubule stability.

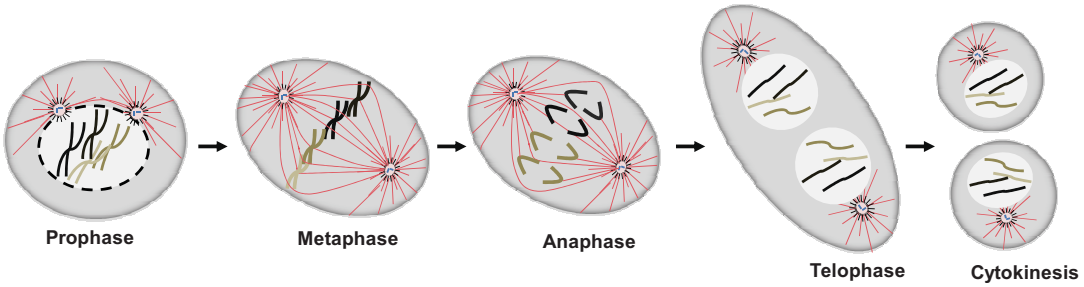

Fig. 2: Mitotic phase of cell division cycle. Prophase is the early phase and telophase is the late phase which is followed by cytokinesis. During prophase two centrosomes move towards opposite poles, chromosomes become shorter and thicker because of condensation and nuclear membrane disappears; in metaphase cells are characterized by high microtubule organization followed by chromosomal attachment to the plus end of microtubules with the help of kinetochores which leads to chromosomal arrangement at metaphase plate; at the end of metaphase two chromatids separate from each other by the action of the anaphase promoting complex (APC) move towards opposite poles during anaphase, telophase is identified by reformation of nuclear membranes by the end of cytokinesis two daughter cells formed each receiving one nucleus with one set of genome.

During metaphase, majority of spindle microtubules appear to pass from one spindle pole to another known as 'centrosomal fibers,' whereas few of them called 'K-fibers' attach to the chromosomes at the centromeres by means of the kinetochore complex. The cell stays in metaphase until the last chromosome gets properly attached to K-fibers originated from both the spindle poles. This is an imperative consensus for the identical allocation of all

chromosomes at the metaphase plate. One (in yeast) to several microtubules (11-40 in humans) attach to kinetochore complexes (21).

Anaphase begins with spindle microtubule depolymerization or catestrophe events due to the action of the microtubule depolymerase XKCM1/MCAK protein (22). This generates drag force or tension on centromeres for chromatid separation or chromosome segregation to the opposite spindle poles. During telophase, chromosomes reach the respective poles and two daughter nuclei are formed, followed by separation into two daughter cells by the end of cytokinesis (6). Thus microtubule dynamics (rescue and catastrophe) is an essential agreement made by mitotic cells for the arrangement of chromosomes at the equatorial plate and their further proper segregation among both daughter cells.

The TACC3 protein is one of the most central PCM components which is known to form a protein complex with colonic and hepatic tumor over expressed gene (chTOG), a member of the evolutionary conserved XMAP215 protein family and Clathrin heavy chain (CHC) molecules (8,23-27). They localize at centrosomes and along the spindle microtubules in an Aurora-A kinase phosphorylation-regulated manner (28-33). Here, TACC proteins along with XMAP215 group members and other MAPs are the key players of spindle microtubule dynamics (8,34). Throughout G_2/M transition phase, prophase and metaphase, cells display high TACC3 proteins level along with numerous other spindle microtubule stabilizing factors. With the beginning of anaphase, TACC3 gets degraded through the Cdh1-dependent proteasomal degradation pathway (35). Although several reports suggest that TACC3 in complex with chTOG plays a crucial role in spindle microtubule dynamics (8,24,25), to date the actual function of TACC3 and mechanism of TACC3-chTOG complex formation at the biochemical and biophysical level has not been clearly characterized.

1.3 The family of centrosomal TACC proteins

The centrosome represents a supra-molecular assembly of protein complexes comprised of more than 100 proteins and considered a fundamental subcellular organelle in all metazoans (36-38). Most centrosomal proteins (71.3%) contain coiled coil (CC)-like structures which add an essential structural role to centrosomal function (39,40). Members of

the centrosomal TACC family can also be identified by their conserved C-terminal CC domain (TACC domain) comprised of about 200 amino acids (34,41,42). TACC proteins evolved only within the metazoan lineage of eukaryotic evolution along with the centrosome and are categorized as a separate protein family (41). Amongst all metazoans, invertebrates have a single known member (Spc72 in *Saccaromyces cereviceae,* Alp7 in *Schizosaccaromyces pombe,* TACC in *Dictyostelium discoideum,* TAC1 in *Caenohabditis elegans,* and D-TACC in *Drosophila melanogaster*), while all vertebrates contain three TACC protein isoforms named TACC1, TACC2, and TACC3 (24,42-45). Of these three isoforms, TACC1 and TACC2 are expressed in various mitotic and postmitotic cell types and tissues. In contrast, the third isoform, TACC3 is exclusively found in proliferating tissues and cells like during embryonic development, in hematopoietic cells and stem cells, reproductive tissues and other postnatally proliferating tissues (12). TACC isoforms in vertebrates are found to be localized at centrosomes in a slightly different manner (42). At the spindle pole, the centrosomal TACC1 localizes weakly whereas TACC2 localizes strongly during mitosis and throughout the cell cycle. On the other hand, TACC3 localizes strongly in a more diffuse region around mitotic centrosomes (42).

1.3.1 Evolution of TACC proteins

TACC1 is the first member of the TACC protein family which was identified and characterized in human breast cancer specimen and found to be localized close to *FGFR1* region at human chromosome 8p11 (46). Subsequently, TACC2 and TACC3 were identified and mapped in human and mouse and also found physically linked with corresponding *FGFR2* and *FGFR3* regions of chromosomes 4p16.3 and 10q26, respectively (45,47). After this finding, it has been postulated that during evolution, TACC/FGFR gene pairs did undergo two gene duplication processes to give rise to the three distinct FGFR/TACC gene pairs on chromosome 4p16.3 (FGFR3/TACC3), 8p11 (FGFR1/TACC1), and 10q26 (FGFR2/TACC2), respectively.

Till date, three isoforms of TACC proteins are recognized in all representative vertebrates except *Xenopus* where only two isoforms TACC3/Maskin (from *Xenopus. laevis*) and TACC2 (from *Xenopus. tropicalis*) have been reported (48,49). Therefore, the existence of a fourth FGFR member indicates consequently to the presence of a fourth TACC member

in all vertebrates. Although TACC4 in *Oryctolagus cuniculus* and RHAMM in humans have been identified as putative TACC family members, their true identity is still under debate (41,50). In an evolutionary tree of coiled coil structure-containing proteins (Fig. 3), the TACC family members are different from other coiled coil containing proteins (e.g. keratins, tropomyosins, and kinesins). However, RHAMM seems to form a separate family and is closer related to tropomyosin and kinesin like-proteins.

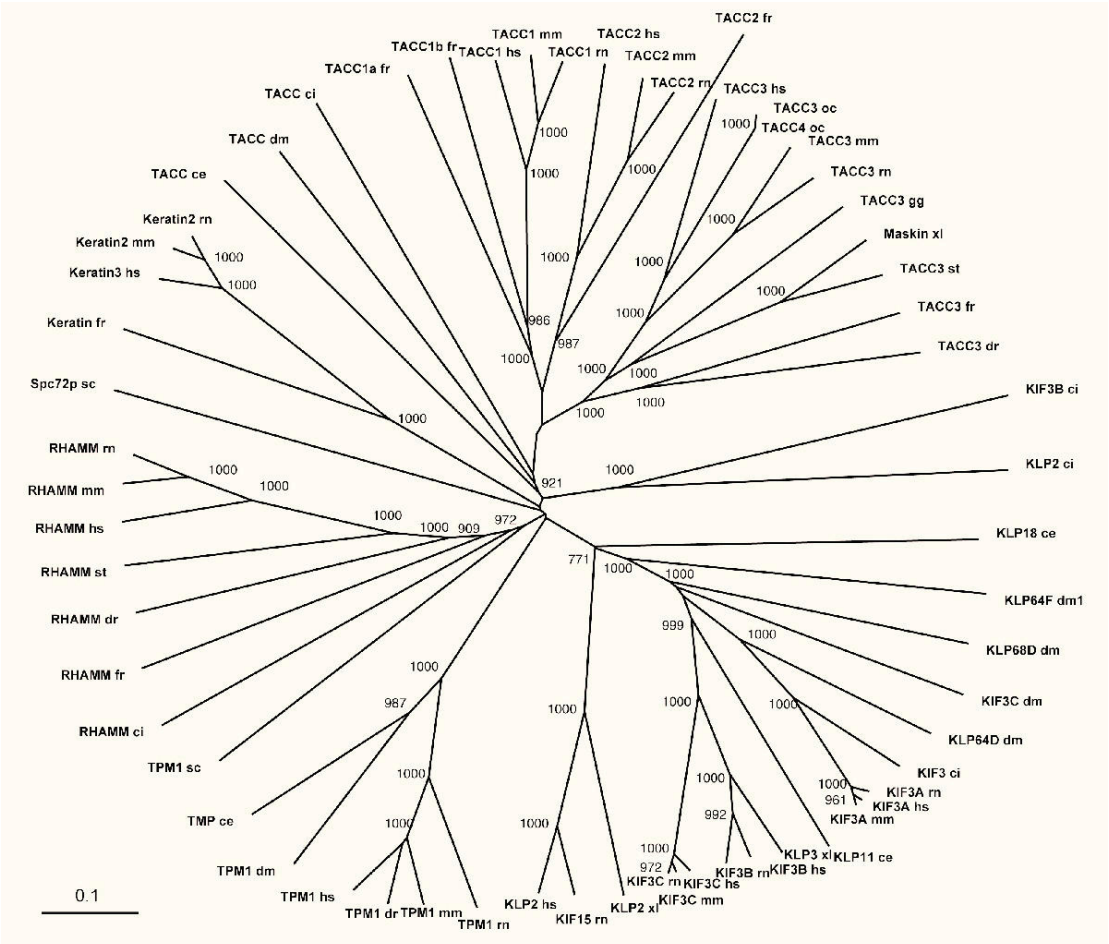

Fig. 3: Phylogenetic tree of TACC family proteins.
The TACC family members constitute a separate subfamily of coiled coil containing proteins, which is different from other coiled coil families such as the keratins, RHAMM, and tropomyosins (41). Number at lower left corner represents scale for branch length (http://www.biomedcentral.com/1471-2148/4/16).

The function of TACC orthologs in simple metazoans (Spc72, Alp7, TACC and TAC1) is to regulate spindle dynamics during mitosis and this function remains conserved throughout evolution in all other metazoans (24,43,44,51). Furthermore, TACC protein family members of lower animals also indirectly play vital roles in different cellular processes, like nuclear export, DNA repair, transcription and translation by interacting with other bridging or intermediate proteins (41,52-55). In vertebrates, the TACC precursor has undergone a gene duplication process and thereby gained diverse functions in addition to its conserved function by generating the TACC isoforms. For example, the TACC3 protein in mouse interacts with FOG1 and ARNT proteins and thereby may functions as a transcriptional coactivator (56-58). The interaction of TACC1 with LSM7 and SmG signifies its putative role in several aspects of mRNA processing and homeostasis in polarized cells (59). Furthermore, involvement of TACC1 in tumor genesis was suggested based on its interaction with the GAS41/NuBI 1 protein (59,60). Similarly, TACC2 interacts with GAS41 and the SWI/SNF chromatin remodeling complex (47). Additional interacting partners of TACC family proteins regulating cellular processes other than spindle microtubule dynamics are tuberous sclerosis complex (TSC2, interacts with human TACC3 and potentially regulates maintenance of nuclear envelop structure during the cell cycle) (61), eIF4E (interacts with *X. laevis* TACC3/Maskin and controls polyadenylation and translation) (62,63), pCAF (histone acetyltransferase interacts with human TACC2 and TACC3 isoforms) (64), and GAS41 (transcription factor interacts with the SPD repeat region of TACC3) (60). Thus, during evolution most of the vertebrates TACC family members gained ability to directly interact with transcriptional and translational factors thereby probably decreasing the dependency on other bridging/intermediate proteins.

1.3.2 Structural organization of TACC proteins

All TACC proteins are characterized by their highly conserved C-terminal TACC domain and an extremely variable N-terminus (Fig. 4). The TAC1 protein (TACC homologue in *C. elegans*) is the smallest member of this family which contains only a CC-domain without the highly variable N-terminus. Spc72 (TACC homologue in *S. cereviceae*) is different from other TACC family members in terms of the distribution of coiled coil regions. It has three coiled coil regions (as predicted by the COIL program), one in the N-terminus, the second very close to the C-terminus and the third in the central region. Alp7 (TACC

homologue in *S. pombe*) has a smaller N-terminal variable region whereas the other known TACC family members from higher eukaryotes contain a longer N-terminal variable region besides the C-terminal TACC signature domain.

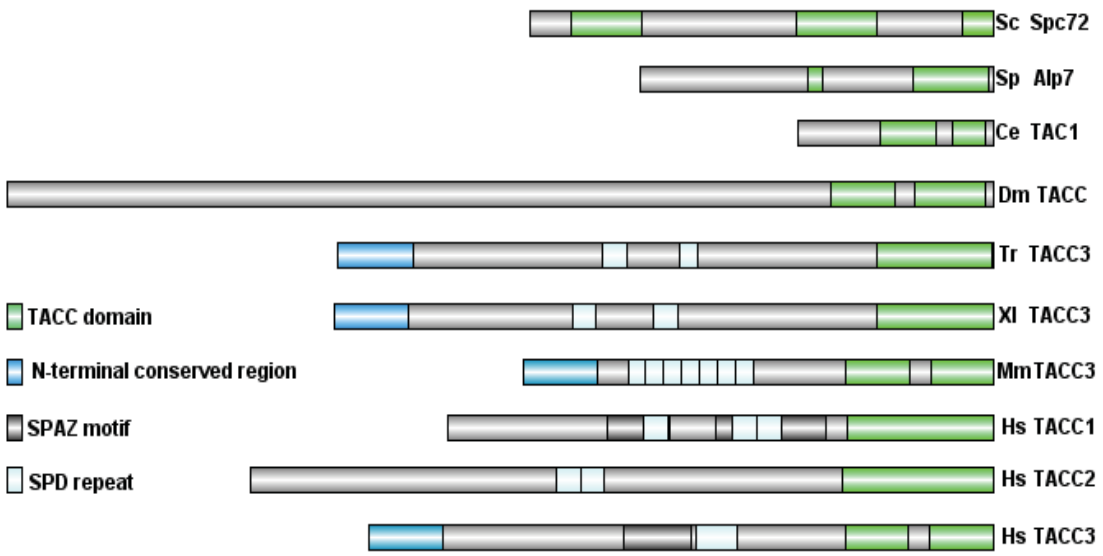

Fig. 4: Domain organization of TACC family members.
The green color shows the highly conserved C-terminal TACC domain in all family members, light blue color indicates the conservation of 100 amino acid residues in the N-terminus of TACC3 isoforms of higher eukaryotes, grey color shows random coil unstructured regions, dark grey indicate SPAZ motif, and the light green color indicates the SP-rich repeat region. Sc-*Saccharomyces cereviceae*, Sp-*Schizosaccharomyces pombe,* Tr-*Takifugu rubripes*, Xl-*Xenopus laevis*, Hs-*Homo sapiens*, Ms-*Mus musculus*, Dm-*Drosophila melanogaster*, Ce-*Caenorhabditis elegans* [Adapted and modified after Peset and Vernos, 2008 (34)].

The longer N-terminal regions are mainly comprised of random coil secondary structures as observed by secondary structure prediction tools. In the case of D-TACC and vertebrates TACC3 isoform, this region has specific binding sites for the serine-threonine kinase Aurora-A (32,33,65). The Aurora-A phosphorylates one serine residue (S863) of D-TACC and three distinct serine residues of vertebrate TACC3 (S33, S620 and S626 in *X. laevis*; S34, S552 and S558 in *H. sapiens*) and thus regulates the localization of three TACC members to centrosomes and the plus end of spindle microtubules (32,33,65,66). The vertebrate TACC3 isoforms show a N-terminal conservation of about 100 residues, however the role of this conservation is not clear (41). In higher eukaryotes, the longer N-terminus of TACC family members displays furthermore the serine/proline (SP) rich repeat region named as ‘SPD [Serine, Prolin, and Glutamate (D) rich] repeats’ and ‘SPAZ (Ser-Pro-Azu-1) motif’

(Fig. 4). These regions are represented in murine TACC3 as seven conservative repeat of 24 amino acids each (45). These repeats are SP rich and contain PXXP motifs as bonafide SH3 binding modules. Single interacting partners for this repeat region are not known yet.

Lastly, the C-terminal TACC domain is comprised of about 200 amino acids (Fig. 4) forming a helical structure and containing unique HXXHCXC heptad repeats, which are the characteristic features of all coiled coil protein domains. The TACC domain of all TACC family members interacts with the C-terminus of XMAP215/chTOG proteins in order to regulate spindle microtubule dynamics (8,24,34). Furthermore, the TACC domain in higher metazoans, especially in vertebrates also interacts with ARNT, hGCN5L2, and MBD2 (58,67). These all proteins are involved in transcriptional regulation and suggesting an unclear role of TACC family members besides their central role in mitosis.

1.4 Biological role of TACC3 in mammalians

The TACC3 gene is vital for embryonic development since it has been shown that TACC3 gene knockouts in the mouse result in embryonic lethality (10,13). In the developing embryo, lack of TACC3 expression results into excessive cellular apoptosis and growth retardation affecting hematopoietic and other organ systems, lastly resulting in prenatal death during mid to late gestation (13). In particular a role of TACC3 has been implicated in a normal mitosis process affecting sclerotome mesenchymal cells and therefore the formation of axial skeleton (10). *In vivo* disruption of TACC3 function results in the regression of mouse thymic lymphoma due to massive apoptosis. Also, TACC3 depletion induces multi-polar spindle formation causing mitotic arrest followed by apoptosis (68). These mutational mouse models provide a clear evidence for the critical role of TACC3 in chromosomal alignment, separation and cytokinesis in association with p53-mediated apoptosis (13). Cell based assays show that TACC3 depletion and dysfunction interferes with normal mitotic process by inducing multipolar spindle formation and aneuploidy. Such depletion induces low to severe mitotic spindle stress resulting in premature senescence and sensitization to paclitaxel-induced cell death via $p21^{WAF}$-mediated cell cycle arrest (11,69).

1.4.1 Expression profile, expression regulation, and subcellular localization of TACC3

The expression of TACC3 is very high in rapidly proliferating cells during early embryonic development (58). In adult tissues, high TACC3 level are confined to haemopoetic (thymus, spleen and leukocytes) and reproductive tissues (ovary and testis) (13). *In situ* hybridization of mouse ovarian tissue sections showed that TACC3 is expressed in ovarian cells undergoing active growth and development (70). In growing oocytes TACC3 has been shown to localize in the cytosol (70). TACC3 is expressed in lung epithelial cells and in all regenerating tissues where cells divide continuously.

In proliferating cells throughout the cell cycle, higher TACC3 expression has been detected during the late S- and G_2/M-phase and succumbs to basal levels in the remaining phases (13). During interphase, TACC3 localizes in the cytosol and/or nucleus depending on the cell and cancer type, although TACC3 does not contain any so far identified nuclear localizing signal (42,71). In the S, G_2 and M-phases, TACC3 associates with the spindle apparatus (centrosomes and spindle microtubules) in an Aurora-A kinase phosphorylation regulated manner (33,66). TACC3 overexpression using artificial constructs results in its accumulation in the cytosol thereby forming punctuate like oligomeric structures (42). The molecular reason for the formation of these oligomeric structures is not well understood.

1.4.2 TACC3 interacting partners and their function

In order to identify interacting partner(s) for TACC family members and to elucidate their interaction in cells, interaction mapping has been performed in different model systems using various approaches (34). So far, about ten different proteins have been identified and characterized which physically bind to TACC family members and exhibit an enzymatic or regulatory function in different cellular processes. The TACC-XMAP215 interaction has been mapped as a highly conserved interaction which is important for spindle pole organization and in particular microtubule dynamics and cell division (34).

XMAP215 is a processive microtubule polymerase which catalyzes the addition of ~25 αβ-tubulin dimers to the plus end of microtubules during elongation (20). It was first isolated from *Xenopus* egg extracts (72). Similar to TACC proteins, XMAP215 is also

conserved in all metazoans that constitute a large family of microtubule-binding proteins. Alp14 (*S. pombe*), CP224 (*D. discoideum*), Zyg9 (*C. elegans*), and Msps (*D. melanogaster*) are members of this family from lower metazoans. XMAP215 (*X. laevis*) and chTOG/CKAP5 (mammals) are the vertebrate orthologs. These proteins were observed to be co-localized with their respective TACC family members at the spindle pole body (in yeast), centrosome (in higher eukaryotes), as well as along the spindle microtubule during mitosis (8). The N-terminus of XMAP215 family members contains two to five TOG domains (2 in yeasts, 3 in nematodes and 5 in higher eukaryotes) binding to tubulin dimers (20,73). The structure for TOG2 of Zyg9 (*C. elegans*) has been solved and found to contain seven HEAT repeat regions folded into a paddle like domain that wraps itself around one tubulin dimer (73). The C-terminus of the protein interacts with the conserved C-terminal TACC domain of TACC family members (44).

Similar to other TACC family members, TACC3 interacts with the C-terminus of chTOG/XMAP215 via its TACC domain (8,34,44). The critical role of TACC3-chTOG interaction in spindle pole organization and spindle microtubule dynamics and stability during mitosis has been proved using RNAi-based approaches and cell based assays (8,74). Formation of the TACC3-chTOG complex has been found to antagonize the microtubule depolymerase activity of XKCM1/MCAK (33). Deletion mapping of XMAP215 suggests that the evolutionarily conserved N-terminal domain has a microtubule-stabilizing activity and stimulates microtubule growth at plus-ends by inhibiting microtubule catastrophes (75). Conversely, in egg extracts from *X. laevis*, the C-terminal part of XMAP215 was described to be capable of suppressing the growth of microtubule by promoting microtubule catastrophes (75). However, although the TACC3-chTOG complex plays a pivotal role in microtubule polymerization and depolymerization, the definite function of TACC3 in this complex and mechanism of this protein-protein interaction are not clear.

The subcellular localization of the TACC3-chTOG complex is regulated through Aurora-A kinase phosphorylation of TACC3 (S33, S620 and S626 in *Xenopus*; S34, S552 and S558 in Human TACC3). In Hs-TACC3, Aurora-A phosphorylation to S558 residues causes their localization to the centrosome (Fig. 5 and 6) (66). The activity of Aurora-A kinase during mitosis is regulated through two different pathways. The first depends on the LIM-

protein Ajuba, which physically interacts with Aurora-A kinase leading to its autophosphorylation and further activation (31). The second mechanism involves a RanGTPase-TPX2 dependent pathway, where RCC1 (Regulator of chromosome condensation 1) acts as a GEF (guanine nucleotide exchange factor) for RanGTPase and convert RanGDP into the GTP-bond form. RanGTP thereby interacts with αβ-importin to relieve the inhibitory binding of αβ-importin on TPX2. Free TPX2 has an inhibitory role on PPI which inactivates Aurora-A. In this way, active Aurora-A phosphorylates its substrates (Eg5, TPX2, PPI, and TACC3) and contributes to centrosome driven spindle assembly (76-78).

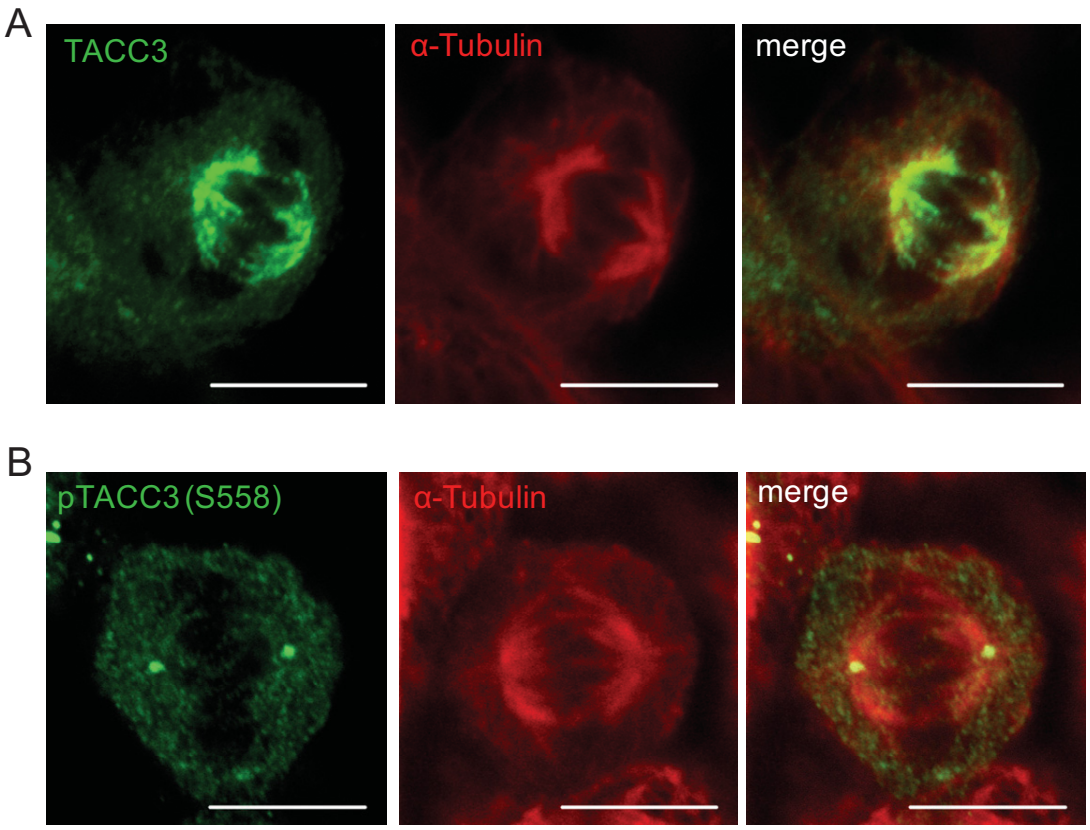

Fig. 5: Subcellular localization of TACC3 and pTACC3 during mitosis in HeLa cells.
A. TACC3 colocalized with spindle microtubule during metaphase; B. Aurora-A phosphorylation of TACC3 at S558 position (pS558TACC3 in green) mediates its localization to the centrosomes during mitosis (In collaboration with Dr. Stephan Schmidt) (79).

Another important regulator of mitosis is the Clathrin heavy chain (CHC) that is known to be mainly involved in endocytotic vesicular trafficking during interphase. During mitosis, CHC also interacts with TACC3 in its phosphorylated form and in Aurora-A kinase

phosphorylation dependent manner (Fig. 6). In immunoflorescence study, CHC has been shown to be co-localized with phosphorylated TACC3 at the centrosome and in slightly diffused region of the centrosome (27,80). Phosphorylation of second and third serine residues (S620 and S626 in Xl-TACC3; S552 and S558 in Hs-TACC3) near to the TACC domains are important for the CHC binding to TACC3 (27,80,81). Interaction of CHC to phosphorylated TACC3 regulates the stability and integrity of centrosomal spindle microtubule during mitosis (27,81,82). The role of CHC has been proposed in spindle microtubule cross linking and its stabilization at the centrosome (28).

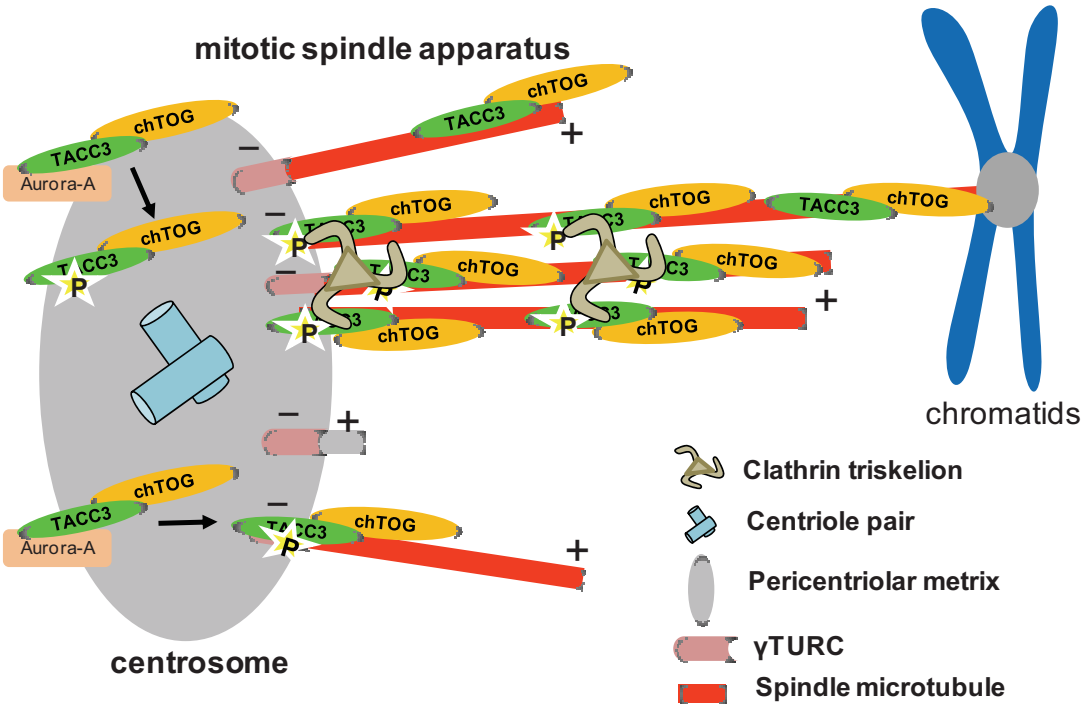

Fig. 6: Proposed model for regulation of mitosis by TACC3.
TACC3 in a complex with chTOG localizes to the centrosome and along the spindle microtubules in an Aurora-A (pink) phosphorylation dependent manner. At the centrosome and along microtubules, the pS558TACC3-chTOG complex interacts with the Clathrin triskelion thereby regulating microtubule growth and providing cross linking.

Lastly, *in vitro* interaction mapping assays identifies the TACC3 binding proteins involved in various cellular process other than mitosis (34). Cep120 interaction with TACC2 and TACC3 regulates the maintenance of the neural progenitor pool during the neocortical development in the mouse (83). DOCK7 has been identified to interact with human or mouse TACC3, and their complex plays a role in regulation of interkinetic nuclear migration and

cortical neurogenesis (84). During interphase, TACC3 interacts with aryl-nuclear translocator (ARNT) (58) and FOG1 (56) proteins and acts as a putative transcriptional regulator or cofactor. TACC3 has been proposed to function as a transcriptional regulator due to its direct physical interaction with GAS41 (YEATS4), the histone acetyl transferase hGCN5L2 (KAT2A), pCAF (KAT2B), retinoid X-receptor beta, and MBD2 proteins (60,64,67,78). TACC family members interact with most of the partner proteins via their TACC domain. Although being such an important molecular hub for the regulation of many cellular processes, the structure of the TACC domain is still not known.

1.4.3 TACC3 mutations and altered expression in tumor cells

The TACC3 gene has been found to be upregulated in a variety of tumor types and has been considered as a putative proto-oncogene. Several somatic mutations (Q4R, S33L, R37C, and Q58Q) and one germ line mutation (S93L) in TACC3 have been identified in human ovarian cancer samples (71,85). Furthermore, substitution missense mutations (E680K in human CNS, A148V & D412G in ovary tumors, G219E in upper digestive tract tumors) and frameshift mutations (M396fs*17 - insertion frameshift and F726fs*87 deletion frameshift) have been reported in the COSMIC (Catalogue of Somatic Mutations in Cancer) database of the Wellcome Trust Sanger Institute. Interestingly, the majority of the mutations examined from human ovarian cancer specimens and other tissues are observed in the N-terminal conserved region. However to which extent these mutations potentially alter the protein interaction and function of the N-terminus of Hs-TACC3 remains to be determined.

In ovarian cancer, an upregulation of TACC3 along with 120 other genes has been observed to be in particular associated with chemoresistance and tumorigenesis (86). Also, an altered TACC3 expression has been detected besides 21 additional genes during breast cancer development (85). In non-small cell lung cancer, elevated expression of TACC3 was correlated with a poor prognosis (87), whereas in breast cancer lower expression was considered as a predictor of poor prognosis (59). The TACC3 gene was mapped physically linked to the FGFR3 region close to the MMSET gene which is rearranged in t(4;14) translocation (45). A significant percentage of glioblastoma multiforme (GBM) tumor patients have been identified expressing a transforming FGFR3-TACC3 fusion protein generated by intrachromosomal translocation (88). In multiple myeloma, TACC3 overexpression was

positively correlated with the t(4;14) (p16·3;q32) translocation and $p21^{WAF}$ expression (89). A single nucleotide polymorphism in the TACC3 gene has been found to be present in a Chinese population and was correlated with increased risk of bladder cancer (90). Interestingly, disruption of TACC3 function leads to *in vivo* tumor regression illustrating that is a vulnerable component of the spindle assembly at least in lymphoma cells (68).

The TACC3 plays a critical role in spindle assembly via the Aurora-A-TACC3-chTOG axis. Therefore, TACC3 function and its inhibition along the Aurora-A-TACC3-chTOG axis during mitosis could represent a promising target for cancer chemotherapy, provided that in particular the TACC3-chTOG interaction becomes molecularly elucidated in a greater detail.

2 Aims of the study

During mitosis spindle microtubule assembly and disassembly is a very dynamic process (20). The centrosomal protein TACC3 in complex with the microtubule polymerase chTOG has been shown to play a pivotal role in the regulation of mitotic spindle assembly, dynamics, and stability (8,9,20,25,28,30,34). TACC3 knockout mice are embryonic lethal and TACC3 gene silencing leads to mitotic defects and cell cycle arrest (13). A role of TACC3 has been implicated in tumor development thereby functioning as putative protooncogene (68,71). Structurally, it has been proposed that after *de novo* synthesis the TACC domain of TACC3 stays in a masked state, and unmasking is required for its proper centrosomal function (49). Furthermore, the TACC domain of TACC3 interacts with the C-terminus of chTOG and this complex localizes to the centrosome and along spindle microtubules in an Aurora-A kinase regulated manner (25,32,33,66,91,92). However, the molecular mechanism(s) of the TACC domain unmasking and subsequent TACC3-chTOG complex formation are still unclear. Therefore, this work aimed to address in particular the following questions:

1. What are the molecular mechanisms of TACC domain masking and its subsequent unmasking?
2. What is the critical region of the TACC domain required for binding to chTOG?
3. What is the molecular structure of the TACC domain and TACC binding domain of chTOG?

Answering these questions should provide novel molecular insight into TACC3-chTOG protein interaction and its regulation. Moreover, given the high expression and possibly the structural alteration of TACC3 linked to cancer development, blocking TACC3 binding to chTOG may represent a long term candidate anti-neoplastic approach. Hence, to answer the questions mentioned above, the following experimental objectives were defined:

1. In depth *in silico* characterization of the TACC3 protein.
2. Designing murine TACC3 and chTOG variants for overexpression in bacterial and mammalian cells followed by protein purification.
3. *In vitro* characterization of murine TACC3 by different biophysical approaches. Protein-protein interaction analysis by means of analytical gel filtration, bait-prey interaction assays, and ITC measurement.

Aims of the study

4. Analysis of the expression and localization of TACC3 variants in mammalian cells.
5. Crystallization and structure determination of the TACC domain of murine TACC3 alone and in complex with the C-terminus of chTOG.

3 Materials

3.1 Chemicals

Tab. 1: List of common chemicals

No.	Name of chemical	Manufacturer and distributor	Storage
1	Acrylamide	Roth, Karlsruhe	RT
2	Advance Milk Powder	Roth, Karlsruhe	RT
3	Adenosine-5'-triphosphate (ATP)	Sigma Aldrich, München	-20˚C
4	Agarose “low melting”	Roth, Karlsruhe	RT
5	Ammonium persulphate (APS)	Sigma Aldrich, München	RT
6	Ampicilin	Sigma Aldrich, München	RT
7	Bovine serum albumin (BSA)	AppliChem, Darmstadt	+4˚C
8	BSA standard (2 mg/ml)	PIERCE, USA	+4˚C
9	Bromophenol blue	Serva, Heidelberg	RT
10	Rotipore 5x Bradford reagent solution	Roth, Karlsruhe	+4˚C
11	Commassie Brilliant Blue (CBB)	Roth, Karlsruhe	RT
12	Chloramphenicol	Sigma Aldrich, München	+4˚C
13	Dimethyl sulfoxide (DMSO)	AppliChem, Darmstadt	RT
14	Dithiothreitol (DTT)	GERBU Biotechnik, Wieblingen	+4˚C
15	dNTP	QIAGEN, Hilden	-20˚C
16	EDTA	Sigma Aldrich, München	RT
17	EDTA free protease inhibitor cocktail	Roche Applied Science	+4˚C
18	EGTA	Sigma Aldrich, München	RT
19	Ethanol	Roth, Karlsruhe	RT
20	Ethidium bromide (EtBr)	Sigma Aldrich, München	RT
21	Glycine	Roth, Karlsruhe	RT
22	Glycerin (glycerol)	Roth, Karlsruhe	RT
23	Glutathione	MERCK Chemicals, Germany	+4˚C
24	Guanidium HCl	Roth, Karlsruhe	RT
25	HCL	Roth, Karlsruhe	RT
26	HEPES	Sigma Aldrich, München	RT

27	Hefe extract	Roth, Karlsruhe	RT
28	Imidazole	Sigma Aldrich, München	RT
29	Igepal (NP40)	Sigma Aldrich, München	RT
30	IPTG	GERBU Biotechnik, Wieblingen	+4˚C
31	Kanamycin	Sigma Aldrich, München	+4˚C
32	KCl	MERCK Chemicals, Germany	RT
33	KH_2PO_4	Roth, Karlsruhe	RT
34	K_2HPO_4	Roth, Karlsruhe	RT
35	LB agar powder	AppliChem, Darmstadt	RT
36	LB powder	AppliChem, Darmstadt	RT
37	$MgCl_2$	Sigma Aldrich, München	RT
38	β-mercaptoethanol	Sigma Aldrich, München	+4˚C
39	Methanol	Roth, Karlsruhe	RT
40	TEMED	AppliChem, Darmstadt	+4˚C
41	NaCl	Sigma Aldrich, München	RT
42	NaH_2PO_4	MERCK Chemicals, Germany	RT
43	Na_2HPO_4	MERCK Chemicals, Germany	RT
44	NaOH	MERCK Chemicals, Germany	RT
45	$NiSO_4$	MERCK Chemicals, Germany	RT
46	Performaldehyde (PFA)	Sigma Aldrich, München	RT
47	D-PBS	GENAXXON, Germany	+4˚C
48	PreCast 4-15% gradient Tris gel	Bio-Rad, München	+4˚C
49	ProQ Diamond	Invitrogen, Darmstadt	+4˚C
50	Ponceau S	Sigma Aldrich, München	RT
51	Potassium acetate	Sigma Aldrich, München	RT
52	PMSF	Sigma Aldrich, München	RT
53	Reblot plus 10x	Millipore, Schwalbach/Ts.	+4˚C
54	2-Propanol	Roth, Karlsruhe	RT
55	SDS	Roth, Karlsruhe	RT
56	Thymidine	AppliChem, Darmstadt	+4˚C
57	Tris	Roth, Karlsruhe	RT
58	Triton-x-100	Sigma Aldrich, München	RT

59	Tween 20	AppliChem, Darmstadt	RT
60	Tetracyclin	ICN Biomedicals, Eschwege	+4˚C
61	Trypton	Becton Dickson and Company	RT
62	TCEP	Roth, Karlsruhe	+4˚C
63	Urea	Calbiochem, Darmstadt, Germany	RT
64	Prestained protein ladder	Fermentas, St. Leon-Rot	-20˚C
65	DNA ladder	Fermentas, St. Leon-Rot	-20˚C

3.2 Antibiotics

Tab. 2: List of antibiotics

No.	Name of Antibiotic	Manufacturer and distributor	Storage
1	Ampicilin	Sigma Aldrich, München	RT
2	Chloramphenicol	Sigma Aldrich, München	RT
3	Kanamycin	Sigma Aldrich, München	+4˚C
4	Tetracycline	ICN Biomedicals, Eschwege	+4˚C

3.3 Enzymes

Tab. 3: List of enzymes

No.	Name of protein/enzyme	Manufacturer and distributor	Storage
1	Aurora-A kinase	SignalChem	-80˚C
2	DNAse I	Calbiochem, Darmstadt, Germany	-20˚C
3	Lysozyme	Calbiochem, Darmstadt, Germany	-20˚C
4	Pfu DNA polymerase	Fermentas, St. Leon-Rot	-20˚C
5	RNAse I	QIAGEN, Hilden	-20˚C
6	Restriction enzymes	Fermentas, St. Leon-Rot	-20˚C
7	TEV protease	Produced and purified in lab	-80˚C
8	Thrombin	Calbiochem, Darmstadt, Germany	-20˚C

9	T4 DNA ligase	Fermentas, St. Leon-Rot	-20˚C
10	Taq DNA polymerase	QIAGEN, Hilden	-20˚C

3.4 Buffers and solutions

Tab. 4: List of buffers and solutions

No.	Buffers and solutions	Stock concentration	Recipes	Storage
1	APS	10%	Dissolve 5 g of APS in 50 ml ddH_2O, prepare 1 ml aliquots.	-20˚C
2	DNAse I	2 mg/ml	Dissolve 100 mg of DNAseI in 50 ml buffer (20 mM Tris-HCl pH 7.6, 50 mM NaCl, 2 mM $CaCl_2$, 2 mM $MgCl_2$, 3 mM DTT, 50% glycerol), prepare 0.5 ml aliquots.	-20˚C
3	DTT	1 M	Dissolve in ddH_2O, prepare 1 ml aliquot.	-20˚C
4	IPTG	1 M	Dissolve in ddH_2O, prepare 1 ml aliquot.	-20˚C
5	Lysozyme	50 mg/ml	Dissolve 2 g of lysozyme in 40 ml of 30 mM Tris-HCl pH 7.5, and prepare 1 ml aliquot.	-20˚C
6	Thrombin	1 U/µl	In 50 mM Tris pH 7.5, 50% glycerol, aliquot 250 µl.	-20˚C
7	Tris-HCl buffer (pH 7.5 and 8.0)	1 M	Dissolve 121.14 g of Tris in 800 ml ddH_2O; adjust pH, make up volume to 1 liter.	RT
8	$MgCl_2$	1 M	Dissolve in ddH_2O	RT
9	NaCl	5 M	Dissolve in ddH_2O	RT
10	$CaCl_2$	1 M	Dissolve in ddH_2O	RT
11	EDTA	0.5 M	Dissolve 93.05 g $Na_2EDTA.2H_2O$	RT

			in 400 ml ddH_2O, adjust pH 8.0 by adding 10 M NaOH, EDTA will dissolve near pH 8.0, make up volume to 500 ml.	
12	PMSF (100x)	100 mM	Dissolve 0.35 g of PMSF in 20 ml Isopropanol, prepare 1 ml aliquot.	+4˚C
13	SDS-PAGE resolving gel buffer	250 mM Tris-HCl pH 6.8; 0.2% SDS	Dissolve 30.3 g Tris-base in 800 ml ddH_2O, adjust the pH to 6.8, add 20 ml of 10% SDS solution, and make up volume to 1 liter.	RT
14	SDS-PAGE stacking gel buffer	750 mM Tris-HCl pH 8.8; 0.2% SDS	Dissolve 90.9 g Tris-base in 800 ml ddH_2O, adjust the pH to 8.8, add 20 ml of 10% SDS solution, and make up volume to 1 liter.	RT
15	SDS-PAGE running buffer	10x (250 mM Tris base, 1.92 M glycine, 1% SDS)	For 1 liter dissolve 30.3 g Tris base, 144.1 g glycine and 10 g SDS in 900 ml ddH_2O, and make up volume to 1 liter.	RT
16	CBB stain for SDS-PAGE		Dissolve 2 g of CBB R250, 2 g of CBB G250 in 400 ml methanol and 100 ml acetic acid, and make up volume with dH_2O to 1 liter.	RT
17	SDS-PAGE destain solution	1x	450 ml methanol, 75 ml glacial acetic acid, and make up volume to 1 liter.	RT
18	Blot transfer buffer	10x (stock)	Dissolve 29 g glucine, 56 g Tris, 3.7 g SDS, and make up volume to 1 liter.	RT
19	Blot transfer buffer	1x (working)	100 ml 10x blot-buffer, 700 ml water and 200 ml methanol.	+4˚C
20	TBS	10x (stock)	Dissolve 30 g Tris, 80 g NaCl, 2 g KCl in 800 ml ddH_2O and make	RT

			up volume to 1 liter	
21	TBST	1x (working)	Add 100 ml of 10x TBS, and 1 ml of Tween 20 (0.1%) to 800 ml ddH_2O, make up volume to 1 liter	RT
22	TAE buffer (Agarose gel electrophoresis buffer)	50x	Dissolve 242 g Tris in 800 ml ddH_2O, add 100 ml of 0.5M EDTA (pH 8.0), 57.1 ml of glacial acetic acid, and make up volume to 1 liter.	RT
23	TCEP	1 M	Dissolve 2.5 g in 5 ml ddH_2O, make up volume to 10 ml, and prepare 1 ml aliquot.	-20˚C

3.5 Chromatography packing materials and columns

Tab. 5: List of chromatography packing materials and columns

No.	Packing material and column	Manufacturer and distributor	Storage
1	Ni^{2+}-NTA Agarose beads	QIAGEN, Hilden	+4˚C
2	GSH-sepharose beads	GE Healthcare, München	+4˚C
3	Superose 6 beads	GE Healthcare, München	+4˚C
4	XK 26/20 column	GE Healthcare, München	RT
5	XK 16/20 column	GE Healthcare, München	RT
6	XK 16/70 column	GE Healthcare, München	RT
7	Superose® 6 HR 10/30 column	GE Healthcare, München	+4˚C
8	Superose® 6 PC 3.2/30 column	GE Healthcare, München	+4˚C
9	Superdex 200 HR 10/30 column	GE Healthcare, München	+4˚C
10	Superdex 200 XK 16/70 column	GE Healthcare, München	+4˚C
11	Superdex 200 XK 26/70 column	GE Healthcare, München	+4˚C
12	Superose 6 XK 16/70 column	Self packed in lab	+4˚C

3.6 Reagents for confocal laser scanning microscopy (cLSM)

Tab. 6: List of reagents for cLSM

No.	Name of antibody (source)	Manufacturer and distributor	Storage
1	Alexa 488 anti-mouse IgG	Invitrogen, Heidelberg	+4 ˚C
2	Alexa 488 anti-rabbit IgG	Invitrogen, Heidelberg	+4 ˚C
3	Alexa 546 anti-mouse IgG	Invitrogen, Heidelberg	+4 ˚C
4	Alexa 546 anti-rabbit IgG	Invitrogen, Heidelberg	+4 ˚C
5	Alexa 568 anti-mouse IgG	Invitrogen, Heidelberg	+4 ˚C
6	Alexa 568 anti-rabbit IgG	Invitrogen, Heidelberg	+4 ˚C
7	Alexa 633 anti-mouse IgG	Invitrogen, Heidelberg	+4 ˚C
8	Alexa 633 anti-rabbit IgG	Invitrogen, Heidelberg	+4 ˚C
9	4',6-diamidino-2-phenylindole (DAPI)	Sigma Aldrich, München	+4 ˚C
10	Prolong Gold Antifade medium	Invitrogen, Heidelberg	-20 ˚C

3.7 Antibodies

Tab. 7: List of antibodies

No.	Name of antibody (source)	Manufacturer and distributor	Storage
1	anti-mTACC3 N18 (rabbit)	Provided by Dr. Roland Piekorz	+4 ˚C
2	anti-mTACC3 C18 (rabbit)	Provided by Dr. Roland Piekorz	+4 ˚C
3	anti-GST polyclonal Ab (goat)	Abcam, Cambridge, UK	-20 ˚C
4	anti-hTACC3 H300 (rabbit)	Santa Cruz Biotechnology, Europe	+4 ˚C
5	anti-hTACC3 D2 (mouse)	Santa Cruz Biotechnology, Europe	+4 ˚C
6	anti-αTubulin (rat)	Abcam, Cambridge, UK	-20 ˚C
7	anti-chTOG (rabbit)	Abcam, Cambridge, UK	-20 ˚C
8	anti-Clathrin heavy chain (rabbit)	Abcam, Cambridge, UK	-20 ˚C
9	anti-rabbit IgG HRP linked (goat)	Cell Signaling, Boston, USA	-20 ˚C
10	anti-mouse IgG HRP linked (goat)	Dako, Denmark	-20 ˚C
11	anti-goat IgG HRP linked (rabbit)	Thermo Scientific, Bonn	-20 ˚C

3.8 Reagents and kits

Tab. 8: List of reagents and kits

No.	Name of reagent and kit	Manufacturer and distributor	Storage
1	MaxiMidi-prep DNA extraction kit	NucleoBond Ax	RT
2	Mini prep DNA extraction kit	QIAGEN, Hilden	RT
3	Gel extraction kit	QIAGEN, Hilden	RT
4	PCR purification kit	QIAGEN, Hilden	RT

3.9 Oligonucleotides

Tab. 9: List of primers

Oligonucleotides for directional cloning	**Restriction Enzymes**
Oligonucleotides for cloning of murine TACC3 variants	
pGEX4t1-nTEV_TACC3wt, Template: pMSCV-GFP_TACC3 wt	
pGEX4t1-nTEV_ TACC3-ΔR, Template: pMSCV-GFP_TACC3 ΔR	
FP 5' AATTGAATTCATGAGTCTGCATGTCTTAAATGACG 3'	EcoRI
RP 5' GGCCGCGGCCGCTCAGATCTTCTCCATCTTAGAGATGAGG 3'	NotI
pGEX4t1-nTEV_ TACC3-ΔN, Template: pMSCV-GFP_TACC3 wt	
pGEX4t1-nTEV_ TACC3-ΔNΔR, Template: pMSCV-GFP_TACC3 ΔR	
FP 5' AATTGAATTCGAAGGCGAGTTACAGGAGG 3' (EcoRI)	EcoRI
RP 5' GGCCGCGGCCGCTCAGATCTTCTCCATCTTAGAGATGAGG 3'	NotI
(RP for amplification of TACC3)	
pET23b_GST-TACC3 N and pET-duet_GST-TACC3 N	
Template: pGEX4t1-nTEV_TACC3 (FP is designed to amplify GST_TACC3-N)	
FP 5' TATACATATGTCCCCTATACTAGGTTATTGG 3'	NdeI
RP 5' GATCCTCGAGCTCACTGTCCAGAAGACTTGTG 3'	XhoI
pGEX4t1-nTEV_TACC3-7R, 3R, & 2R, Template: pGEX4t1-nTEV_TACC3	
FP 5' TATAGGATCCATGGAAGGCGAGTTACAGGAGG 3'	BamHI
RP 5' TCGACTCGAGTCAACCTAGGACTTCTGATGGGTC 3'	XhoI
pGEX4t1-nTEV_TACC3-NR, Template: pGEX4t1-nTEV_TACC3	

FP 5' AATTGAATTCATGAGTCTGCATGTCTTAAATGACG 3'	EcoRI
(FP for amplification of TACC3 wt)	
RP 5' TCGACTCGAGTCAACCTAGGACTTCTGATGGGTC 3'	XhoI
(RP for amplification of TACC3 7R)	
pGEX4t1-nTEV_TACC3-CC1, Template: pGEX4t1-nTEV_TACC3	
FP 5' GATCGGATCCGGTCTCCTTCCTGCTGAG 3'	BamHI
RP 5' TCGACTCGAGGCCTTCAATCACTTCCTTCC 3'	XhoI
pGEX4t1-nTEV_TACC3-CC2, Template: pGEX4t1-nTEV_TACC3	
FP 5' GATCGGATCCGGCTACCAGAAGAATGAAGAG 3'	BamHI
RP 5' GGCCGCGGCCGCTCAGATCTTCTCCATCTTAGAG 3'	NotI
pGEX4t1-nTEV_TACC3-CC, Template: pGEX4t1-nTEV_TACC3	
FP 5' GATCGGATCCGGTCTCCTTCCTGCTGAG 3'	BamHI
RP 5' GGCCGCGGCCGCTCAGATCTTCTCCATCTTAGAG 3'	NotI
pFastBac-Htb_TACC3wt, Template: pMSCV-GFP_TACC3	
FP 5' AATTGAATTCAAATGAGTCTGCATGTCTTAAATGACG 3'	EcoRI
RP 5' GGCCGCGGCCGCTCAGATCTTCTCCATCTTAGAGATGAGG 3’	NotI
pET23b_TACC3-7R, Template: pGEX4t1-nTEV_TACC3	
FP 5' TATACATATGCACCATCACCATCACCATGAAGGCGAGTTAC	NdeI
AGGAGG 3'	
RP 5' GATCGGATCCTCAACCTAGGACTTCTGATGGGTC 3'	BamHI
pCDNA 3.1_TACC3wt_GFP, Template: pMSCV-GFP_TACC3	
pCDNA 3.1_TACC3-ΔR_GFP, Template: pMSCV-GFP_TACC3 ΔR	
FP 5' AGTCAAGCTTGCCACCATGAGTCTGCATGTCTTAAATG 3'	HindIII
RP 5' GGCCGCGGCCGCGATCTTCTCCATCTTAGAGATG 3'	NotI
pCDNA 3.1_TACC3-ΔN _GFP, Template: pMSCV-GFP_TACC3	
FP 5' TTAAGCTTGCCACCATGGCTTCCACAAGTCTTCTG 3'	HindIII
RP 5' GGCCGCGGCCGCGATCTTCTCCATCTTAGAGATG 3'	NotI
pcDNA 3.1_TACC3-ΔCC_GFP, Template: pMSCV-GFP_TACC3	
FP 5' GCGCGGCCGCCACAATAGGCTCAGCAGGA 3'	HindIII
RP 5' GGCCGCGGCCGCGATCTTCTCCATCTTAGAGATG 3'	NotI
pcDNA 3.1_TACC3-ΔCC2_GFP, Template: pMSCV-GFP_TACC3	
FP 5' AGTCAAGCTTGCCACCATGAGTCTGCATGTCTTAAATG 3'	HindIII

RP 5' GGCCGCGGCCGCTTCAATCACTTCCTTCC 3'	NotI
Oligonucleotides for cloning of murine TACC3 variants	
pcDNA4/TO-hTACC3-3xFlag, Template: pReceiver-M15-hTACC3wt	
FP 5' TTAACTTAAGCTTGCCACCATGAGTCTGCAGG 3'	AflII
RP 5' GGCCGCGGCCGCTTGATCTTCTCCATC 3'	NotI
Oligonucleotides for cloning of murine chTOG variants	
pET23b_chTOG-C, Template: murine cDNA from lever and brain	
FP 5' GATCGGATCCAAGCTGAAGCTATGTCTGGC 3'	BamHI
RP 5' TCGACTCGAGCAGCTTCATTTGCGACTGC 3'	XhoI
pGEX4t1-nTEV_chTOG-C, Template: murine cDNA from lever and brain	
FP 5' GATCGGATCCAAGCTGAAGCTATGTCTGGC 3'	BamHI
RP 5' TCGACTCGAGCAGCTTCATTTGCGACTGC 3'	XhoI
Oligonucleotides for cloning of murine CHC variants (pTACC3 binding domain)	
pGEX4t1-nTEV-CHC317-549, Template: murine cDNA from lever and brain	
FP 5' GATCGGATCCGGAGTCAACAGAAAGGGAC 3'	BamHI
FP 5' GGCCGCGGCCGCTCCTGGGTGATATCAGCAAGAG 3'	NotI
Oligonucleotides for site directed mutagenesis	
pcDNA 3.1_TACC3-ΔCC1_GFP, Template: pMSCV-GFP_TACC3wt	
Primer1 5' TCTTCTGGTAGCCAAGGAGACCTCGAGGC 3'	
Primer2 5' CTCGAGGTCTCCTTGGCTACCAGAAGAATGAAGAG 3'	
pGEX4t1-nTEV_TACC3 S347E, Template: pGEX4t1-nTEV_TACC3	
Primer1 5' GTCGGCCTGGAGGAAGCAGGAGTTGTACGTGAAATTT GACC 3'	
Primer2 5' GGTCAAATTTCACGTACAACTCCTGCTTCCTCCAGGCC GAC 3'	
pGEX4t1-nTEV_TACC3 S347A, Template: pGEX4t1-nTEV_TACC3	
Primer1 5' GTCGGCCTGGAGGAAGCAGGCTTTGTACGTGAAATTT GACC 3'	
Primer2 5' GGTCAAATTTCACGTACAACGACTGCTTCCTCCAGGC CGAC 3'	
Sequencing primer for site directed mutagenesis	
FP 5' CAGTGAGCTGGTGACCCC 3'	
RP 5' TCCAAGTTCTCCTGCTGC 3'	

3.10 Bacterial culture media

Tab. 10: List of Bacterial culture media

No.	Type of media	Composition	Recipes
1	Luria-Bertani (LB) media	LB powder (5 g/l) yeast extract, 10 g/l NaCl, 10 g/l Trypton)	Dissolve LB powder (25 g/l) in dH_2O, sterilize by autoclaving (121˚C & 15 lb), store at +4˚C.
2	LB Agar plate	LB Agar powder (Yeast extract 5 g/l, NaCl 10 g/l, Trypton 10 g/l, Agar 15 g/l)	Dissolve LB agar powder (40 g/l) in dH_2O, sterilize by autoclaving (121˚C & 15 lb), cool to 60˚C temperature, add antibiotic, pore 20-25 ml in 10 cm petri dish, wait till solidify; and store at +4˚C.
3	Terrific Broth (TB) media	Trypton (12 g/l), Hefe extract (24 g/l), Glycerol (0.4%), KH_2PO4 (2.31 g/l)and K_2HPO4 (12.5 g/l)	Dissolve 12 g Trypton, 24 g yeast extract and 4 ml glycerol in 900 ml dH_2O. In parallel make 10x phosphate buffer solution by dissolving 23.1 g KH_2PO_4 and 125 g K_2HPO_4 in 1 liter dH_2O, sterilize both solution by autoclaving and store at +4˚C. Before using add 100 ml of 10x phosphate buffer to 900 ml medium.

3.11 Vectors and plasmids

Tab. 11: List of vectors and plasmid

No.	Vectors and plasmids	Selection marker	Vendor
1	pGEX4t1-nTEV	Ampicilin	GE Healthcare, München
2	pET 23b	Ampicilin	Novagen, USA
3	pET-Duet	Ampicilin	Novagen, USA
4	pCDNA 3.1	Ampicilin	Invitrogen, Heidelberg

3.12 Bacterial strains

Tab. 12: List of bacterial strain

No.	Bacterial strains	Selection marker	Vendor
1	*Escherichia coli* XL1 blue	Tetracycline	Agilent Technologies, USA
2	*Escherichia coli* Rosetta (DE3)	Chloramphenicol	Novagen

3.13 Cell lines and culture media

Tab. 13: List for mammalian cell lines and culture media

No.	Cell lines	Culture Media
1	HeLa	DMEM supplemented with 10% FCS and 1x penicillin/streptomycin
2	COS7	DMEM supplemented with 10% FCS and 1x penicillin/streptomycin

3.14 Crystallization kits

Tab. 14: List of kits for crystal screen

No.	Name of the screen	Manufacturer
1	Nextal Classic I & II	QIAGEN, Maryland USA
2	Nextal PEGs I & II	QIAGEN, Maryland USA
3	Nextal JCSG Core I, II, III, & IV	QIAGEN, Maryland USA
4	Nextal $AmSO_4$	QIAGEN, Maryland USA
5	Nextal PACT	QIAGEN, Maryland USA
6	Nextal Mb class I & II	QIAGEN, Maryland USA
7	Nextal protein complex	QIAGEN, Maryland USA
8	JB Membran 1, 2, 3, (72)	QIAGEN, Maryland USA
9	MD MemStart MD1-21 (48)	QIAGEN, Maryland USA
10	MD MemStart MD1-25 (48)	QIAGEN, Maryland USA
11	Crystal Screen 2	Hampton Research, USA

3.15 Instruments and equipments

Tab. 15: List of Instruments

No.	Name of instrument	Facility center
1	Acta Purifier (GE Healthcare)	Institute of Biochemistry and Molecular Biology II, HHU, Düsseldorf
2	Acta Prime (GE Healthcare)	
3	Acta FPLC (GE Healthcare)	
4	Bio-Rad SDS-PAGE gel apparatus	
5	Bio-Rad agarose gel apparatus	
6	Beckman Coulter Avanti J-20-XP centrifuge	
7	Beckman Coulter optima LE80K ultracentrifuge	
8	Beckman Coulter DU800 spectrophotometer	
9	Confocal Microscopy (cLSM 510-Meta/Zeiss)	
10	Diana UV-lamp agarose gel scanner	
11	Eppendorf Mastercycler/Thermocycler	
12	Eppendorf centrifuge 5410R, 5415D, 5417R	
13	INTAS Chemocam Imager	
14	INTAS UV lamp agarose gel scanner	
15	Infors-HT Multitron incubation shaker	
16	MicroCal ITC	
17	Nikon Microscope (TE2000)	
18	PEQLAB Nanodrop 200c spectrophotometer	
19	Fluidizer	
20	Mass spectrometry facility	BMFZ, HHU, Düsseldorf
21	Multi Angle Light Scattering Facility	Institute of Biochemistry, HHU Düsseldorf
22	Crystallization Screening facility	Crystal and X-Ray Facility, HHU Düsseldorf
23	CD spectroscopy facility	Institute of Physical Biology, HHU Düsseldorf
24	Analytical Ultracentrifugation facility	
25	Electron Microscopy (EM)	MPI for Molecular Physiology, Dortmund

4 Experimental methods

4.1 Microbiological methods

In microbiology and molecular biology studies, because of the well characterized genome and widely studied genetics, *Escherichia coli* is the most commonly used model organism. Work of Stanley Cohen and Herbert Boyer in *E. coli* to create recombinant DNA revolutionized the modern protein technology (93). *E. coli* became the frequently used host for recombinant or heterologous protein production (94). In this work, *E. coli* strains have been used as microbiological tools for recombinant protein production.

4.1.1 Bacterial culture

Transformed *E. coli* was grown on a solid (LB Agar antibiotic selection plate) and/or in broth (LB and TB) media with selection antibiotic. In order to pick up single cell colonies an aliquot of *E. coli* inoculums were streaked on a LB Agar antibiotic plates and kept in incubation chamber (37℃ for overnight) for growth of single cell colonies (95). For plasmid multiplication and protein production *E. coli* were grown in broth media in a two step process. In the first step, a single cell colony was inoculated into 5 ml of sterile LB or TB media (in a sterile 50 ml falcon tube) with the proper antibiotics for selection and allowed to grow by shaking (150 rpm) on the incubation shaker (37˚C for overnight). In a second step, overnight grown cultures from single cell colonies were inoculated into fresh sterile TB media in a ratio of 1:100 in a flask and bacteria were allowed to grow by shaking on an incubation shaker (37˚C). OD_{600} was recorded at 30 minute (min) intervals.

Overnight grown pre-cultures were directly harvested for small scale plasmid isolation (plasmid mini preparation), whereas for large scale plasmid isolation (midi- and maxi-preparations) second cultures were grown [for 4-5 hours (h) at 37˚C until OD_{600} reached 0.6-0.8] and then harvested and processed for plasmid DNA isolation. For protein production second cultures were grown until OD_{600} reached above 0.7 and after that culture was induced

with an appropriate concentration of IPTG and then allowed to grow at 20˚C overnight. Next day, cultures were harvested and processed for protein isolation and separation.

4.1.2 Growth curve analysis of *E. coli*

Growth curves of *E. coli* rosetta strain were analyzed for calculating the time required to reach the mid log phase or OD_{600} >0.7. In order to analyze the growth curve, bacteria were pre-cultured in TB media and 100 ml of second culture (as mentioned in section 4.1.1) was grown for recording absorbance at a wavelength of 600 nm (OD_{600}) at 20 min intervals. Absorbance data were plotted against time to obtain a sigmoid curve (96). Time (in hours) to reach OD_{600} >0.7 was calculated from this plot, which is a very helpful factor for preparative cultures particularly when using IPTG induction for protein production.

4.2 Bioinformatics

In order to perform *in silico* characterization of TACC family members, the protein sequences of TACC family members from representative metazoans were retrieved from the NCBI database (Tab. 16). Different bioinformatics tools/programs were used for sequence based characterization of the TACC3 protein. Blast algorithm was used for similarity search and to identify a functional domain or motif in the less conserved N-terminal part of murine TACC3. To analyze the conservation of amino acids residues, motifs and domains and creating the evolutionary tree of vertebrate TACC family members, multiple sequence alignment was performed using the ClustalW algorithm (97). The alignment file was analyzed using the JALVIEW program (98). For the further analysis of coiled coil regions for redefining the coiled coil boundary in the murine TACC3 protein the COILS program was used in 14, 21 and 28 residues scan modes (99). Different proteomic tools from the EXPASY-SIB bioinformatics resource portal were used for *in silico* characterization of the TACC3 protein sequence (pI and theoretical molecular weight determination, phosphosite prediction, secondary structure prediction) (100). JAVA based DOG (domain graph) program was used to draw the schematic diagram of protein domain structures with functional motifs/sites (101).

Tab. 16: List of protein sequences retrieved from NCBI database

No.	Protein	Organism	NCBI protein sequence ID
1	TACC1	*Homo sapiens*	Accession: NP_006274.2; GI: 170763517
2	TACC2	*Homo sapiens*	Accession: NP_008928.1; GI: 11119414
3	TACC3	*Homo sapiens*	Accession: NP_006333.1; GI: 5454102
4	TACC1	*Mus musculus*	Accession: NP_796063.3; GI: 110681727
5	TACC2	*Mus musculus*	Accession: NP_001004468.1; GI: 52486843
6	TACC3	*Mus musculus*	Accession: NP_001035525.1; GI: 94681040
7	TACC3	*Oryctolagus cuniculus*	Accession: NP_001075615.1; GI: 126722961
8	TACC3	*Bos taurus*	Accession: NP_001093775.1; GI: 154152109
9	TACC3	*Xenopus laevis*	Accession: NP_001081964.1; GI:148235419
10	TACC3	*Takifugu rubripes*	Accession: NP_001011729; GI: 348041275
11	chTOG	*Mus musculus*	Accession: NP_001159461.1; GI: 260166721
12	chTOG	*Homo sapiens*	Accession: NP_001008938.1; GI: 57164942

4.3 Molecular biology methods

4.3.1 Preparation of competent *E. coli*

Development of competency is an important prerequisite for bacterial transformation. Chemical and electro-competent cells of *E. coli XL1 Blue* and *E. coli* Rosetta *(DE3)* strains were useful for transformation of recombinant TACC3 and chTOG variants plasmids for their multiplication and protein production. To prepare the electro-competent bacteria, the bacterial culture was grown (section 4.1.1) in the presence of antibiotics (tetracycline for *E. coli XL1 Blue* and chloramphenicol for *E. coli* Rosetta) for selection. The secondary culture (500 ml) was grown until OD_{600} reached in between 0.4-0.5 and the further procedures were followed on ice temperature or at +4˚C according to standard protocols (102). In brief, harvest bacteria (by centrifugation at 5000×g; +4˚C for 10 min), resuspend two times (in ice cold sterile ddH_2O) and wash the pellet gently followed by single wash with sterile 10% glycerol. Finally, resuspend pellet in 2 ml of sterile 10% glycerol, prepare aliquots of 50 µl in pre-chilled eppendorf tubes, snap freeze in liquid N_2 and store at -80°C. For chemical competent cell preparation all the steps performed were identical with two changes - in place of sterile

ddH_2O and sterile 10% glycerol, sterile ice chilled 0.1 M $CaCl_2$ without and with 15% glycerol was used, respectively (103).

4.3.2 Plasmid vector maps

pGEX-4t1-nTEV (Fig. 7A): This vector has the tac-promoter region and coding DNA for GST-tag followed by multiple cloning site (MCS). Used for cloning of TACC3, chTOG and CHC variants and N-terminal GST fused soluble protein production in bacterial expression host. Ampicillin resistance gene gives the benefit of double selection of transformed '*E. coli* Rosetta' strain during expression culture together with chloramphenicol. This vector also inserts a TEV (tobacco-etch-virus) protease cleavage site along with a thrombin site in between the GST-tag and fusion partner which was useful for purification of TACC3 variants with the internal thrombin site.

pCDNA3.1-GFP (Fig. 7B): Provided by Dr. Doreen Floss, Institute of Biochemistry and Molecular Biology II. Eukaryotic expression plasmid vector contains HindIII and NotI cloning sites followed by the EGFP coding DNA sequence. Used for cloning of TACC3 variants fused to C-terminal EGFP and for its expression in mammalian cells.

pET 3a (Fig. 7C): T7 promoter based plasmid vector, in which coding DNA for TACC3-CC with a C-terminal His-tag was inserted for protein production in *E. coli* expression strains. The ampicillin resistance gene gives the benefit of double selection of transformed '*E. coli* Rosetta' strain during expression culture together with chloramphenicol.

pET 23b (Fig. 7D): T7 promoter based plasmid vector, used for cloning of TACC3-N, TACC3-7R, and chTOG-C. This vector gives the advantage of a C-terminal His-tag fused to the protein to be produced in *E. coli* expression strains. The ampicillin resistance gene gives the benefit of double selection of transformed '*E. coli* Rosetta' strain during expression culture together with chloramphenicol.

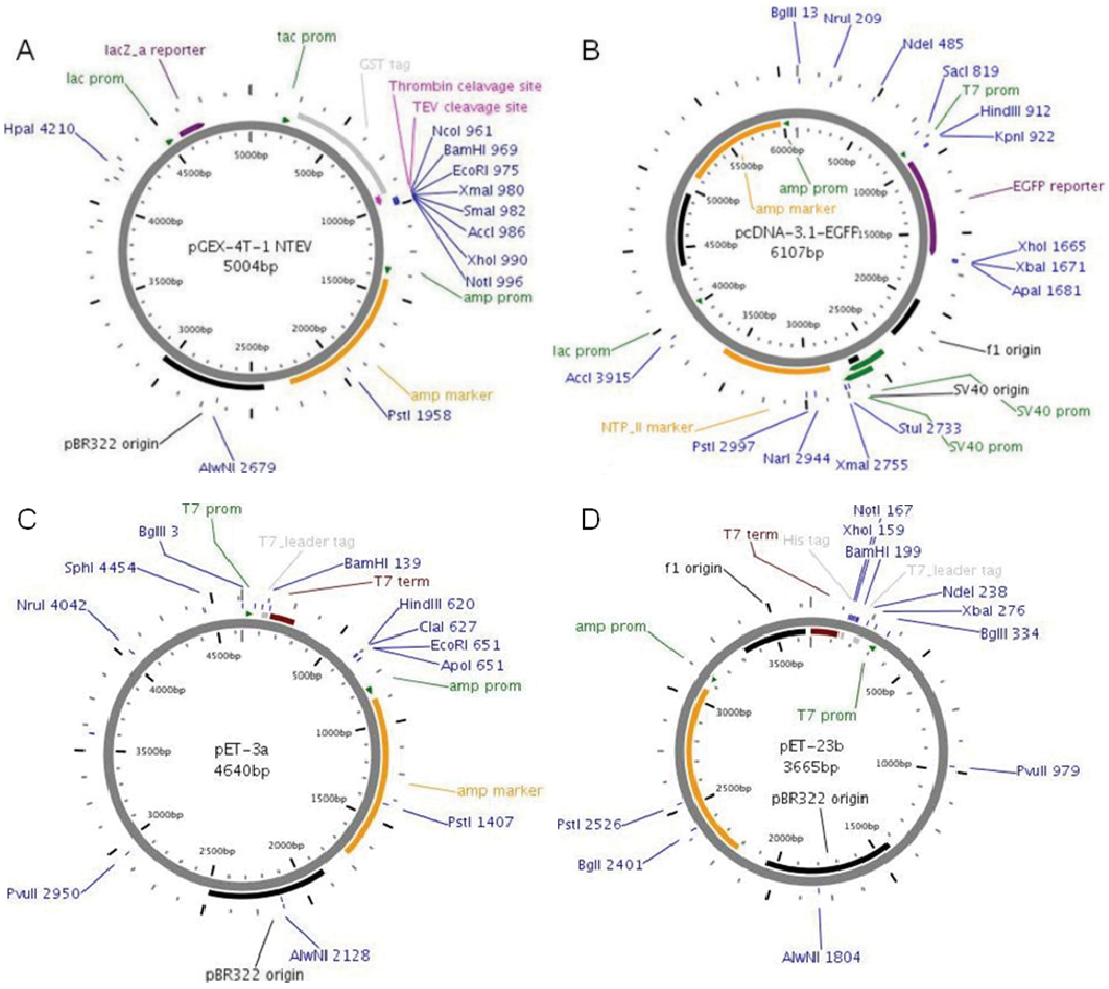

Fig. 7: Plasmid vector maps with unique restriction sites.

4.3.3 Bacterial transformation

Standard transformation protocols were applied according to the type of competent *E. coli* strains (102,104). Briefly, plasmid DNA (0.2-0.5 µg) was added to competent bacteria, followed by 5-20 min incubation on ice. Further heat shock (42˚C for 90 sec; for chemical competent bacteria) or short electrical pulse/shock (in an electroporater for electrocompetent bacteria) followed by cold shock (5 min incubation on ice) was provided to competent bacteria for DNA uptake. The transformed bacteria were grown in sterile LB media (1 ml; 37˚C; 150 rpm for 30-60 min). After centrifugation (5000 rpm for 2 min), 800 µl media was discarded and the pellet was resuspended in the remaining 200 µl media. Afterwards resuspended bacteria were spread on LB agar plates with antibiotics for selection and kept in

an incubation chamber (37˚C; overnight) for growth of single cell colonies. Electroporation was performed for colony screening after molecular cloning and chemical transformation for large scale plasmid isolation.

4.3.4 Bacterial glycerol stock preparation

Transformed *E. coli* Rosetta *(DE3)* bacteria were stored at -80˚C as 25% glycerol stocks. To prepare glycerol stocks, 5 ml bacterial cultures were grown up to log phase (section 4.1.1). Then 1.2 ml of log phase culture was mixed with 400 µl of autoclaved 100% glycerol in a labeled 1.8 ml sterile cryovial, vortexed to mix well, snap frozen in liquid N_2, and stored at -80˚C.

4.3.5 Agarose gel electrophoresis

In order to separate, identify, and purify amplified DNA fragments or plasmids, agarose gel electrophoresis was performed using standard protocols (102). In brief, prepare 1% agarose gel in 1x TBE or 1xTAE buffer (section 3.4) with EtBr (ethidium bromide), transfer gel into electrophoresis chamber, load DNA sample with sample loading dye, perform electrophoresis (65V; 30-60 min or for a time period to achieve optimal separation). Finally, visualize DNA bands by illumination with UV light. Images were visualized and captured with the INTAS imager connected to an UV illuminator (102,105).

4.3.6 Polymerase chain reaction (PCR)

PCR was performed for fast copying and amplification of specific DNA fragments from a pool using sequence-specific primers (Oligonucleotides; section 3.11) and thermosensitive DNA polymerase (Taq, Pfu, and Vent polymerase) (106). All reaction ingredients (as mentioned in Tab. 17-19) were mixed in a 0.5 ml sterile thin walled tubes and reactions were carried out in 25 µl of total reaction volume. The reactions were carried out in an eppendorf thermocycler followed programming. The thermocycler program (Tab. 20) was designed according to the size of fragments to be amplified and the melting temperature (T_m) of primers. Amplification of targeted DNA fragments was analyzed on agarose gels (section 4.3.5) and fragments were purified by a PCR purification kit.

Tab. 17: Composition for Pfu polymerase reaction mixture

Component	Stock concentration	Final concentration	Volume (µl)
Pfu DNA polymerase (Fermentas)	2.5 U/ µl	1.25 U	0.5
10x PCR buffer with 20 mM $MgSO_4$	10x	1x	2.5
$MgSO_4$	20 mM	0.6 mM	0.3
dNTPs mix	25 mM	2.5 mM	1.0
Forward (upstream) primer	10 pM	1.5 pM	1.5
Reverse (downstream) primer	10 pM	1.5 pM	1.5
Nuclease-free ddH2O			17.2
DNA template	0.25 µg/µl	0.125 µg	0.5
Total reaction volume			25 µl

Tab. 18: Composition for Vent polymerase reaction mixture

Component	Stock concentration	Final concentration	Volume (µl)
Vent DNA polymerase (New England Biolab)	2 U/ µl	1U/reaction	0.5
10x PCR buffer	10x	1x	2.5
$MgSO_4$	20 mM	2.0 mM	1.0
dNTPs mix	25 mM	2.5 mM	1.0
Forward (upstream) primer	10 pM	1.5 pM	1.5
Reverse (downstream) primer	10 pM	1.5 pM	1.5
Nuclease-free ddH2O			16.5
DNA template	0.25 µg/µl	0.125 µg	0.5
Total reaction volume			25 µl

Tab. 19: Composition for Taq polymerase reaction mixture

Component	Stock concentration	Final concentration	Volume (µl)
Taq DNA polymerase (QIAGEN)	5 U/ µl	1.25 U	0.25
10x PCR buffer	10x	1x	2.5
$MgCl_2$	25 mM	2.5 mM	1
dNTPs mix	25 mM	2.5 mM	1
Forward (upstream) primer	10 pM	1.5 pM	1.5
Reverse (downstream) primer	10 pM	1.5 pM	1.5
Nuclease-free ddH2O			16.75
DNA template	0.25 µg/µl	0.125 µg	0.5
Total reaction volume			25 µl

Tab. 20: PCR program for

Step	Temperature	Duration	No. of Cycles
Initial denaturation	95 ˚C	3 min	
Denaturation	95 ˚C	0.5-1 min	24-29
Annealing	60-62 ˚C	2 min	
Extension	72 ˚C	2 min/kb for Pfu polymerase 1 min/kb for Taq polymerase	
Final extension	72 ˚C	10 min	
Store	4 ˚C		

4.3.7 Plasmid DNA isolation

Alkaline lysis in presence of SDS detergent is the basic principle for isolating plasmid DNA from *Escherichia coli*, which is followed by all currently available protocols (102,107). In this work, QIAGEN miniprep, Nucleobond AX midi and maxi-prep kits, and respective protocols were used to isolate plasmid DNA. In brief, harvest bacterial culture (section 4.1.1) (centrifugation at 5000 g, 10 min) resuspend pellet in pre-chilled resuspension buffer with RNAseI (P1 mini-prep buffer; RES midi- maxi-prep buffer), add lysis buffer (P2 mini-prep buffer; LYS midi-maxi-prep buffer), add neutralization buffer (miniprep buffer N; NEU midi-maxi-prep buffer), clean cell debris, pass solution through DNA-binding column and subject column to high salt wash (miniprep buffer PB; WASH midi-maxi-prep buffer). Thereafter, wash the mini-prep column with PE buffer and elute the DNA with elution buffer or nuclease free water. For midi-maxi-prep columns, DNA was eluted with elution buffer followed by isopropanol precipitation and 70% ethanol washing of the DNA pellet. Upon drying, the DNA pellet was re-dissolved in nuclease free water. The purity of the DNA was analyzed by agarose gel electrophoresis and concentration was measured using a Nanodrop at OD_{260} nm.

4.3.8 DNA cleavage by restriction enzymes

In order to create recombinant plasmid DNA, amplified DNA (insert) and plasmid vector were digested with site specific restriction enzymes (REs). In this work some common REs (according to MCS and site inserted in primers) were used to cleave the duplex DNA generating sticky/cohesive end on both sides of linear DNA. The DNA (1-5 µg) was mixed with RE (1 U) and 1x RE buffer in a volume of 20-25 µl and the reaction were carried out by

incubation at 37˚C for 3-4 h. After heat inactivation of the first enzyme, sequential digestion was performed using another specific RE to cleave the DNA at a second site. Digested DNA was separated on agarose gels and isolated using a gel elution kit (QIAGEN).

4.3.9 Ligation of DNA fragments

Digested amplified DNA (inserts) was ligated into plasmid vector (with complementary sticky end) using recombinant T4-DNA ligase. The reaction mixtures were prepared by mixing insert(s) and vector(s) in a ratio of 1:1 to 1:5 ratios (100-500 ng insert with 100 ng of plasmid vector) with T4-DNA ligase (2U), 1x T4-ligase buffer and 1 mM ATP. The reaction was carried out at 16 ˚C for overnight. Thereafter, the complete mixture was used to transform electrocompetent *E. coli* XL1 Blue bacteria. Clones were selected on recombinant DNA specific antibiotic selection LB agar plates.

4.3.10 Molecular cloning

In this work murine TACC3 and chTOG variants were inserted into prokaryotic plasmid expression vectors for protein production and purification. To facilitate the cloning, respective DNA fragments were amplified by PCR (section 4.3.6) using sequence specific primers and template DNA (section 3.9). Plasmid vectors were isolated (section 4.3.7) and vectors and inserts (PCR amplified product) were cleaved with site-specific REs (section 4.3.8). Respective inserts and vectors were ligated and the ligated plasmid was selected following transformation on vector specific antibiotic selection LB agar plates (section 4.3.9). Bacterial colonies were screened by PCR followed by double digestion of cloned plasmids. Finally, correct insertion and identity of targeted DNA was confirmed by sequencing using vector specific sequencing primers (GATC biotech).

4.3.11 Site directed mutagenesis

To create single amino acid residue variants or internal deletion mutants of murine TACC3, full recombinant plasmid was amplified by PCR using Pfu polymerase and primers were designed for mutation. PCR amplification was achieved in a 25 µl reaction mixture

(Tab. 21) and reaction was carried out in a thermocycler by programming SDM specific temperature cycle (Tab. 22).

Tab. 21: Composition of PCR reaction mixture for mutagenesis

Component	Stock concentration	Final concentration	Volume (µl)
Pfu DNA polymerase	2.5 U/ µl	1.25 U	0.5 µl
10x PCR buffer with 20 mM $MgSO_4$	10x	1x	2.5 µl
$MgSO_4$	20 mM	0.6 mM	0.3 µl
dNTPs mix	25 mM	2.5 mM	1.0 µl
Primer 1	10 pM	1.5 pM	1.5 µl
Primer 2	10 pM	1.5 pM	1.5 µl
Nuclease-free ddH2O			17.2 µl
DNA template	0.25 µg/µl	0.125 µg	0.5 µl
Total reaction volume			25 µl

Tab. 22: PCR program for mutagenesis

Steps	Temperature	Duration	No. of Cycles
Initial denaturation	94 ˚C	3 min	
Denaturation	94 ˚C	0.5-1 min	16
Annealing	80 ˚C	45 sec	
Extension	68 ˚C	8 min	
Final extension	72 ˚C	10 min	
Store	4 ˚C		

4.3.12 Recombinant gene test expression

In order to check the expressibility of recombinant DNA, *E. coli* Rosetta strain was transformed and test expression cultures (5 ml for pre-culture and 50 ml for secondary culture) were grown after induction with 0.2 mM of IPTG (section 4.1.1). Bacteria were harvested, lysed by pulse ultrasonication (at 4˚C; 30 sec pulse and 1 min rest) in normal Tris-NaCl buffer (30 mM Tris-HCl pH 7.5, 150 mM NaCl, 3 mM DTT, 2 mM EDTA, 1 mM PMSF, and one protease inhibitor cocktail tablet per 50 ml of buffer) and centrifuged (10.000 g, 10 min, 4 ˚C). Protein expression levels in the supernatant were analyzed by SDS-PAGE and immunoblotting.

4.4 Protein chemical methods – protein separation

4.4.1 SDS-polyacrylamide gel electrophoresis (SDS-PAGE)

SDS-PAGE is a widely used and elaborately described protein separation method (108,109). This method was performed on polyacrylamide gel (7.5, 10, & 12.5 %; gels casted in lab, composition are mentioned in Tab. 23, and 4-15% precasted gradient gels from BioRad were used) using standard protocols. For sample preparation cell lysate, cell pellets or protein samples were mixed with 2x Laemmli buffer, boiled at 100˚C for 10 min and centrifuged at 8000 rpm for 5 min. The samples were loaded onto the gels, proteins were separated by electrophoresis and protein bands were analyzed either by staining (with CBB dye or ProQ-Diamond stain) or by immunoblotting.

Tab. 23: SDS-PAGE gels with resolving gels of different percentages

Ingredients	Stacking gel 3%	Resolving gel 7.5 %	Resolving gel 10 %	Resolving gel 12.5 %
Acrylamide-bisacrylamide (30%)	0.3 ml	1.5 ml	2 ml	2.5 ml
Stacking gel buffer	1.5 ml	-	-	-
Resolving gel buffer	-	3 ml	3 ml	3 ml
H_2O	1.25 ml	1.5 ml	1 ml	0.5 ml
TEMED	10 µl	15 µl	15 µl	15 µl
10% APS	20 µl	45 µl	45 µl	45 µl

4.4.2 Immobilized metal ion affinity chromatography (IMAC)

The IMAC protein separation method is based on interfacial interactions between histidine and cysteine residues of protein in solution and metal ions like Zn^{2+}, Ni^{2+}, Co^{2+}, Cu^{2+}, and Ca^{2+} fixed to a solid support made of hydrophilic cross linked polymer (110,111). In this work Ni^{2+}-NTA agarose matrix (Ni^{2+} immobilized by nitrilotriacetic acid cross linked with agarose; QIAGEN) was used for purification of 6xHis-TACC3-7R and 6xHis-chTOG-C proteins using standard protocols (QIAGEN handbook). In brief, the steps were as follows: Harvesting cells in lysis buffer (30 mM Tris-HCl pH 7.5, 200 mM NaCl, 5 mM β-ME, 15 mM imidazole and EDTA-free protease inhibitor cocktail); protein extraction by incubating (4˚C for 10-15 min) the bacteria with DNaseI (10 µg/ml) followed by cell lysis in a fluidizer

(Microfluidics Corporation); soluble fraction isolation by centrifugation (30,000 g for 45 min at 4 ˚C); applying the supernatant to a pre-equilibrated (30 mM Tris-HCl pH 7.5, 200 mM NaCl, 5 mM β-ME, 20 mM imidazole) Ni^{2+}-NTA agarose column followed by washing with 3-5 column volumes of purification buffer; and finally, elution of the protein in fractions by setting a gradient of 50 mM imidazole (elution buffer I; 30 mM Tris, 200 mM NaCl, 5 mM β-ME, 50 mM imidazole) to 500 mM imidazole (elution buffer II; 30 mM Tris, 200 mM NaCl, 5 mM β-ME, 500 mM imidazole). Elution fractions were analyzed on SDS-PAGE for final purity.

4.4.3 Glutathione (GSH) affinity chromatography

The Glutathion-S-transferase (GST) fusion system is a frequently used method for high level soluble protein production and purification from bacterial lysates (112,113). The pGEX-4t1-nTEV vector was used for the production of GST fused TACC3 and chTOG variants in *E. coli* expression host (114). GST-fused proteins were isolated by passing the soluble fraction from the cell lysate through pre-equilibrated (with standard GSH-purification buffer; 30 mM Tris-HCl pH 7.5, 150-200 mM NaCl, 3 mM DTT, 1-2 mM EDTA) glutathione agarose column, followed by three times washing (each with two column volume of buffer; two times with standard GSH-purification buffer and once in between with high salt buffer - 30 mM Tris-HCl pH 7.5, 150-200 mM NaCl, 3 mM DTT, 10 mM $MgCl_2$, 10 mM ATP). Lastly, bound protein was eluted by passing GSH-elution buffer (30 mM Tris-HCl pH 7.5, 150-200 mM NaCl, 3 mM DTT, 1-2 mM EDTA, 20 mM glutathione; adjust final pH 7.5) through the column. The purity of GST-fused protein was analyzed by SDS-PAGE (section 4.4.1).

This method was also used to remove the cleaved GST-tag (reverse GSH-affinity chromatography) after cleaving the tag from fusion protein with TEV (tobacco-etch-virus) or thrombin protease. To isolate TEV or thrombin cleaved protein, samples were passed through a pre-equilibrated (standard GSH-purification buffer) glutathione agarose column and elution fractions (containing the protein of interest) were collected. Fractions were analyzed on SDS-PAGE and by immunoblotting for purity determination. Further the bound GST in the column was removed by passing one column volume of 6 M Guanidium-Cl followed by passing 2-3 column volume of filtered ddH_2O.

4.4.4 Gel filtration or size exclusion chromatography

Gel filtration chromatography represents a widely used approach to separate protein molecules according to their size and shape (molecular mass and stock radii) in native or solution state. This method was also used for fast exchanging of the appropriate buffers as an alternative to the dialysis procedure. This method was employed to, separate protein molecules (GST from protein of interest after TEV or thrombin cleavage) or to exchange the buffer (of affinity purified proteins for sample preparation before ITC, CD spectroscopy & analytical ultracentrifugation). Protein samples were passed through gel filtration columns (Superdex 200 or Superose 6) using specific buffer: Tris-NaCl buffer (30 mM Tris-HCl pH 7.5, 150-200 mM NaCl, 3 mM DTT, 1-2 mM EDTA); phosphate buffer [50 mM sodium phosphate (1.08% Na_2HPO_4 and 0.13% NaH_2PO_4) pH 7.5, 150 mM NaCl, 1 mM EDTA]; ITC buffer (30 mM Tris-HCl pH 7.5, 200 mM NaCl, 1 mM TCEP, 2 mM EDTA); and AUC buffer (30 mM Tris-HCl pH 7.5, 200 mM NaCl, 3 mM DTT, 1 mM EDTA). Elution fractions (fraction size: 0.5 ml for analytical column and 5 ml for preparative column) were collected and peak fractions were analyzed by SDS-PAGE and immunoblotting.

4.5 Protein chemical methods – protein production and purification

4.5.1 Preparative culture for recombinant protein production

Preparative cultures (5-20 liter for each construct) were generated using enriched TB media for large scale protein production. *E. coli* Rosetta strain transformed with recombinant plasmid DNA of interest was grown as mentioned in section 4.1.1. To induce protein expression and overproduction in transformed *E. coli*, IPTG (0.2 mM, 20 ˚C) was added and cultures were allowed to grow at this temperature for overnight.

4.5.2 Cell lysis and protein extraction

Bacteria with overexpressed protein were harvested by centrifugation (10,000 g for 10 min; Backman JLA 8.1000 rotor) and pellets were resuspended using IMAC-protein purification buffer (section 4.4.2) or GSH-purification buffer (section 4.4.3). Protein extraction was carried out by incubating (4˚C for 10−15 min) the cells with DNaseI (10

µg/ml) and cell lysis was performed in a fluidizer (Microfluidics Corporation) at a pressure of 10,000 psi (~690 bar). Soluble fractions were separated by centrifugation (30,000 g for 45 min at 4 ˚C) and supernatants were transferred into clean flasks for further purification by affinity chromatography (section 4.4.2 and 4.4.3).

4.5.3 Large scale purification of recombinant proteins

For large scale recombinant protein purification GSH-agarose and Ni^{2+}-NTA-agarose affinity purification methods were used (section 4.4.2 and 4.4.3). The supernatants (soluble fraction) after cell lysis and centrifugation (section 4.5.2) were applied to column with a flow rate of 1 ml/min. The remaining steps were performed as mentioned in section 4.4.2 and/or 4.4.3. Purified His- or GST-fusion proteins were concentrated and passed through gel filtration columns (section 4.4.4; Superdex 200 XK26/60 or Superpose 6 XK16/60 column) for buffer exchange. GST fusion proteins were subjected to TEV (4 U/mg) or thrombin (2 U/mg) digestion at 4˚C for overnight. GST was removed by performing either reverse glutathione affinity purification or gel filtration chromatography or both in combination. Finally, the purity of proteins was analyzed by SDS- PAGE and CBB staining.

4.6 Protein chemical methods – protein analytics

4.6.1 Determination of protein concentration

For any *in vitro* biochemical reaction or protein characterization, the correct concentration of a protein is an important factor. Especially for crystallization and protein characterization by ITC, there is a need for a higher protein concentration. To achieve the required concentration of a protein obtained after preparative scale, the protein was concentrated using Millipore amicon centricon columns followed by centrifugation at 4000 rpm. Several methods are available for the determination of protein concentration with the representing Bradford assay the method of interest. The assay was performed according to a standard protocol (115). In brief, standard curves (amount of protein vs. absorbance) were plotted by mixing increasing amount of BSA (0.5-20 µg) to 500 µl Bradford reagent and absorbance at OD 595 nm was recorded in triplicate. The absorbance data were averaged and the standard linear equation was derived from the amount of BSA vs. absorbance (XY

distribution) plot. Protein samples were analyzed in an analogous manner and the concentration was calculated by analyzing the absorbance data using the obtained standard linear equation. TACC3 protein variants have an acidic pI and the purified proteins precipitated and formed clots in Bradford solution because of the acidic nature. Therefore, protein samples for concentration determination were prepared by diluting them in 1 M NaOH solution (116). Lastly, several aliquots (250 or 500 µl) were made for the highly concentrated purified proteins and were snap-frozen in liquid N_2 and stored at -80 ˚C for further use.

4.6.2 Immunoblotting (Western blotting)

Protein samples were loaded onto SDS-PAGE and transferred to nitrocellulose membranes (Hybond C, GE Healthcare) by the tank blot (Bio-Rad wet/tank blotting system) method. Blots were blocked with 5% milk in TBST and probed (overnight at 4 ˚C) with primary antibodies (1:5000 dilutions or according to manufacturer's instructions): anti-mTACC3 N18, anti-mTACC3 C18 (both generated in rabbits); anti-GST (pAb Abcam, Cambridge, UK), and anti-chTOG (mAb Abcam, Cambridge, UK). After washing three times for 10 min with 1x TBST (1x TBS with 0.1% Tween 20) the blots were subjected for incubation (1h at RT) with respective horseradish peroxidase (HRP)-coupled secondary antibodies (1:5000 dilution or according to manufacturer's instructions). Thereafter, blots were washed three times for 5 min with 1x TBST and specific signals were visualized using the ECL detection system (GE Healthcare, München) and visualization by INTAS chemostar imager.

4.6.3 Analytical gel filtration chromatography

AGFC was performed using Superose 6 10/300 GL column (GE Healthcare) connected to an ÄKTA™ purifier with an UV900 detector (GE Healthcare). The column was equilibrated by passing two column volume of filtered and degassed Tris-NaCl buffer (30 mM Tris-HCl pH 7.5, 150 mM NaCl, 3 mM DTT and 2 mM EDTA) with a flow rate of 0.5 ml/min and calibrated with standard proteins of known molecular weight (GE healthcare): Thyroglobulin (669 kDa); Ferritin (440 kDa); Aldolase (158 kDa); Ovalbumin (43 kDa); Carbonic Anhydrase (29 kDa); Ribonuclease A (13.7 kDa); Aprotinin (6.5 kDa). Following calibration each protein sample (~50-200 µg) was injected into the column and elution

fractions (500 µl) were collected. For protein-protein interaction analysis proteins were mixed at an equimolar ratio (7-10 nmol of TACC3 and chTOG variants), incubated on ice for 30 min, and then injected onto the column. Elution profiles were recorded using the UNICORN4.11 software program and peak fractions were analyzed on SDS-PAGE followed by CBB staining and immunoblotting.

4.6.4 Immunoprecipitation

Purified TACC3 before and after thrombin digestion (~10-15 µg) was mixed with 2 µl of stock antibodies (anti-mTACC3 N18 and anti-mTACC3 C18) and incubated at 4 °C for overnight. Thereafter, 25 µl of Protein A/G agarose beads presoaked in BSA were added, volume made up to 100 µl with IP buffer (30 mM Tris-HCl pH 7.5, 200 mM NaCl, and 2 mM EDTA) and samples incubated at 4 °C for 1 h by continuous mixing on a rotor. Following 4-5 washing steps with IP buffer, immune complexes were subjected onto SDS-PAGE and immunoblotting was performed with primary (anti-mTACC3 C18 and anti-mTACC3 N18) and HRP conjugated secondary (anti-rabbit) antibodies, respectively.

4.6.5 GST pull down assay

The GST pull down (bait-prey interaction) assay was performed by using GSH-sepharose (GE Healthcare) beads to analyze the interaction between purified TACC3 and chTOG variants. The prey proteins were obtained by cleaving the GST tag with TEV protease followed by removing of the GST tag by gel filtration or reverse GSH affinity purification. GSH-sepharose beads (GE healthcare) in a volume of 100 µl were washed three times with Tris-NaCl buffer (30 mM Tris-HCl pH 7.5, 200 mM NaCl, 3 mM DTT, and 2 mM EDTA). GST and GST-fused proteins (10-20 µM) were added and incubated (at 4 °C for 1 h) in a final volume of 200 µl. Blocking (2 h at 4 °C) with 5% BSA was performed followed by three times washing with Tris-NaCl buffer followed by the next incubation (4 °C for 2 h) with an equimolar ratio of the “prey” protein. After five washing steps, 100 µl of 2x Laemmli buffer was added, samples were heat denaturated at 100°C for 5 min and finally SDS-PAGE was performed followed by CBB staining and immunoblotting. Because of the weak interaction the pull down of TACC3-CC (prey) with GST-TACC3-7R (bait) was performed with a small modification in this method. For this, first bait and prey were mixed and incubated (overnight

at 4°C), and then GSH-sepharose beads presoaked in 5% BSA were added for the final pull down.

4.6.6 Isothermal titration calorimetry (ITC)

The ITC experiment was performed with the assistance of M.Sc. Eyad Fansa (AG Ahmadian, Institute of Biochemistry and Molecular Biology II). Purified TACC3 variants and chTOG protein samples were prepared by exchanging the buffer by gel filtration chromatography (Superose 6 XK 16/70 column; GE Healthcare) using ITC buffer (30 mM Tris-HCl pH 7.5, 200 mM NaCl, 1 mM TCEP, 2 mM EDTA). For the TACC3-7R protein, buffer was exchanged by an overnight dialysis against ITC buffer using Slide-A-Lyzer cassettes (Thermo Scientific). All measurements were carried out at 20 °C using a VP-ITC microcalorimeter. Proteins in the syringe were titrated with 10-30 fold higher concentrations to the proteins in the thermo-sensitive cell. For each titration 10-30 injections were made at 150-180 sec intervals, with each consisting of 8 µl, 10 µl, or 15 µl of the titrant. The reference power was set at 13 µcal sec^{-1} and the cell was stirred continuously at 310 rpm. Final data analysis was carried out using Origin software (Microcal Software). A non-linear least squares fit to a single binding site model was considered to obtain values for the binding constant, stoichiometry, and heat of binding. Control measurements were performed by titrating buffer to the protein and *vice versa* for comparison.

4.6.7 Aurora-A kinase assay

Human Aurora-A kinase (SignalChem) was used and all reaction steps were followed according to the manufacturer's instructions. In brief, the assays were performed in a volume of 25 µl by adding 5 µl (0.1 µg/µl) of Aurora-A kinase (diluted in kinase assay buffer: 5 mM MOPS pH 7.2, 2.5 mM β-glycerol phosphate, 5 mM $MgCl_2$, 1 mM EGTA, 0.4 mM EDTA and 50 ng/µl BSA) together with 1 µg of purified TACC3 protein. The final volume was adjusted to 20 µl with sterile ddH_2O and reactions were started by adding 5 µl of 10 mM ATP (dissolved in 25 mM MOPS pH 7.2, 12.5 mM β-glycerol phosphate, 25 mM $MgCl_2$, 5mM EGTA and 2 mM EDTA) followed by incubation (at 30°C for 15 min). Reactions were stopped by the addition of 10 µl of 6x Laemmli buffer followed by heat denaturation (100°C for 5 min). Phosphorylated proteins were then separated onto SDS-PAGE gel and detected by

Pro-Q Diamond phosphostaining followed by subsequent CBB staining for the visualization of the total protein loaded.

4.6.8 Pro-Q Diamond phosphoprotein gel staining

Fluorescent staining of SDS-PAGE gel using the Pro-Q Diamond phosphoprotein gel stain (Molecular Probes, Invitrogen) was performed to analyze the phosphorylation status of purified TACC3. Following the kinase assay, protein samples were resolved by SDS-PAGE and gels were incubated two times in the fixation solution (50% methanol, 10% acetic acid), first for 30 min and then for overnight. Thereafter, the gels were washed three times for 10 min with deionized ultrapure water, followed by incubation in Pro-Q Diamond phosphoprotein gel stain solution. The gels were destained with destaining solution (20% acetonitrile in 50 mM sodium acetate, pH 4) and washed two times for 5 min with ultrapure water. Images were obtained after 120 min of staining followed by three successive destaining washes. Pro-Q Diamond fluorescent gel images were acquired with the INTAS imager attached to a 300 nm UV transilluminator. Subsequent to image acquisition, gels were stained for total protein loading using CBB staining for comparing phosphorylated protein profiles and protein loading.

4.7 Protein biophysical methods

4.7.1 Sample preparation for MALDI-TOF mass spectrometry

For mass spectrometric analysis, protein samples were desalted by exchanging the buffer using NAP-25 columns (GE healthcare). Protein samples (5-10 µl) followed by ddH_2O were applied to the column and elution fractions were collected in drops. Desalted protein samples were sent to the central mass spectrometry facility (BMFZ) of the Heinrich-Heine-University.

4.7.2 Multi angle light scattering (MALS)

The MALS experiment was performed in collaboration with the lab of Prof. Lutz Schmitt (Institute for Biochemistry, Heinrich-Heine-University). The light scattering

measurements were done on a MALS instrument (miniDAWN™ TREOS; Wyatt Technology) under an asymmetric Field Flow Fractionation condition (Eclipse™ AF4, Wyatt Technology). Protein separation according to size was achieved within a very thin flow, which is exposed to a perpendicular force field. For exact mass calculation, UV absorptions at 280 nm (Agilent Infinity 1260) and refractive index signals (OptilabRex, Wyatt Technology) were also collected. For both TACC3 protein samples (before and after thrombin digestion) the same experimental procedures were performed. In brief, the AF4 membrane was equilibrated with Tris-NaCl buffer (30 mM Tris-HCl pH-7.5, 150 mM NaCl and 2 mM EDTA). Fifty microliter of protein sample (~3 to 4 mg/ml) was injected on the membrane under inflow of buffer. The movement of the sample on the terminal point of the AF4 membrane was monitored and the amount of scattered light and UV absorption (A_{280}) were detected in a time-dependent manner. The raw data were analyzed and processed with ASTRA software (Wyatt Technology). The amount of scattered light at maximum UV absorption was used to calculate molecular mass averages and polydispersity index of the protein samples. The amount of light scattered is related to the molar mass by the equation: $(K*C)/R(\theta,c)=[1/MwP(\theta)] + 2A_2C$. Where Mw is weight averaged molar mass, K is constant, C is solute concentration, $R(\theta,c)$ is excess Rayleigh ratio of the solution as a function of scattering angle q and concentration C, $P(\theta)$ is angular dependence of scattered light, and A_2 is the second virial coefficient and depend on osmotic pressure.

4.7.3 Analytical ultracentrifugation - sedimentation velocity (AUC-SV)

The AUC-SV experiment was performed in collaboration with Dr. Luitgard Nagel-Steger (AG Willbold, Institute for Physical Biology, Heinrich-Heine-University). The experiment was performed using an Optima XL-A analytical ultracentrifuge (Beckman Coulter) with a 4-hole titanium rotor (AnTi-60; Beckman). For SV experiments, cells with a standard aluminum two-channel centerpiece and quartz windows were used. Samples were prepared by gel filtration using Tris-NaCl buffer (AUC buffer; 30 mM Tris-HCl pH-7.5, 200 mM NaCl, 3 mM DTT and 1 mM EDTA) and concentrated up to 20 µM. The rotor temperature was equilibrated at 10°C in the vacuum chamber. After loading the sample (400 µl) as well as reference buffer (420 µl), radial scans at 280 nm with 20 µm radial resolution were recorded at 3 to 5 min intervals during sedimentation at 37.000 rpm. Partial specific volume of the protein, solvent density, and solvent viscosity were calculated from standard

tables using the UltraScan II program (Version 14.3). The collected radial scans were analyzed using the continuous distribution [c(s)] analysis module in the SEDFIT program (Version 12.1) as well as two-dimensional spectral analysis combined with genetic algorithm (GA) and final Monte Carlo statistics (MC) as implemented in UltraScan II. SEDFIT data evaluation was performed as follows: Sedimentation coefficient increments of 0.1 S were used in the appropriate range for each sample. The frictional coefficient was allowed to float during the fitting. The weight average sedimentation coefficient was obtained by integrating the range of sedimentation coefficients in which peaks were present. The c(s) distribution was converted to a c($s_{20,\ w}$) distribution using the SEDFIT program. Additional data were evaluated with the UltraScan II software, which in contrast to c(s) in SEDFIT provides each detected species with an individual shape factor, i.e. frictional ratio. After a primary data evaluation by 2DSA the time invariant noise was subtracted. These noise corrected data were fitted according to a model of non-interacting species with a parsimoniuosly regulated genetic algorithm to find the sum of solutions of the Lamm equation with the lowest number of individual species that describes the measured data best.

4.7.4 Circular dichroism (CD) spectra analysis

The CD spectroscopic measurements were performed at the Institute for Physical Biology, AG Willbold, Heinrich-Heine-University. The measurements were accomplished on a J715 spectropolarimeter (JASCO) using sodium phosphate buffer [50 mM sodium phosphate (1.08% Na2HPO4 and 0.13% NaH2PO4) pH 7.5, 150 mM NaCl, 1 mM EDTA] as a control. Protein samples were prepared by buffer exchange (against sodium phosphate buffer) by gel filtration. The CD spectrum was measured in the wavelength range of 190 nm to 260 nm with a data pitch of 0.2 nm with ten accumulations per reading. The spectrum was recorded as change in ellipticity [Δε] (milli degree or mdeg) and converted into molar ellipticity (in deg.cm^2/dmol) using the following formula: Molar ellipticity [ɵ] in deg.cm^2/dmol = [Δε (in mdeg) × mean residue weight]/[pathlength (in mm) × concentration (mg/ml)]. The standard value of mean amino acid residue weight (110 kDa) was considered in above formula. Final data processing was carried out with the help of the K2D3 CD spectra analysis program by selecting 41 data points from 200 nm to 240 nm at a data pitch interval of 1 nm followed by final curve fitting (117).

4.7.5 Negative staining and electron microscopy (EM)

The staining and electron microscopy (EM) was carried out with the help of M.Sc. Daniel Prumbaum and Dr. Stefan Raunser, Max-Planck-Institute for Molecular Physiology, Dortmund, Germany. For sample preparation, purified proteins were passed through gel filtration column, the peak elution fractions were collected, and concentrated to 1-2 mg/ml. Specimens were prepared using the conventional negative staining procedure (118). Briefly, a 4 µl drop of diluted samples were adsorbed for 40 s to a thin carbon film on a freshly glow-discharged 400 mesh copper grid (G2400C, Plano GmbH, Wetzlar). Excess solution was blotted onto filter paper (Whatman No. 4). After washing with two drops of deionized water and once with freshly prepared 0.75% uranyl formate (SPI Supplies/Structure Probe), specimen were exposed to the staining solution for about 2 min. Excess stain solution was removed and specimen were air-dried (118). For EM imaging, a Joel JEM-1400 electron microscope equipped with a LaB_6 filament was used and operated at an acceleration voltage of 120 kV. Digital micrographs were taken at a corrected magnification of 53,800x and a defocus value of -1.5 µm using a 4k x 4k CMOS camera F416 (TVIPS) at low-dose conditions.

4.7.6 Crystallization trials

The crystallization trials were made with collaboration of Dr. Astrid Höppner, Crystal and X-ray facility, Heinrich-Heine-University. The crystallization trials were performed for TACC3 before and after thrombin digestion, alone and in complex with chTOG-C as well as for TACC3-CC1 alone and in complex with chTOG-C. The samples were prepared by passing the protein through gel filtration column, pooling the single peak elution fractions and concentrating them to 5-10 mg/ml. The purity of proteins was confirmed by SDS-PAGE. In order to screen the crystallization conditions, the crystallization drops were set up in 96 well plates using the sitting drop method performed by HYDRA II Matrix robotics and crystal screens from QIAGEN. The screens used for the trial are listed in Tab. 14. The plates were kept in a vibration free incubator at 12˚C and/or room temperature for crystal nucleation and growth. Images were documented with the FORMULATRIX robotic scanner and imager at 1, 2, 3, 5, 7, 9, 11, 13, 15, and 21 days interval and analyzed further for the growth of crystals.

To determine the minimal stable domain(s) of TACC3 that can be crystallized, protein samples were subjected to partial protease (trypsin and chymotrypsin) digestion. The proteins were mixed with the protease in a molar ratio of 1:1000, 1:500 and 1:100 followed by time dependent incubation at 37˚C. Reactions were stopped by adding 2x Laemmli buffers and heat denaturation. Samples were analyzed on SDS-PAGE followed CBB staining.

4.8 Cell biological methods

The mammalian cell culture work and confocal laser scanning microscopy were performed with the help of M.Sc. Madhurendra Singh, Institute for Biochemistry and Molecular Biology II.

4.8.1 Mammalian cell culture and transfection

HeLa and COS7 cells were cultured in Dulbecco's Modified Eagle's Medium (DMEM) supplemented with 10% fetal calf serum (FCS; Invitrogen), 100 U/ml penicillin and 100 µg/ml streptomycin (Genaxxon) at 7% CO_2 and 37°C in standard cell culture incubator. Cell culture work was performed in six well cell culture plates (TPP) containing sterile glass cover slips in each well. Cells were allowed to grow up to a confluency of 50-70% and then transfected with 2 µg of recombinant plasmid DNA by using the FuGENE^{R}HD transfection reagent (for COS7 cells) or Calcium phosphate method (for HeLa cells). Cells were allowed to grow for 8 h after adding the transfection mixture, thereafter the medium was replaced with fresh medium followed by a further incubation period of 24-48 h. Transfection efficiency of recombinant DNA (EGFP alone and EGFP-fused TACC3 variants) was analyzed on a NIKON TE2000 microscope at a 40x magnification.

4.8.2 Confocal laser scanning microscopy (cLSM)

HeLa and COS7 cells were grown on sterile glass coverslips, washed once with $PBS^{+/+}$, fixed in 4% paraformaldehyde in 1x PBS for 20 min and permeabilized with 0.2% Triton X-100 in 1x PBS for 5 min at room temperature. Paraformaldehyde was neutralized with 1% glycine in 1x PBS for 20 min. After washing one time with $PBS^{+/+}$, cells were

blocked with 4% BSA in 1x PBS for 30 min and then incubated with primary antibodies diluted in PBS containing 1% BSA overnight at 4˚C. The following antibodies were used: anti-Human TACC3 (D2 mouse mAb; Santa Cruz), anti-Tubulin (Rat mAb; Acris GmbH), anti-chTOG (Rabbit polyclonal antibody; abcam), and anti-CHC (Rabbit polyclonal antibody; abcam). Following incubation with these primary antibodies, cells were washed three times with 1x PBS. Thereafter, incubation with secondary antibodies (Alexa 488-IgG anti-Mouse; Alexa 546-IgG anti-Rabbit; Alexa 633-IgG anti-Rat) dissolved in PBS containing 1% BSA was performed for 1 h. For visualizing DNA/chromosomes, cells were treated with DAPI (1:10,000) for 5 min and finally coverslips were mounted on glass slides using Prolong Gold. The slides were examined under a Zeiss cLSM 510 Meta (Zeiss) microscope at a 63x magnification under emersion oil. Images were collected and processed with the Zeiss LSM image browser software. Alternatively, slides were analyzed and pictures were taken using Nikon TE2000 microscope at 40x magnification.

5 Results

5.1 Subcellular colocalization of TACC3 with its known effectors

TACC3 localizes in the cytosol and nucleus in interphase cells (42). During the G_2/M and mitotic phases of the cell cycle it co-localizes with its partner and effector proteins CHC and chTOG at the centrosome and along spindle microtubules (8,27,29,30,33,34). To validate their colocalization, immunostainings of HeLa cells were performed in the lab by using primary antibodies (against TACC3, αTubulin, chTOG, CHC) and Alexafluor (Alexa 488, 546, 633)-labeled secondary antibodies (Fig. 8). The cells were stained with DAPI to detect chromosomes/DNA. As expected, during metaphase TACC3 clearly appears to be colocalized with chTOG as well as CHC at the mitotic spindle apparatus.

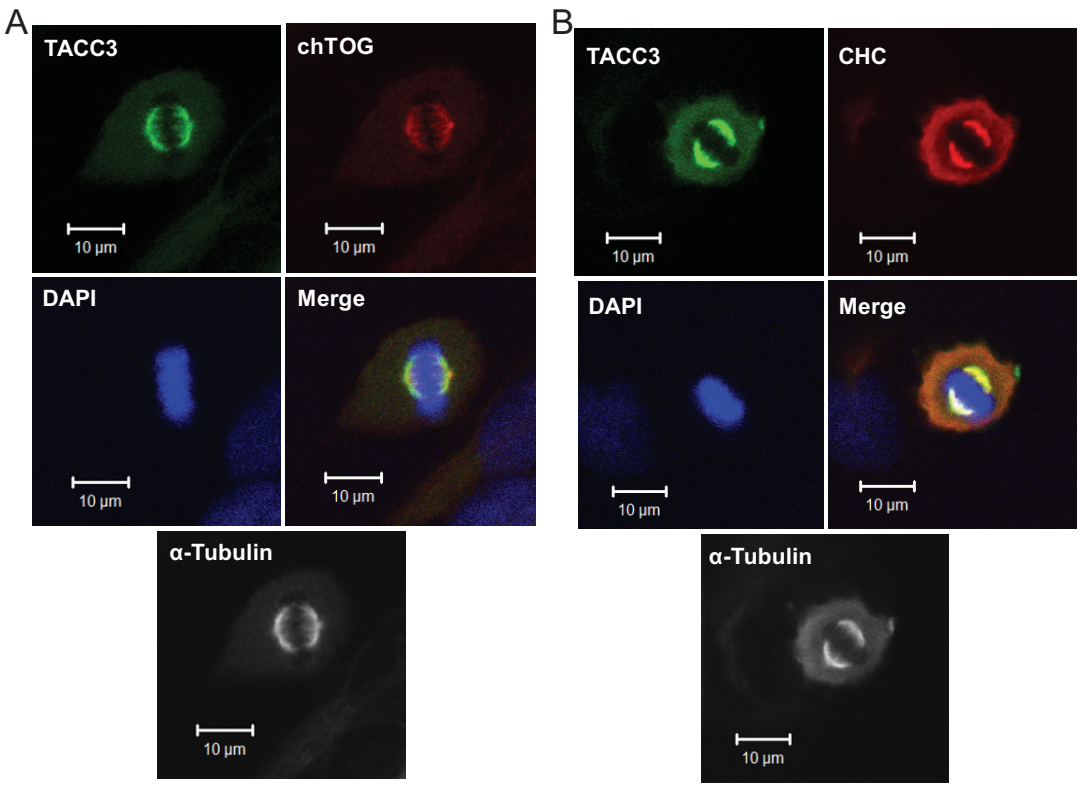

Fig. 8: Colocalization of TACC3 with chTOG and CHC in metaphase cells.
Images of metaphase cells were collected under a Zeiss cLSM 510 Meta microscope at a 63x magnification. A, at the spindle apparatus TACC3 colocalizes with chTOG and spindle microtubules (white). B, CHC co-localizes with TACC3 at centrosomes and a slightly diffused region around the centrosomes.

5.2 Sequence based *in silico* analysis of TACC protein family members

The TACC protein family evolved separately in the metazoan lineage, parallel to other protein families containing the coiled coil structure. All vertebrates express three TACC isoforms (TACC1, TACC2, and TACC3), while in other metazoans only one member is known (41). The phylogenetic distance tree of the TACC family members in higher eukaryotes was analyzed by multiple sequence alignment using the ClustalW program. The alignment data (newick file format) was used to make the final evolutionary tree by means of the iTOL (interactive tree of life) online program (Fig. 9).

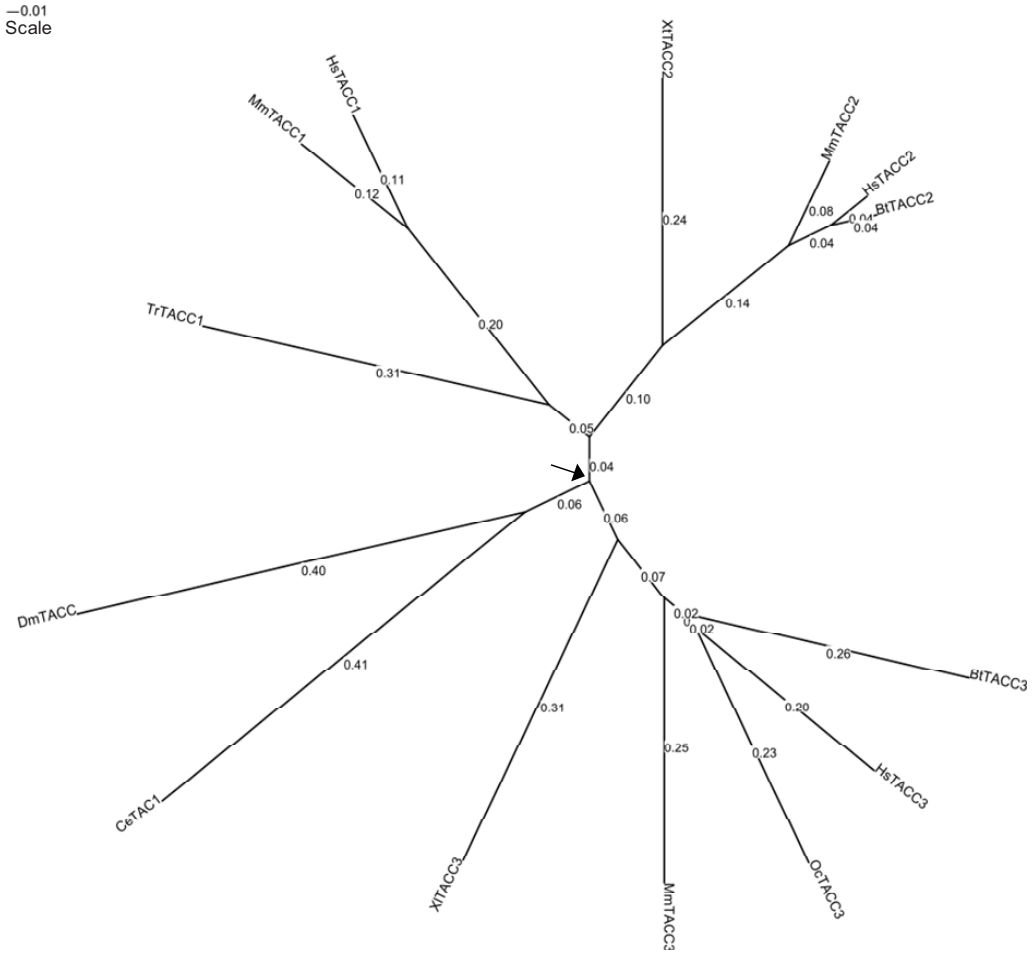

Fig. 9: Phylogenetic tree of TACC protein family members in higher eukaryotes.
The TACC3 evolutionary branch is separated from TACC1 and TACC2 earlier during evolution. The arrow in the center indicates the origin of the tree. The number indicates the branch length. On to left corner is a scale (0.1) for branch length. (Tr-*Takifugu rubripes*; Xl-*Xenopus laevis*; Bt-*Bos taurus*; Oc-*Oryctolagus cuniculus*; Hs-*Homo sapiens*; Ms-*Mus musculus*; Dm-*Drosophila melanogaster*; Ce-*Caenorhabditis elegans*).

Results

The evolutionary distance tree of TACC family members in higher eukaryotes reveals a separate branch for the evolution of TACC3. The TACC1 and TACC2 isoforms evolved together and they also got separated earlier during evolution. The tree further indicates that the TACC1 and TACC2 isoforms are relatively close to the D-TACC (*D. melanogaster*) and TAC1 (*C. elegans*) TACC family members in contrast to all TACC3 isoforms. The reason(s) behind the separate evolutionary branch for TACC3 isoforms are still unknown. Nevertheless, the separate evolutionary branch of vertebrate TACC isoforms indicates the adoption of some non-overlapping functions different from the conserved role in mitosis.

All TACC protein family members share the C-terminal conserved CC-domain consisting of about 200 amino acids residues, referred to as TACC domain (42). The COILS program based scanning (in a 14, 21 and 28 residues window scanning mode) of the C-terminal 250 residues displays a high score (COILS score=1) for CC-structure formation for all TACC family members (Fig. 10). This program is based on a mathematical algorithm and scans for heptad repeats (HXXHCXC; H-hydrophobic residues, X-any amino acid, and C-charged residues) in the backbone of the α-helix (99).

Surprisingly, a fall in the COILS score (in 28 residues window scan mode; Fig. 10, red arrows) was observed in the center of the CC-domain of the TACC3 isoforms from human, mouse, and other higher vertebrates. The residues with low COILS scores in the center of the CC-domain were identified as a CC-structure breaking peptide region. Interestingly, thus low COILS score region was absent in the CC-domains of TACC1, TACC2, and all lower vertebrates (*X. laevis* and *T. rubripes*) TACC3 isoforms. The central region with a low COILS score is indicated as the CC-structure breaking peptide region.

Sequence alignment of vertebrate TACC family members demonstrates a very high conservation of amino acid residues in their C-terminal region (Fig. 11) (41,42). In the TACC domain, residues in the left part of the C-terminus are comparatively less conserved than the residues towards the end of the C-terminus. The CC-structure breaking peptide region is present in the highly conserved region of the CC-domain. Only few residues in this region are different from TACC1, TACC2, and the lower vertebrate TACC3 sequences.

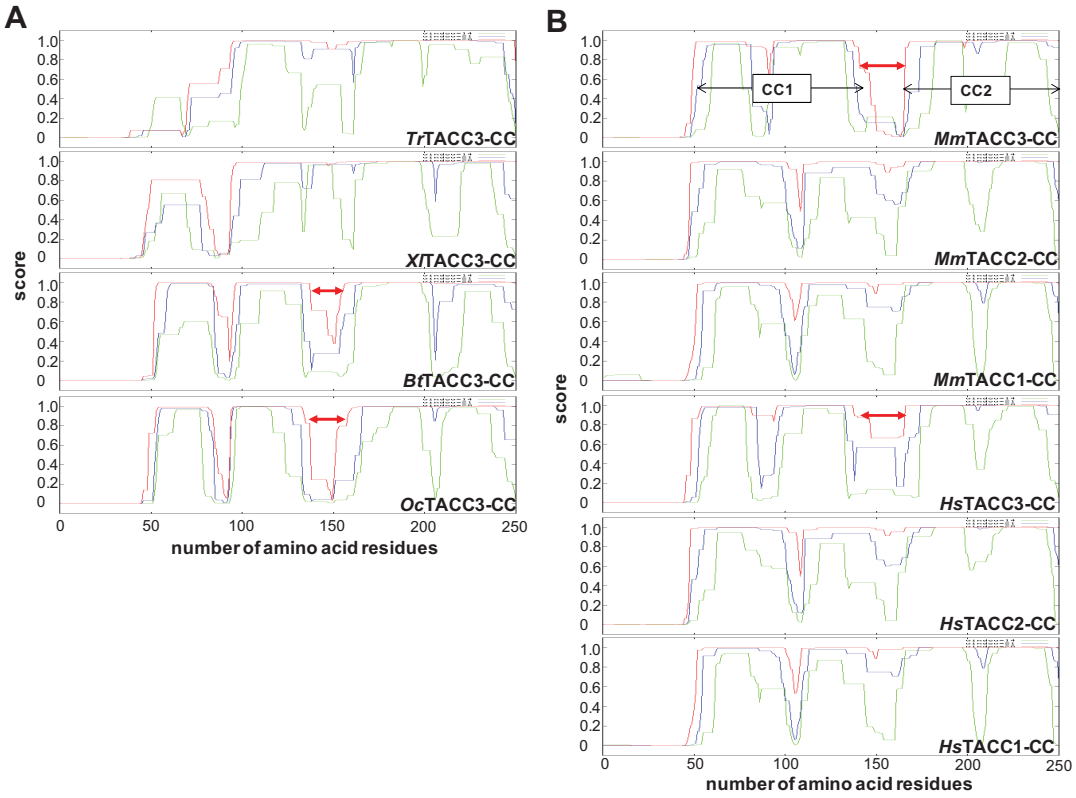

Fig. 10: *In silico* prediction of coiled coil structures in the C-terminus of the TACC protein family members using COILS program.
The C-terminal 250 amino acid residues were scanned in 14 (green line), 21 (blue line), and 28 (red line) residues window scanning modes. High scores for CC-structure formation were observed at the C-terminus of TACC protein family members. Double headed red arrows indicate the region with lowest probability for forming CC-structures in the center of the TACC domain of human, mouse and other higher vertebrate TACC3 isoforms. Fig. A, and B, displays the COILS scores for the TACC domain of vertebrate TACC family members. For murine TACC3, CC-structures before and after the low COILS score region are named the CC1 and CC2 modules respectively [Tr- *Takifugu rubripes*, Xl- *Xenopus laevis*, Bt- *Bos Taurus*, Oc- *Oryctolagus cuniculus,* Hs- *Homo sapiens* and Ms- *Mus musculus*].

The presence of the CC-structure breaking peptide in the highly conserved region of the CC-domain could be possibly explained as inability to meet up the regular heptad repeat pattern required to form a CC-structure in this region. The sequence alignment (Fig. 11) also reveals a difference in the pattern of sequence conservation before and after the CC-structure breaking peptide region. The residues before this region are less conserved than the residues following this region. In murine TACC3, the CC-modules before and after the breaking peptide were named as CC1 and CC2, respectively (Fig. 10B). Thus, the evolution of the CC-structure

breaking peptide region gives a clue at the structural level about the separate evolutionary branch of the TACC3 isoforms.

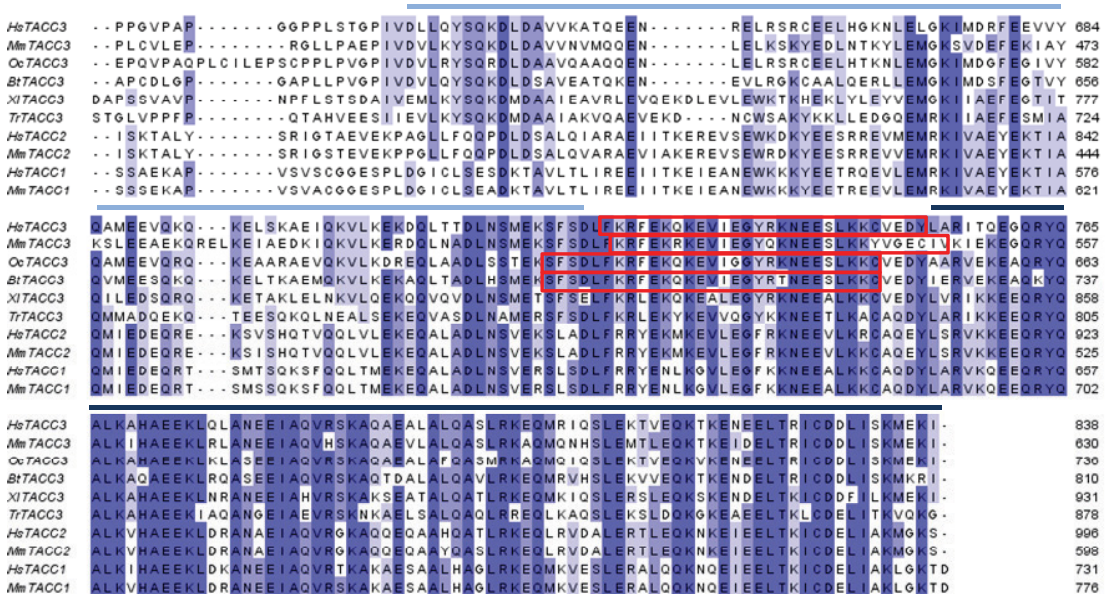

Fig. 11: Sequence alignment showing conservation of residues in the CC-domain of vertebrate TACC family members.
The red box indicates the CC-structure breaking peptide region. Light and dark blue color indicates less and highly conserved residues, respectively. Lines with a light and dark blue color correspond to the CC1 and CC2 regions of murine TACC3, respectively.

A sequence alignment for the variable N-terminal part of TACC family members was also performed. This analysis revealed a conservation of about hundred N-terminal residues only in the TACC3 isoforms (Fig. 12A). The sequence blast analysis, of the first 100 residues from the N-terminus of TACC3 isoforms shows sequence identities of up to 74% (Fig 12C). The high percentage of sequence identity in the N-terminal region of TACC3 isoforms indicates functional specificity compared to TACC1 and TACC2, and this could be the second possible explanation for the separate TACC3 evolutionary branch. Hitherto interacting partners for the conserved N-terminal region are unknown and its functional role is unclear. Some mutations in this region of TACC3 in human breast cancer samples have been reported, however, a putative role of these TACC3 variants in tumor growth are not known (71).

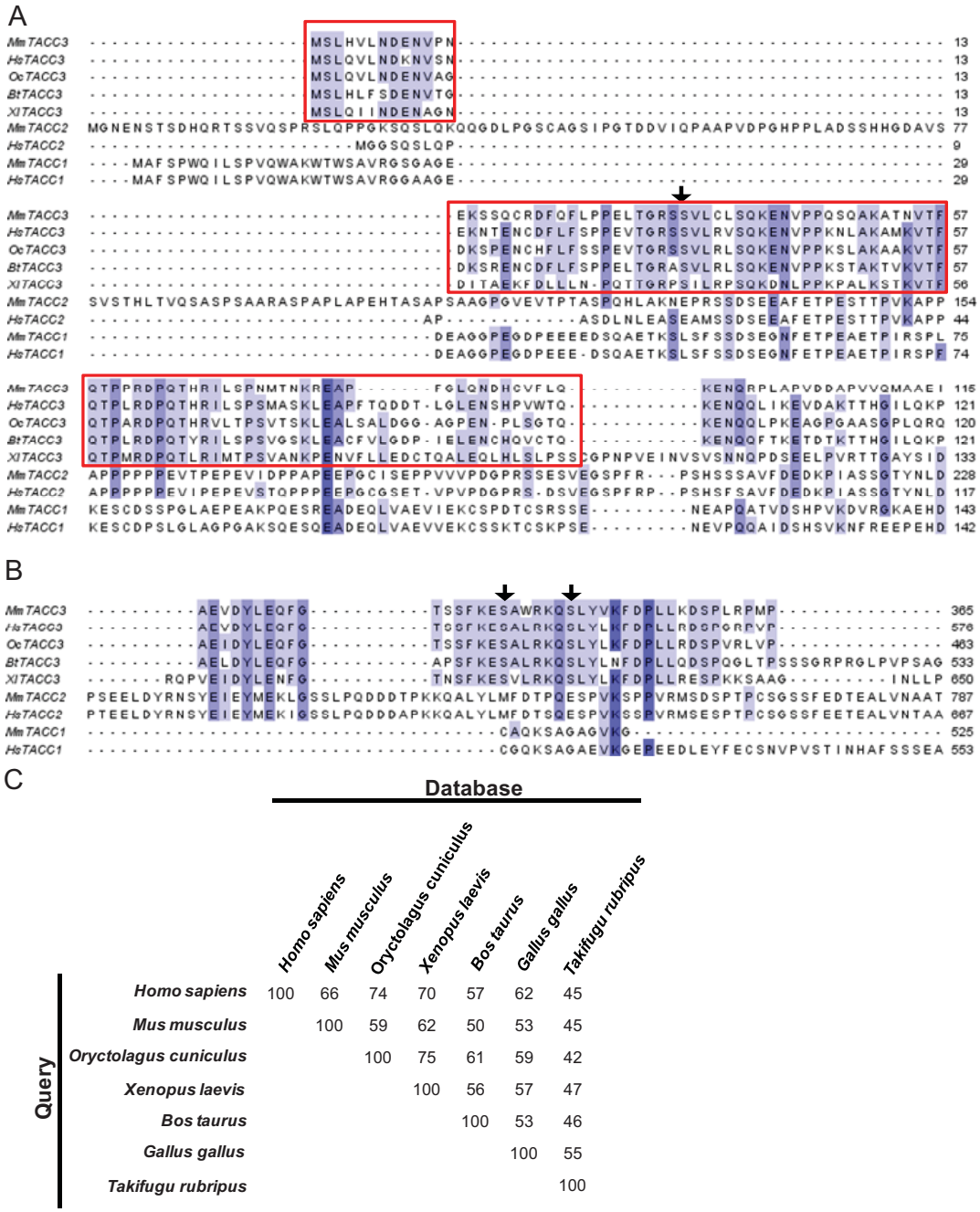

Fig. 12: Conservation of N-terminal residues and Aurora-A phosphorylation sites in TACC3 isoforms.

A, Sequence alignment demonstrates conservation of about hundred amino acid residues from the N-terminus and one Aurora-A phosphorylation site (indicated with the arrow) only in TACC3 isoforms (red box). B, Further, Aurora-A phosphorylation sites (indicated with arrows) are conserved only in TACC3 isoforms. C, Up to 74% identity was observed in the N-terminal region of TACC3. Query indicates the input sequence (100 residues from the TACC3 N-terminus) used for NCBI blast analysis. Database indicates the output aligned sequence. Numbers represent the percentage identity between two respective sequences.

TACC3 displays in total three known Aurora-A phosphorylation sites. One is present in the N-terminal region (S33 in *Xenopus* and S34 in human and mouse TACC3 isoforms; Fig. 12A, indicated with arrow) and another two phosphorylation sites are present close to the CC-domain (S620 & S626 in *X. laevis* and S552 & S558 in *H. sapiens*; Fig. 12B). Similar to Hs-TACC3 (*H. sapiens*-TACC3) and Xl-TACC3 (*X. laevis*-TACC3), sequence comparison also identified analogous Aurora-A phosphorylation sites (S34, S341, & S347) in murine TACC3. However, the role of the Aurora-A phosphorylation site (S33/S34) in the highly conserved N-terminal part is still unclear. The role of Aurora-A phosphorylation at S626 (Xl-TACC3) or S558 (Hs-TACC3) has been shown in the regulation of TACC3 recruitment to the centrosome during mitosis (27,33,66). The role of Aurora-A phosphorylation of Xl-TACC3 at S620 and S626 seems to be critical for CHC binding and RanGTP-dependent spindle assembly (27).

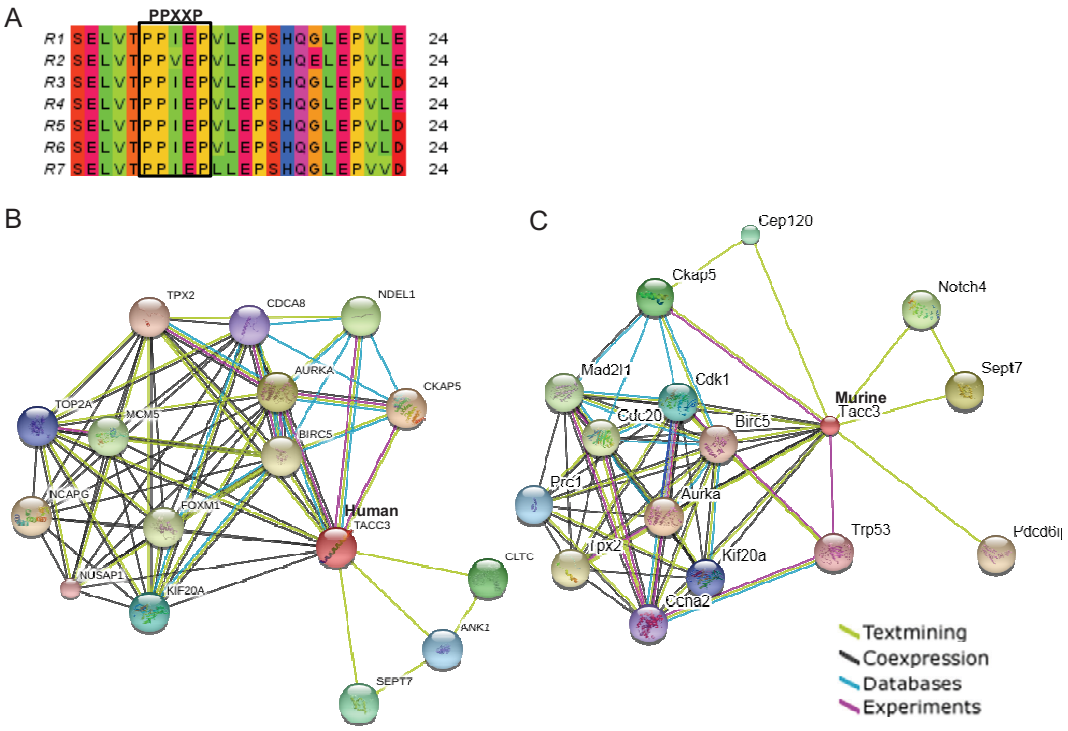

Fig. 13: The interaction network for human (A) and murine (B) TACC3.
A, Alignment of the seven repeats (R1-R7) of TACC3 each contains 24 amino acids. The box shows the PPXXP motif conserved in all seven repeats (P-prolin; X-any amino acid). B, and C, Web based interaction was analyzed on 31 August 2012 by the use of the String 9.0 program. The program combines various database and scientific literatures to find a connection between two proteins. The color of the line joining two proteins indicates the type of evidence or type of connection as indicated in index (lower right corner).

Murine TACC3 is distinct from the human and other vertebrate TACC3 isoforms by having seven perfect repeats, each comprising 24 amino acids (Fig. 13A). Interestingly, these repeats contain several serine (S), prolin (P) and glutamate (E) residues which are identical to the imperfect SPD repeats of Hs-TACC3 and Xl-TACC3 (34,60). One PPXXP motif was identified to be present in each repeats of murine TACC3 (Fig 13A, black box). Indeed, such motifs are known to interact with SH3 domains (119). However, interactome analysis using the String 9.0 program did not reveal any SH3 domain-containing protein(s) interacting with murine TACC3 (Fig. 13B & C).

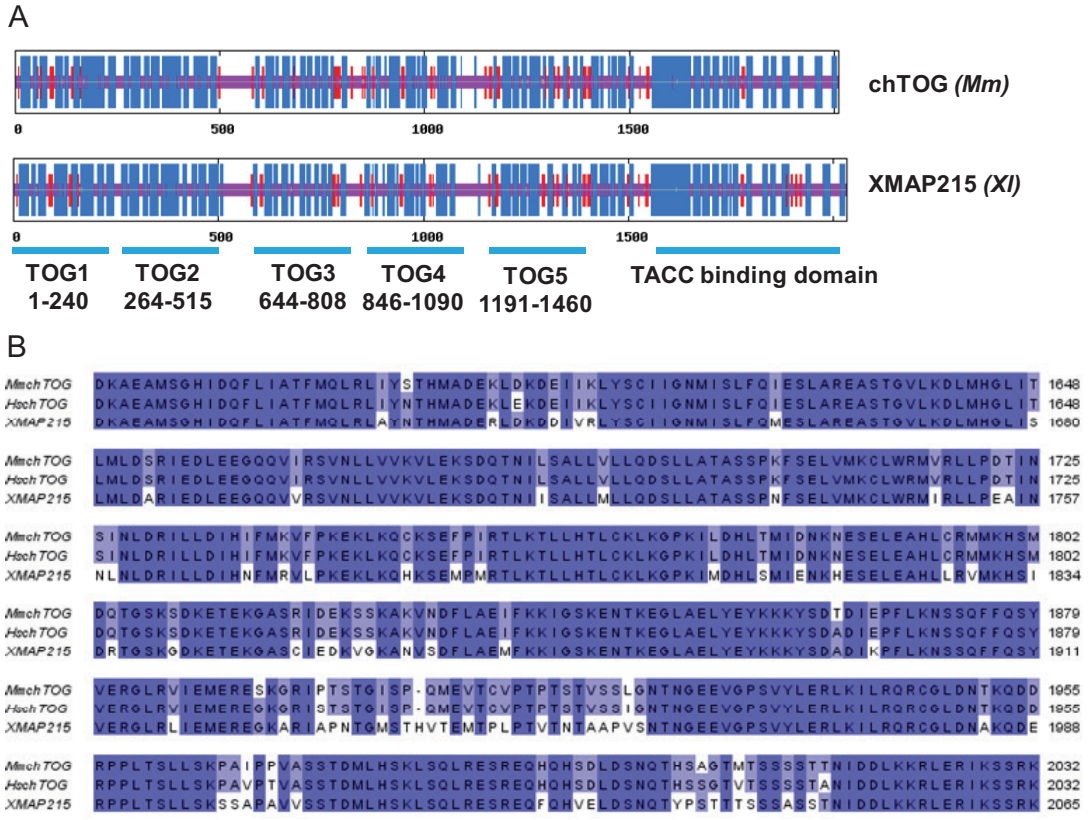

Fig. 14: The C-terminus of XMAP215/chTOG is highly identical in vertebrates and contains mainly α-helical secondary structures.
A, Secondary structure prediction (using NPS@ server at Lyon, France) results for murine chTOG and XMAP215 from *X. laevis* shows a high percentage of α-helical secondary structure (blue color). Red and purple colors represent extended and random coil regions, respectively. TOG1-5 indicates αβ-tubulin heterodimer binding domains and numbers below show their exact position in XMAP215. The TACC binding domain is present at the C-terminus of the protein and similar to the TOG domains it also contains α-helical repeats. B, Sequence alignment of C-terminal sequence from chTOG (*H. sapiens* and *M. musculus*) and XMAP215 reveals a very high conservation of residues.

The chTOG/XMAP215 family members are major interacting and effector proteins of TACCs. The CC-domain of TACC proteins is known to interact with the C-terminus of chTOG/XMAP215 proteins throughout metazoans (8,24,34,51,92). The N-termini of chTOG/XMAP215 proteins contain two to five highly conserved TOG domains (Fig. 14A) that are known to bind to tubulin heterodimers (20,73,75). Apart from its N-terminal conservation, the C-terminus of the chTOG/XMAP215 is also conserved. The sequence alignment of chTOG (*H. sapiens and M. musculus*) with XMAP215 (*X. laevis*) displays a very high amino acid conservation of the C-terminus (Fig. 14B). The chTOG sequences from *H. sapiens* and *M. musculus* are almost identical. Sequence based secondary structure prediction demonstrated the presence of α-helical multi-repeat arrays in both TOG domains and the C-terminal TACC binding domain of chTOG/XMAP215 (Fig. 14A). This pattern of secondary structure is typically present in the Ankyrin, tetratrico peptide, HEAT [**H**untingtin, elongation factor 3 (**E**F3), protein phosphatase 2A (PP2**A**), and the yeast kinase **T**OR1] and ARM (**Arm**adillo) (120-124) repeats. These repeats are characterized by an array of α-helices, packed against each other around a common axis to form a continuous superhelix or solenoid (125). The structure for the TOG2 domain from *C. elegans* has been solved and found to contain seven HEAT repeats (73). However, no evidence suggests the presence of such repeats in the C-terminus of chTOG.

5.3 Generation of recombinant plasmids for the expression of murine TACC3 and chTOG variants

Cell based studies showed that TACC interaction with chTOG plays an important role in spindle microtubule dynamics and stability during mitosis (8). By considering the importance of these molecules, this work aimed to investigate the biochemical, biophysical, and atomic details of the individual proteins and their complex formed upon interaction. After defining this objective, the foremost requirement was to design all recombinant expression plasmids based on previous and current information. Retroviral pMSCV-TACC3 and pMSCV-TACC3-ΔR expression vectors and pGEX-5x3-TACC3 bacterial expression plasmid were provided by Dr. Roland Piekorz. Those were used to further subclone TACC3 variants. The cDNA from mouse liver, brain, and heart were provided by Dr. Fabian Kuck from where the coding DNA sequence for the C-terminus of chTOG was amplified.

5.3.1 Cloning of TACC3 full length and TACC3 mutants

Coding DNA sequences for TACC3 variants in mammalian and bacterial expression vectors were sub-cloned into pGEX-4t1-NTEV (bacterial expression) and pcDNA3.1-EGFP (mammalian cell expression) vectors. Complete list of the recombinant constructs designed for this study is depicted in Tab. 24. Fig. 15 provides an overview of the domain organization of all TACC3 and chTOG variants over-expressed in bacteria and mammalian cell lines. The pGEX-4t1-NTEV plasmid based construct was designed to produce and isolate the N-terminal GST fused protein with an additional TEV protease site in addition to the thrombin site for cleaving the GST-tag. The pET series vector based construct was designed for His-tag fused protein production and its isolation by the IMAC technique. For cloning of GST-TACC3-N into the pET series vector (Tab. 24, No. 12), complete cassette (GST-TACC3-N) was amplified from the pGEX-4t1-NTEV-TACC3 construct and inserted into the target vector after restriction digestion. The murine TACC3 coding DNA was also inserted into a vector (pFastBack-htb) for protein expression in Sf9 insect cells. To analyze the S347 phosphorylation site, TACC3-S347E and TACC3-S347A mutants were obtained by site-directed mutagenesis (Tab. 24, No. 16-17) in the pGEX-4t1-NTEV-TACC3 construct. In order to analyze the subcellular localization of TACC3 variants, respective cDNAs were inserted into the mammalian cell expression vector pcDNA 3.1 EGFP (Fig. 15B). During the screening of the pGEX-4t1-NTEV-TACC3-7R clones, clones containing only two or three repeats were identified. The work also aimed to identify new interacting partners for TACC3, especially proteins binding to variable N-terminal region of TACC3. Thus the coding sequence for human TACC3 was cloned into the pcDNA4/TO-3xFLAG mammalian cell expression vector. The identity of all constructs was confirmed through DNA sequencing (GATC Biotech).

5.3.2 Cloning of the C-terminal domain of chTOG (chTOG-C) and the pTACC3 binding domain from Clathrin heavy chain (CHC)

The C-terminus of chTOG has been shown to mediate the interaction with the CC-domain of TACC3 (34,92). Therefore for an in depth *in vitro* TACC3-chTOG interaction analysis, the cDNA for the C-terminus of murine chTOG was cloned into the bacterial expression vector pGEX-4t1-NTEV (Tab. 24, No. 18). Fig. 15D displays domain arrangement of the full length chTOG (with the N-terminal five TOG domains and C-terminal TACC

binding domain) and GST-chTOG-C. Further to this, we also cloned the pTACC3 binding motif from CHC (Tab. 24, No. 19) in the pGEX-4t1-NTEV vector, with the intention to characterize the *in vitro* TACC3-CHC complex formation and interaction.

Tab. 24: List of constructs cloned for bacterial and mammalian expression of TACC3 and chTOG variants.

No.	Insert	Cloning region†	Vector	Cloning sites
Recombinant plasmid construct for bacterial expression of murine TACC3				
1	TACC3	1-630	pGEX-4t1-NTEV	EcoRI and NotI
2	TACC3-ΔR	Δ141-308	pGEX-4t1-NTEV	EcoRI and NotI
3	TACC3-ΔN	119-630 (Δ1-118)	pGEX-4t1-NTEV	EcoRI and NotI
4	TACC3-ΔNΔR	Δ1-118 & Δ141-308	pGEX-4t1-NTEV	EcoRI and NotI
5	TACC3-NR	1-322	pGEX-4t1-NTEV	EcoRI and XhoI
6	TACC3-7R	119-324	pGEX-4t1-NTEV	BamHI and XhoI
7	TACC3-3R	119-212	pGEX-4t1-NTEV	BamHI and XhoI
8	TACC3-2R	119-288	pGEX-4t1-NTEV	BamHI and XhoI
9	TACC3-CC	414-630	pGEX-4t1-NTEV	BamHI and NotI
10	TACC3-CC1	414-530	pGEX-4t1-NTEV	BamHI and XhoI
11	TACC3-CC2	530-630	pGEX-4t1-NTEV	BamHI and NotI
12	GST-TACC3-N	1-124	pET23b	NdeI and XhoI
13	TACC3-7R	119-322	pET23b	NdeI and BamHI
14	GST-TACC3-N	1-124	pET Duet	NdeI and XhoI
15	TACC3	1-630	pFastBack-htb	EcoRI and NotI
Site directed mutagenesis of murine TACC3				
16	TACC3 S347A	1-630	pGEX-4t1-NTEV	EcoRI and NotI
17	TACC3 S347E	1-630	pGEX-4t1-NTEV	EcoRI and NotI
18	TACC3-ΔCC2	Δ413-529	pcDNA3.1-EGFP	HindIII and NotI
Murine chTOG variant				
19	chTOG-C	1574-2032	pGEX-4t1-NTEV	BamHI and XhoI
Murine Clathrin Heavy Chain Variants (pTACC3 binding motif)				
20	CHC(317-549)	317-549	pGEX-4t1-NTEV	BamHI and NotI
Recombinant plasmid construct for mammalian cell expression of murine TACC3				
21	TACC3	1-630	pcDNA3.1-EGFP	HindIII and NotI
22	TACC3-ΔR	Δ141-308	pcDNA3.1-EGFP	HindIII and NotI
23	TACC3-ΔN	119-630	pcDNA3.1-EGFP	HindIII and NotI
24	TACC3-ΔCC	1-413	pcDNA3.1-EGFP	HindIII and NotI
25	TACC3-ΔCC2	1-530	pcDNA3.1-EGFP	HindIII and NotI
Recombinant plasmid construct for mammalian cell expression of human TACC3				
26	TACC3	1-838	pcDNA4/TO-3xFlag	AflII and NotI

'Δ' indicates deletion mutants; '†' indicates the position of amino acid residues cloned

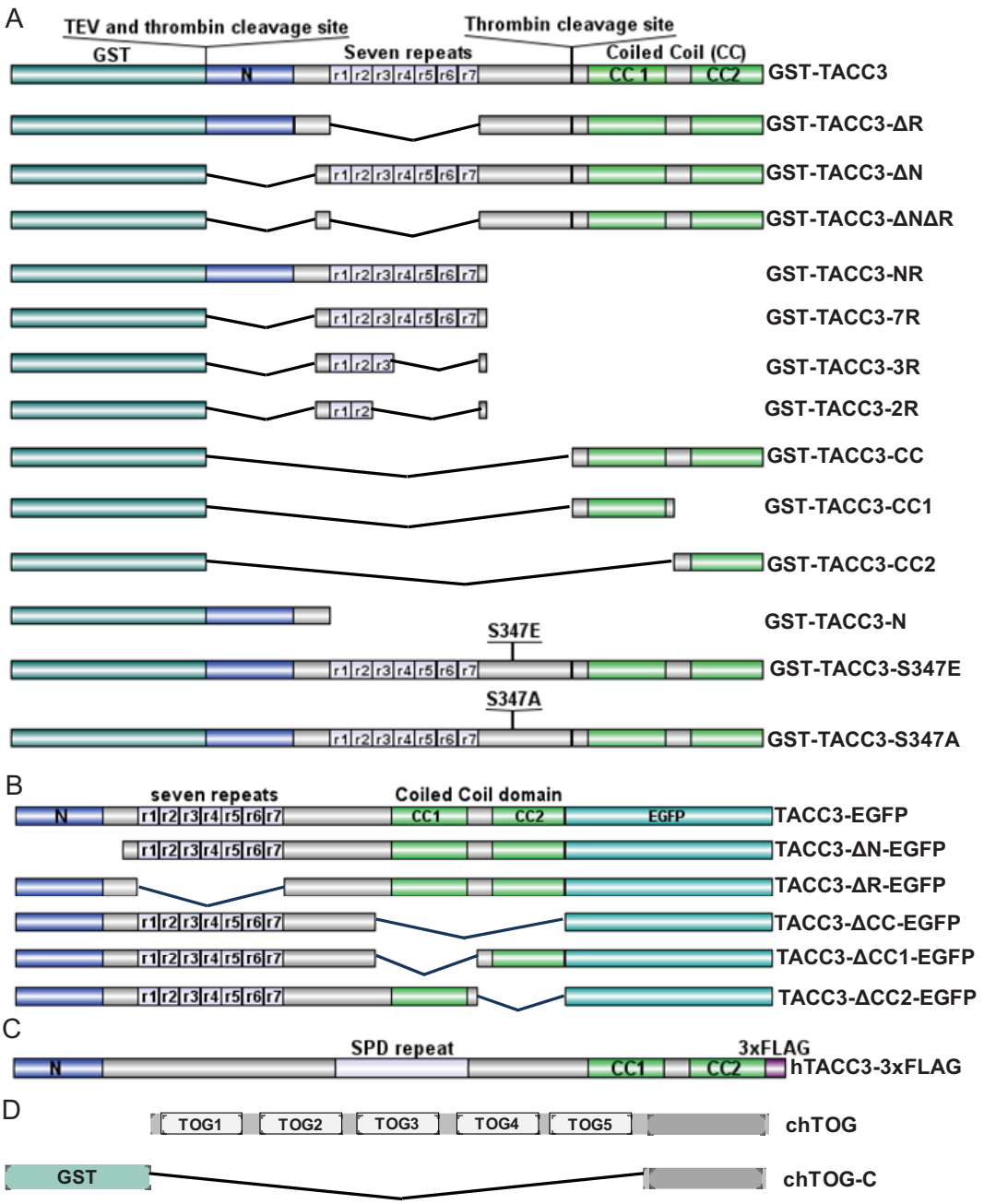

Fig. 15: Domain organization of expressed fusion protein variants.
A, N-terminal GST fused murine TACC3 variants. B, C-terminal EGFP fused murine TACC3 variants. In A and B, repeats are represented with a small 'r' followed by their number beginning from the N-terminus. C, C-terminal 3xFLAG tag fused human TACC3 construct. Light grey color in center denotes the SPD repeat region. Blue color indicates the N-terminal conserved region and the green color marks the highly conserved coiled coil domain. CC1 and CC2 indicate two separate coiled coil modules in the CC-domain of murine and human TACC3. D, the primary structure of murine chTOG (upper) and GST-fused chTOG-C protein (lower).

Tab. 25: Expression and purification status of cloned constructs

No.	Fusion protein	Expression status	Purification status
1	pGEX-4t1-NTEV-TACC3	Expressed in *E. coli* rosetta	purified
2	pGEX-4t1-NTEV-TACC3-ΔR	Expressed in *E. coli* rosetta	purified
3	pGEX-4t1-NTEV-TACC3-ΔN	Expressed in *E. coli* rosetta	purified
4	pGEX-4t1-NTEV-TACC3-ΔNΔR	Expressed in *E. coli* rosetta	purified
5	pGEX-4t1-NTEV-TACC3-NR	Expressed in *E. coli* rosetta	purified
6	pGEX-4t1-NTEV-TACC3-7R	Expressed in *E. coli* rosetta	purified
7	pGEX-4t1-NTEV-TACC3-3R	Expressed in *E. coli* rosetta	n.d.
8	pGEX-4t1-NTEV-TACC3-2R	Expressed in *E. coli* rosetta	n.d.
9	pGEX-4t1-NTEV-TACC3-CC	Expressed in *E. coli* rosetta	purified
10	pGEX-4t1-NTEV-TACC3-CC1	Expressed in *E. coli* rosetta	purified
11	pGEX-4t1-NTEV-TACC3-CC2	Expressed in *E. coli* rosetta	purified
12	pET23b-GST-TACC3-N	Expressed in *E. coli* rosetta	purified
13	pET23b-TACC3-7R	Expressed in *E. coli* rosetta	n.d
14	pET Duet-GST-TACC3-N	Expressed in *E. coli* rosetta	n.d.
15	pFastBack-htb-TACC3	n.d.	n.d.
16	pGEX-4t1-NTEV-TACC3 S347A	Expressed in *E. coli* rosetta	purified
17	pGEX-4t1-NTEV-TACC3 S347E	Expressed in *E. coli* rosetta	purified
18	pGEX-4t1-NTEV-chTOG-C	Expressed in *E. coli* rosetta	purified
19	pGEX-4t1-NTEV-CHC(317-549)	n.d.	n.d.
20	pcDNA3.1-EGFP-TACC3	Expressed in COS7 cells	n.a
21	pcDNA3.1-EGFP-TACC3-ΔR	Expressed in COS7 cells	n.a.
22	pcDNA3.1-EGFP-TACC3-ΔN	Expressed in COS7 cells	n.a
23	pcDNA3.1-EGFP-TACC3-ΔCC	Expressed in COS7 cells	n.a.
24	pcDNA3.1-EGFP-TACC3-ΔCC1	Expressed in COS7 cells	n.a
25	pcDNA3.1-EGFP-TACC3-ΔCC2	Expressed in COS7 cells	n.a.
26	pcDNA4/TO-hTACC3wt-3xFLAG	Expressed in HeLa Cells	n.d.

n.d. not done; n.a., not applicable

5.4 Overexpression and purification of recombinant TACC3 and chTOG-C variants

To check the functionality of pGEX and pET backbone-based expression recombinant plasmid, they were transformed into the competent *E.coli* rosetta expression host. The expression and purification status for all recombinant plasmids is summarized in Tab. 25. Most of the GST-fused proteins were purified on a large scale using a combination of approaches mentioned in the method section. Thereafter, proteins were subjected for tag

cleavage using thrombin and TEV protease (Tab. 26). A temperature around 0 ˚C (on ice) was found to be most suitable for cleaving GST from all fusion proteins except for GST-chTOG-C. The GST tag from GST-chTOG-C fusion protein could be rather removed completely by elevating the reaction temperature to +4-8 ˚C. Subsequent to GST tag separation, the proteins were subjected to further characterization by different biochemical and biophysical techniques. The GST-tag from GST-TACC3-ΔN and GST-TACC3-ΔNΔR protein could be only cleaved by thrombin, but not by TEV protease. It seems that the binding site is masked by other secondary structures in the protein which makes it inaccessible for TEV protease.

Tab. 26: Thrombin and TEV digestion to remove the GST-tag from fusion proteins

No.	GST fusion protein	Reaction temperature (overnight)					
		Ice temperature		+4-8 ˚C		Room temperature	
		Thr.	TEV	Thr.	TEV	Thr.	TEV
1	GST-TACC3	+	+	+	+	n.d.	n.d.
2	GST-TACC3-ΔR	+	+	+	+	n.d.	n.d.
3	GST-TACC3-ΔN	+	-	+	-	n.d.	n.d.
4	GST-TACC3-ΔNΔR	+	-	+	-	n.d.	n.d.
5	GST-TACC3-NR	+	+	+	+	n.d.	n.d.
6	GST-TACC3-7R	+	+	+	+	n.d.	n.d.
7	GST-TACC3-CC	+	+	+	+	n.d.	n.d.
8	GST-TACC3-CC1	+	+	+	+	n.d.	n.d.
9	GST-TACC3-CC2	+	+	+	+	n.d.	n.d.
10	GST-TACC3-N	+	+	+	+	n.d.	n.d.
11	GST-chTOG-C	partial	partial	+	+	+	+

Thr.-Thrombin; '+' means cleaved the GST tag; '-' means GST tag could not be cleaved; n.d. not done

5.5 TACC3 displays an unique interdomain/intramolecular interaction

5.5.1 Identification of a novel and unique thrombin site in TACC3

To enable the characterization of the TACC3 full-length protein, purified GST-TACC3 protein was digested with thrombin protease. Very surprisingly, even after the complete removal of the cleaved GST-tag (by reverse GSH-affinity purification), still two fragments were observed on SDS-PAGE followed by CBB staining (Fig. 16A, inset). This finding could be only explained by the presence of an internal thrombin site in the murine TACC3 protein. In order to identify a putative thrombin cleavage site, MALDI-TOF mass

spectrometry after desalting the sample was performed (Dr. Sabine Metzger, BMFZ, central mass spectrometry facility, Heinrich-Heine-Universität).

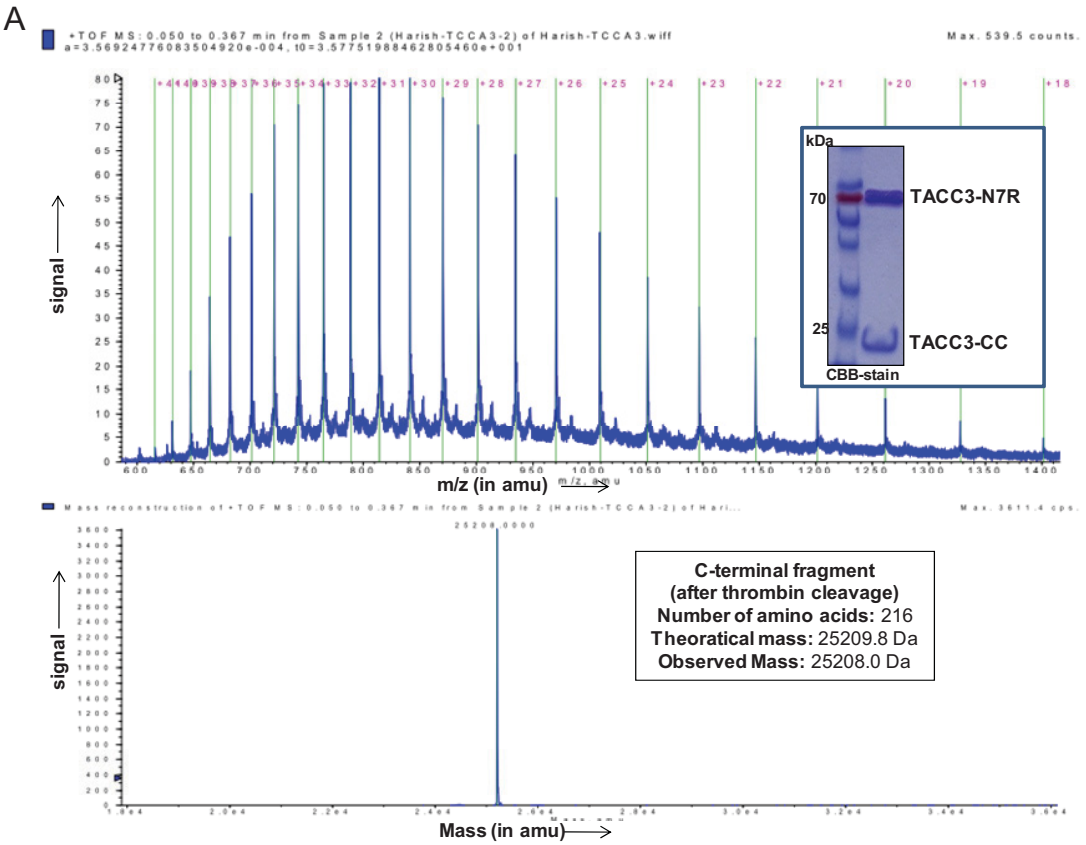

Fig. 16: MALDI-TOF mass spectrometry based determination of molecular sizes confirms the presence of a novel thrombin site in murine TACC3.
A, Upper panel shows plot of signals obtained against mass/charge (m/z) ratio. The lower panel indicates the measured mass for the smaller fragment after thrombin digestion. Inset (upper panel) displays the two protein fragments obtained after thrombin digestion followed by reverse GSH-chromatography. B, Sequence alignments showing conservation of the PR/G (thrombin cleavage site) in the TACC3 protein sequence from *M. musculus* (amu–atomic mass unit).

The measured mass for the smaller fragment was found to be 25208.0 Da (Fig. 16A, lower panel). In parallel the protein sequence of the murine TACC3 was also scanned manually for the presence of a thrombin site. An unique PR/G sequence adjacent to the CC-domain was identified which is similar to a typical thrombin cleavage site (Fig. 16B) (126). To verify this further the theoretical mass of the protein fragment following this thrombin site

(216 amino acid residues) was calculated and found to be 25209.8 Da (Fig. 16A, lower panel, inset). This result was comparable to the mass of smaller fragment obtained by mass spectrometry. Further to this, the smaller fragment was identified as the C-terminal part and larger fragment as the N-terminal part of the TACC3, by uses of N- and C-terminal specific antibodies (Fig. 18C). Combining all together, the data confirm the presence of a putative thrombin site in vicinity of the CC-domain of murine TACC3. Based on this finding, the TEV protease was used to cleave the GST tag (Fig. 17). The purified proteins were subjected to thrombin digestion to reconfirm its action on murine TACC3 (Fig. 17A-D). Although this thrombin site might not have any functional relevance, it was used as an unique and important tool for the *in vitro* characterization of TACC3 as described below.

Tab. 27: Sequence based properties of TACC3 and chTOG variants.

No.	Protein	Polypeptide chain length (aa)	Molecular size (kDa)	Isoelectric point (pI)
1	TACC3	630	70.468	4.56
2	TACC3-ΔR	462	52.323	4.94
3	TACC3-ΔN	512	57.241	4.45
4	TACC3-ΔNΔR	344	39.096	4.80
5	TACC3-NR	322	35.197	4.23
6	TACC3-7R	204	21.970	3.81
7	TACC3-CC	216	25.209	5.32
8	TACC3-CC1	122	14.448	5.01
9	TACC3-CC2	101	11.683	6.36
10	TACC3-N	124	13.930	5.31
11	chTOG-C	459	51.889	8.08

aa, amino acid

To next perform an *in vitro* biophysical and biochemical characterization of TACC3 and chTOG, the required wild type proteins and deletion mutants were purified after bacterial overexpression (Fig. 17). The sequence based theoretical properties (molecular size and pI; Tab. 27) of all the variants were determined by using the ProtParam tool from the ExPASy (http://expasy.org/proteomics) bioinformatics resource portal (127). The theoretical molecular weight of the wild type murine TACC3 protein is 70.4 kDa. However, on SDS-PAGE this protein migrates like ~120 kDa molecular size (Fig. 17A, lane 2). A similar abnormal migration behavior has been also reported for TACC3 from other species (71). After thrombin digestion of murine TACC3, the C-terminal (smaller) fragment migrates on SDS-PAGE gel according to its size while the N-terminal fragment (~45 kDa) migrates like a ~90 kDa

molecular size (Fig. 17A, lane 3). The GST-TACC3-ΔN deletion mutant shows the same migration pattern on SDS-PAGE (Fig. 18C). Interestingly, when the central seven repeat region was deleted (TACC3-ΔR), the protein migrated normally on SDS-PAGE, according to its molecular size (Fig. 17B lane 2). In contrast and very remarkably the repeat region (TACC3-7R) migrates like a 60 kDa molecular size (Fig. 17E, lane 5) although its real size is ~22 kDa. Even the acidic nature of proteins (pI values shown in Tab. 27) was considered for this abnormal migration on SDS-PAGE gels, however, the actual cause for this migration behavior are still missing. The conformational rigidity of polyproline regions (PP or PPP) in the polypeptide backbone could be a possibility for this abnormal migration behavior.

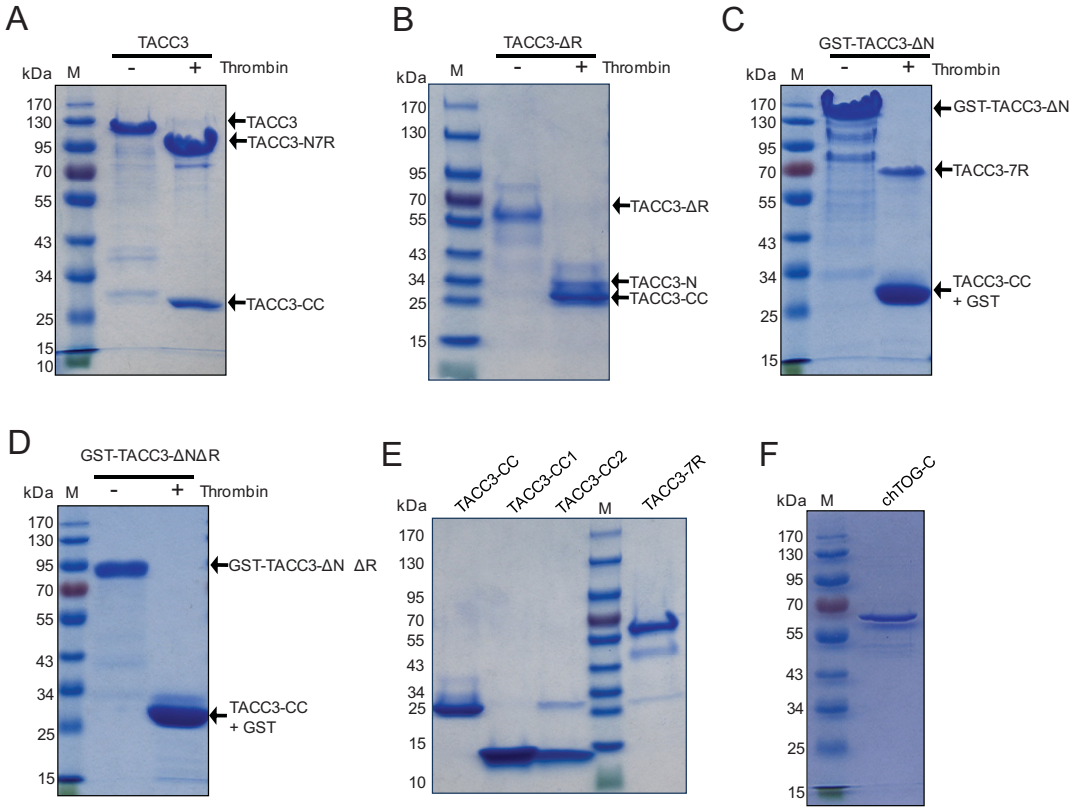

Fig. 17: Purity of murine TACC3 and chTOG variants as analyzed by SDS-PAGE and CBB staining.
Thrombin cleaves the purified murine TACC3 protein at an unique internal site. A to D, purified proteins before and after thrombin cleavage are shown. E, Purified fragments of the murine TACC3 is indicated. F, Purified C-terminal of the murine chTOG, which interacts with TACC proteins (M, Marker or protein ladder; Δ, deletion).

5.5.2 The N- and C-terminal fragments of TACC3 form an intramolecular complex

Thrombin cleaves the murine TACC3 at the internal site localized near to the CC domain and divides the protein into two fragments, TACC3-N7R and TACC3-CC (Fig. 18A). To facilitate the separation of both the fragments and to determine the native approximate molecular mass, TACC3 protein before and after thrombin digestions was injected to a pre-equilibrated Superose 6 10/300 column. The column was calibrated with standard molecular weight proteins (LMW and HMW calibration kit; GE Healthcare) and a linear equation (from lnMr. *vs* K_{av} plot) was derived for calculation of the molecular mass (Fig. 18B, inset).

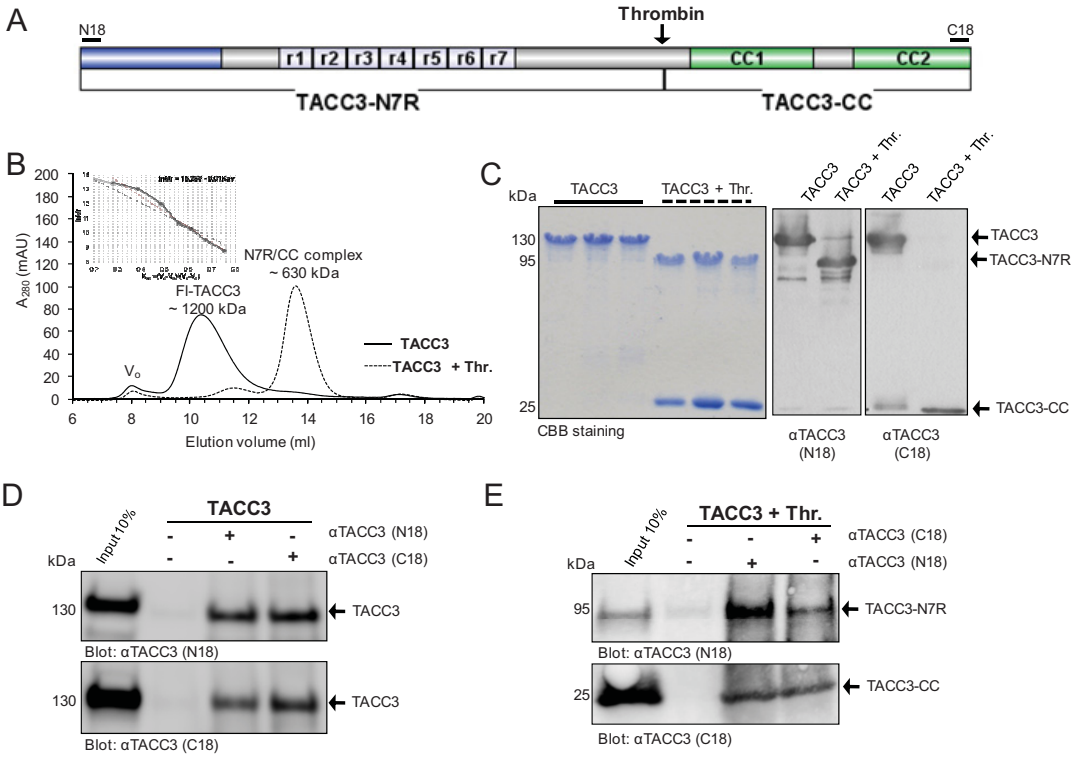

Fig. 18: TACC3-N7R and TACC3-CC form an intramolecular complex.
A, The primary structure of murine TACC3 shows the thrombin site (Thr.) in the vicinity of the CC-domain. N18 and C18 depict the epitopes for antibodies specifically recognizing the N- or C-terminal of murine TACC3. B, Analytical gel filtration (Superose 6 10/300 column) elution profiles for TACC3 before (solid line) and after the thrombin digestion (dotted line). 'V_o' denotes the void volume of the column. Inset shows the plot of lnMr *vs*. elution volume for standard molecular weight proteins. C, SDS-PAGE analysis shows the protein in peak elution fractions followed by CBB staining and immunoblotting by the use of TACC3 specific antibodies (αTACC3-N18 and αTACC3-C18). Immunoprecipitation of TACC3 before and after thrombin cleavage by use of αTACC3-N18 and αTACC3-C18 antibodies (D and E).

Before and after thrombin cleavage murine TACC3 eluted in rather earlier peak fraction of ~1200 kDa and ~630 kDa respectively (Fig. 18B). This indicated a higher oligomeric mass of the protein or an elongated rod like structure, or both. Interestingly, only one peak appeared for the thrombin cleaved TACC3 and the peak profile shifted to the right as compared to uncutted protein. The elution peak fractions were analyzed on SDS-PAGE followed by CBB staining and immunoblotting using TACC3 specific antibodies (αTACC3-C18 and αTACC3-N18). In case of thrombin digestion, two fragments were observed to co-elute on gel filtration (Fig. 18C). Coelution of two fragments on a gel filtration column indicates an intramolecular interaction and the formation of one protein complex.

Thereafter immunoprecipitation, using N- and C-terminal specific antibodies (αTACC3 N18 and αTACC3 C18, respectively), was performed (Fig. 18D & E). In the case of thrombin cleavage, TACC3-CC could be immunoprecipitated with αTACC3 N18 and TACC3-N7R could be immunoprecipitated with αTACC3 C18 antibodies, respectively. Thus these results confirm the interaction and co-elution of both thrombin cleaved TACC3 fragments as observed by analytical gel filtration.

5.5.3 The central repeat region of TACC3 is required for its intramolecular interaction

To identify the domain(s) involved in the intramolecular interaction of TACC3, the N-terminal conserved region (Fig. 19A) and the central seven repeat regions (Fig. 20A) were deleted one by one. Analogous to the wild-type TACC3 protein, elution profiles for these mutants before and after thrombin digestion were analyzed using Superose 6 10/300 based analytical gel filtration columns. Since the GST-tag could not be cleaved from the GST-TACC3-ΔN mutant using the TEV protease (Tab 26), thus GST-fusion protein was directly subjected to thrombin digestion and further analysis.

Deletion of the conserved N-terminal region did not show any effect on the elution pattern of the GST-TACC3-ΔN mutant. The ΔN mutant elutes earlier in the peak fraction of ~1200 kDa protein similar to wild-type TACC3 (Fig. 19B, solid line). Following thrombin digestion, the protein fragments eluted into two separate peak fractions. Similar to the thrombin cleaved wild type protein, the earlier eluting peak has an approximate size of 630 kDa, and the calculated mass for the late eluting peak was ~50 kDa. Employing SDS-PAGE

followed by CBB staining and immunoblotting, the first peak from left was identified as an intramolecular complex of two fragments (TACC3-7R/TACC3-CC) and second peak as GST protein (Fig. 19C). Thus, these results suggested that the deletion of the N-terminal conserved region does not impair the intramolecular interaction of TACC3.

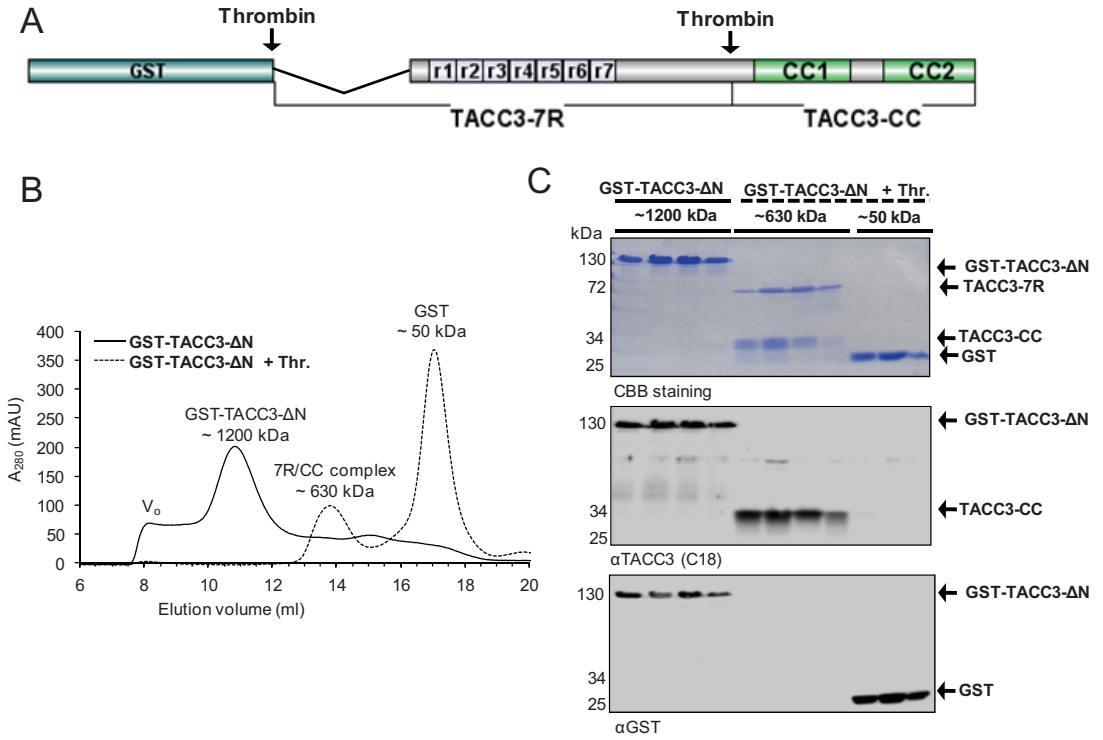

Fig. 19: Deletion of the first 118 amino acid residues from the N-terminus of TACC3 does not impair the intramolecular complex formation of TACC3 after thrombin digestion.
A, Primary structure of GST-TACC3-ΔN, two thrombin sites are indicated with arrow. B, Analytical gel filtration (Superose 6 10/300 column) elution profiles of GST-TACC3-ΔN before (solid line) and after (dashed line) thrombin cleavage. 'V_o' denotes the void volume of the column. C, SDS-PAGE based analysis of peak elution fractions followed by CBB staining and immunoblotting. In the lower panel a GST specific antibody was used.

Next, the role of the central repeat region in intramolecular complex formation was addressed. Interestingly, thrombin digestion of TACC3-ΔR resulted in the separation of two fragments as two separate peaks on gel filtration (Fig. 20B). SDS-PAGE followed by immunoblotting analysis identified an earlier eluting peak as the C-terminal fragment and a late eluting peak as the N-terminal fragment of TACC3 (Fig. 20C). The TACC3-CC protein was still eluting in the same peak fraction like the intramolecular complex (Fig. 18B), but the peak for TACC3-N now shifted right to a peak fraction of 160 kDa. Thus, these results

suggested an important role of the seven repeat regions in the intramolecular complex formation of TACC3.

Moreover, deletion of the seven repeat region not only affected the migration behavior on SDS-PAGE (shown earlier; Fig. 17), but also had an impact on the elution pattern on the gel filtration column. In comparison to the wild-type protein (~1200 kDa; Fig. 18B solid line), the peak for the TACC3-ΔR deletion mutant shifted slightly right and appeared in a peak fraction of ~1100 kDa of molecular size (Fig. 20B, solid line). Thus, in contrast to the role in intramolecular interaction, the seven repeat region contributes also to the overall native structure (shape, size, and stock radii) of the TACC3 protein.

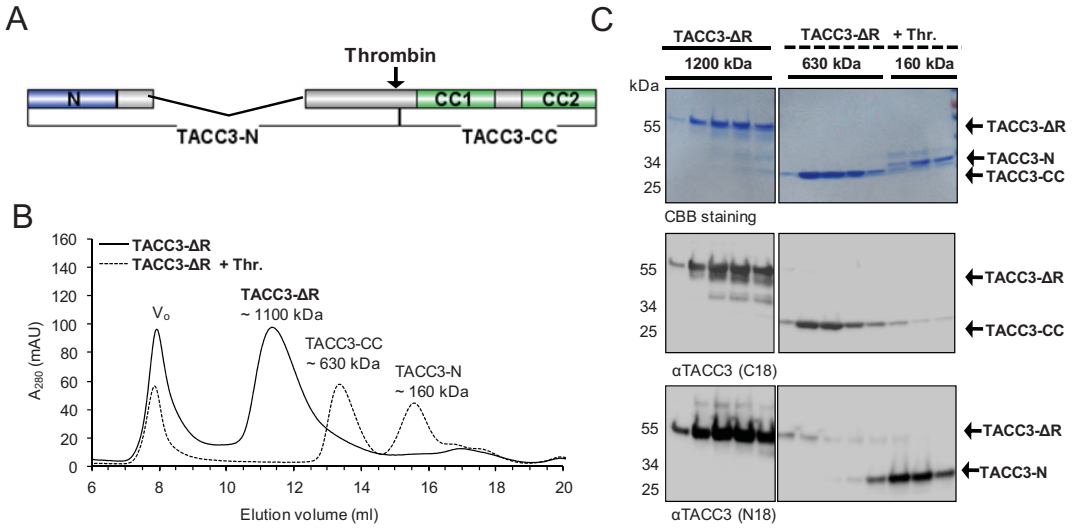

Fig. 20: Deletion of the serine prolin-rich seven repeat region precludes the intramolecular complex formation of TACC3.
A, Primary structure of TACC3-ΔR with one internal thrombin site that divides this mutant into two parts: TACC3-N and TACC3-CC. B, Analytical gel filtration (Superose 6 10/300 column) elution profile of TACC3-ΔR before (solid line) and after (dashed line) thrombin cleavage. 'V_o' denotes the void volume of the column. C, Peak elution fractions were analyzed on SDS PAGE (4-15% gradient gels) followed by CBB staining (upper panel) and immunoblotting (middle panel, blot with αTACC3 C18 antibody; lower panel blot with αTACC3 N18 antibody).

5.5.4 The central repeat region interacts with the CC2 region of TACC domain

In order to prove a direct interaction between the seven repeat region (TACC3-7R) and TACC3-CC, pull down assays were performed together with all required controls. GST-TACC3-7R was employed as bait and purified TACC3-CC was used as prey. The results were

analyzed on SDS-PAGE gradient gel (4-15 %) followed by immunoblotting. As indicated in Fig. 21 (lane 9), when mixing GST-TACC3-7R with TACC3-CC, TACC3-CC could be efficiently precipitated using GSH-sepharose beads. This indicates that TACC3-7R can directly interact with TACC3-CC. The weaker signal for TACC3-CC in lanes 7 and 8 indicates unspecific binding of the protein with the beads (as compared to the clearly higher level of TACC3-CC in lane 9 that is visualized by the C18 antibody, but not by the αGST antibody).

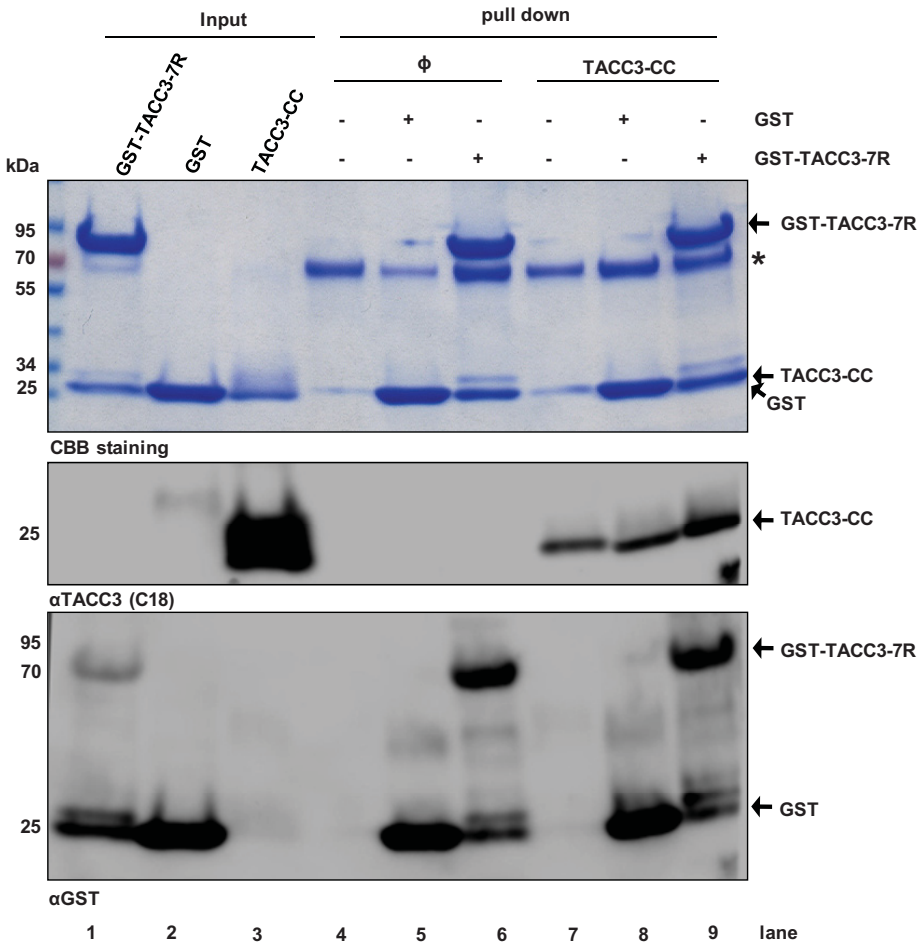

Fig. 21: Pulldown assay-based interaction analysis between TACC3-7R and TACC3-CC.
Purified GST-TACC3-7R was used as bait to pull down TACC3-CC (prey). The probes from the pull down experiment were analyzed on SDS-PAGE (4-15% gradient gel) followed by CBB staining and immunoblotting (αTACC3 C18 and αGST antibodies). First three lanes from left (lane 1, 2, & 3) are the input (10%), followed by the central three lanes (lane 4, 5, & 6) of buffer control (indicated with ϕ). The last three lanes (lane 7, 8, & 9) show the pull down of TACC3-CC. Lane 9 depicts the pull down of TACC3-CC by GST-TACC3-7R. * indicates BSA.

Next to this, the interaction of TACC3-7R with the TACC3-CC domain was further characterized using an alternative experimental approach, i.e. ITC measurements. In ITC, when two protein interacts with each other heat of the system changes (increase for exothermic reaction and decrease for endothermic reaction) in comparison to reference samples. In order to identify the region of the CC domain interacting with the seven repeat region, shorter mutants (Fig. 17E; CC1 and CC2) were purified and heat changes after association between two molecules (CC1 *vs*. seven repeat region and CC2 *vs*. seven repeat region) were determined in ITC experiment (Fig. 22A to D). The results were compared to control experiments (Fig. 23E to G) in which either of the purified proteins was titrated to buffer or the buffer was titrated to the proteins.

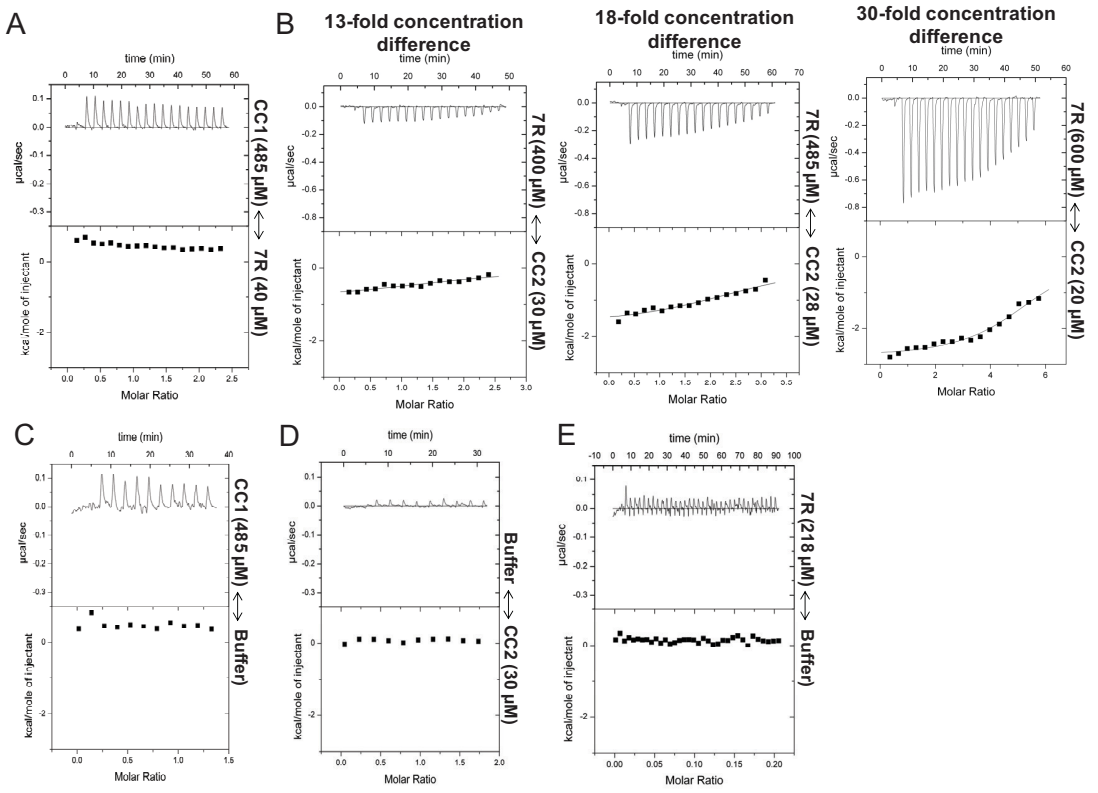

Fig. 22: TACC3-7R interacts with the CC2 region, but not with the CC1 region of the CC-domain.

In each figure the upper panel shows the raw data and the lower panel shows the integrated data from the titration. A, Heat changes were not observed after titration of CC1 (485 µM) to 7R (40 µM) indicating lack of association. B, Titration of 7R to CC2 with 13-fold, 18-fold, and 30-fold protein concentration difference reveals an increased level of heat change within this titration. C, D, & E, indicates control experiments for comparison.

Interestingly, a significant heat change was observed after titration of the seven repeat regions to CC2 (Fig. 22B). However, association was not observed when CC1 was titrated to the seven repeat regions. Surprisingly, in the case of titration of these repeats to CC2, the saturation level could not be obtained at the end of titration even at an increased fold concentration difference (7R concentration in syringe 13, 18 and 30 fold higher than the CC2 concentration in the ITC cell). The failure to reach the saturation level could be explained as continuous association and dissociation between both proteins because of multiple binding sites in seven repeat.

The repeat region has seven identical repeats and six identical junctions (Fig. 23). Therefore, 6-7 binding sites in the seven repeat regions could be possible for CC2. In order to find a perfect binding position, association and dissociation (between CC2 and the seven repeat region) may continue. This could be a possible reason for the observation that the heat changes fail to reach the saturation level during titration even at a 30-fold concentration difference. Despite this problem the results altogether suggest an interaction between CC2 and the seven repeat region. A nonlinear curve fitting in a single and sequential binding site mode indicates thereby a low affinity between the seven repeat region and CC2.

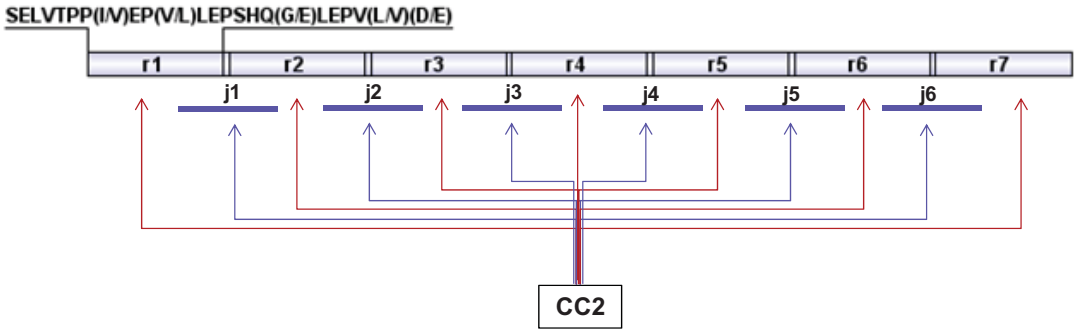

Fig. 23: Model showing multiple sites in the seven repeat regions for CC2 binding.
In the seven repeat region, either seven (repeats, r1-r7) or six (junctions between the repeats, j1-j6) different binding sites are possible for CC2.

5.5.5 Synopsis of the studies addressing the intramolecular interaction of TACC3

To summarize the data obtained from the studies based on 'deletion mutant' analysis of TACC3 employing gel filtration, the bait-prey based protein-protein interaction assays and the determination of heat changes after protein association in ITC experiments, a model for

the intramolecular interacting state of TACC3 is proposed (Fig. 24). Here, the central repeat region has been shown to interact with the CC2 module, thereby the N-terminal part likely masks the TACC domain of TACC3. Deletion of the conserved N-terminal region (the first ~118 amino acids; TACC3-ΔN) does not have any detectable impact on the intramolecular interaction. However, deletion of the seven repeat (TACC3-ΔR) precludes the intramolecular interaction between the two N- and C-terminal fragments of TACC3 after thrombin cleavage.

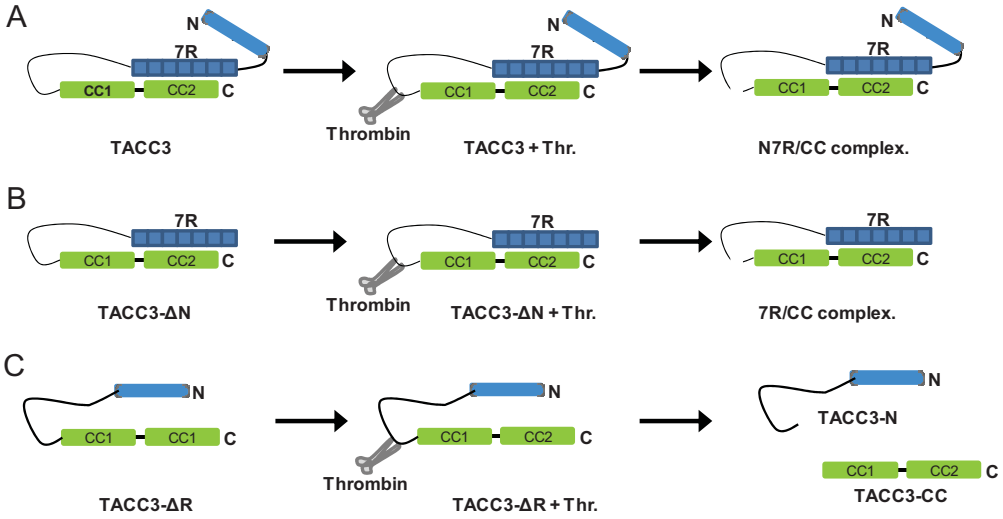

Fig. 24: Schematic diagram depicting the intramolecular interaction between the seven repeat region and the CC2 module.
A, Two fragments (N7R and CC) stay together in a complex after thrombin cleavage of murine TACC3. B, Deletion of the N-terminal conserved residues fails to interfere with the intramolecular interaction between the two TACC3 fragments after thrombin cleavage. C, Deletion of the seven repeat region results in separation of the two TACC3 fragments following thrombin cleavage.

5.6 *In vitro* characterization of the TACC3-chTOG intermolecular interaction

5.6.1 The C-terminal TACC domain of TACC3 interacts with the C-terminus of chTOG

In metazoans, the TACC family members have been shown to colocalized with their respective XMAP215 family members at the centrosome and along the spindle microtubule and thereby regulating the spindle dynamics (8,34). The TACC family members in *S. pombe* (Alp7), *D. discoideum* (TACC), C. *elegans* (TAC-1), *D. melanogaster* (D-TACC), *X. laevis* (TACC3/Maskin), and *H. sapiens* (TACC1, TACC2 and TACC3) interact with their

respective XMAP215 partners (8,24,25,33,44,51,66). Here, *in vitro* characterization of the murine TACC3-chTOG protein complex was performed. For that, two independent sets of experiments were carried out. In the first set up, purified TACC3 protein was mixed with an excess amount of purified chTOG-C followed by incubation for 30 min on ice. Thereafter, the mixed protein sample was injected to the pre-equilibrated Superose 6 10/300 column and elution fractions (0.5 ml/fraction) were collected and analyzed on SDS-PAGE followed by CBB staining (Fig. 25). Furthermore, both proteins were also injected to the column separately and the shift in elution peaks of the mixed sample was compared to the peak profile of both individual proteins.

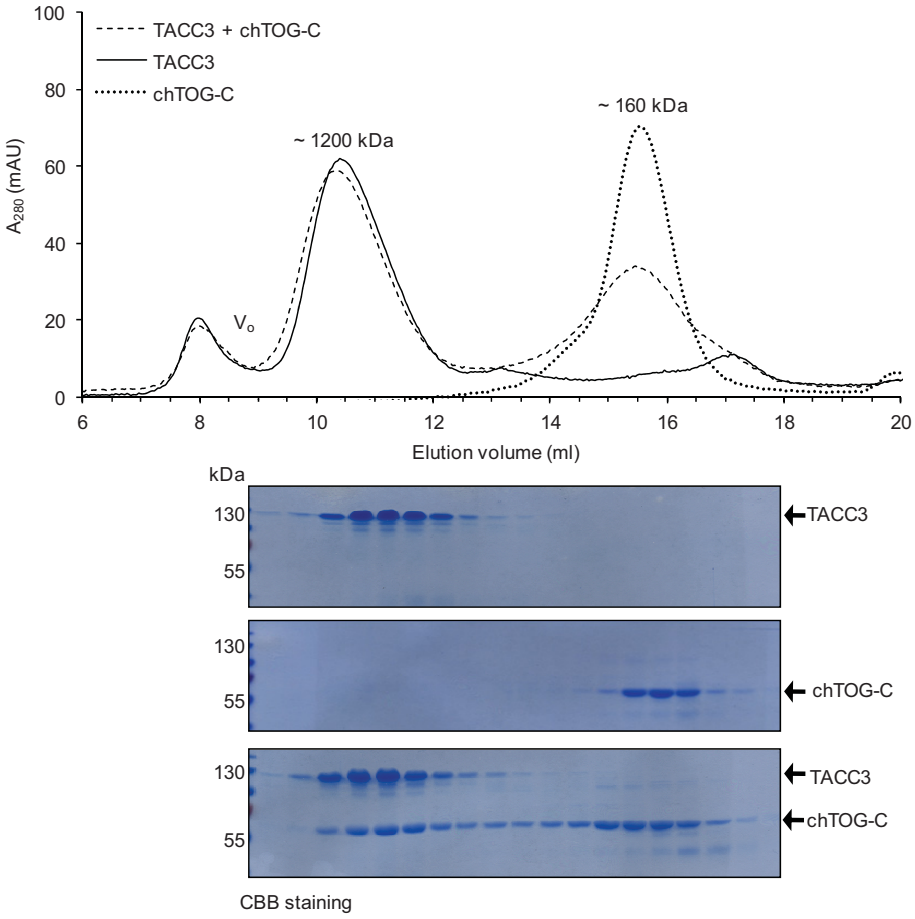

Fig. 25: TACC3 interacts with the C-terminus of chTOG.
The upper panel shows the elution profile for TACC3 (solid line), chTOG-C (dotted line), and the complex of both proteins (small dashed line) from a Superose 6 10/300 column. The lower panel depicts CBB stained 10% SDS-PAGE gels, showing elution fractions (9-18 ml) from respective protein profiles. 'V_o' denotes the void volume of the column.

As indicated in Fig. 25, the TACC3 and chTOG proteins elute in peak fractions corresponding to molecular size of ~1200 kDa and ~160 kDa. The earlier elution of TACC3 has been discussed in section 5.5.2 (Fig. 18). The chTOG-C protein has a monomeric size of 52 kDa and its elution in the peak fraction of 160 kDa protein indicates a trimeric (52 × 3 = 156 kDa) structure. Evidence showing such a trimerization of chTOG/XMAP215 proteins is still missing. Interestingly, the yeast homologue (Stu2 and Alp 14) of XMAP 215 family contains a coiled coil domain in their C-terminal region and is responsible for homodimerization of the protein (128). Further, upon mixing of both proteins (TACC3 and chTOG-C), a clear and significant left shift of the chTOG-C peak fraction was observed. Analysis of the elution fractions (9-18 ml) by SDS-PAGE clearly revealed an interaction between TACC3 and chTOG-C nearly at a 1:1 stoichiometric ratio. Comparable results have been described for the interaction of Xl-TACC3 (Maskin) with XMAP215 (33).

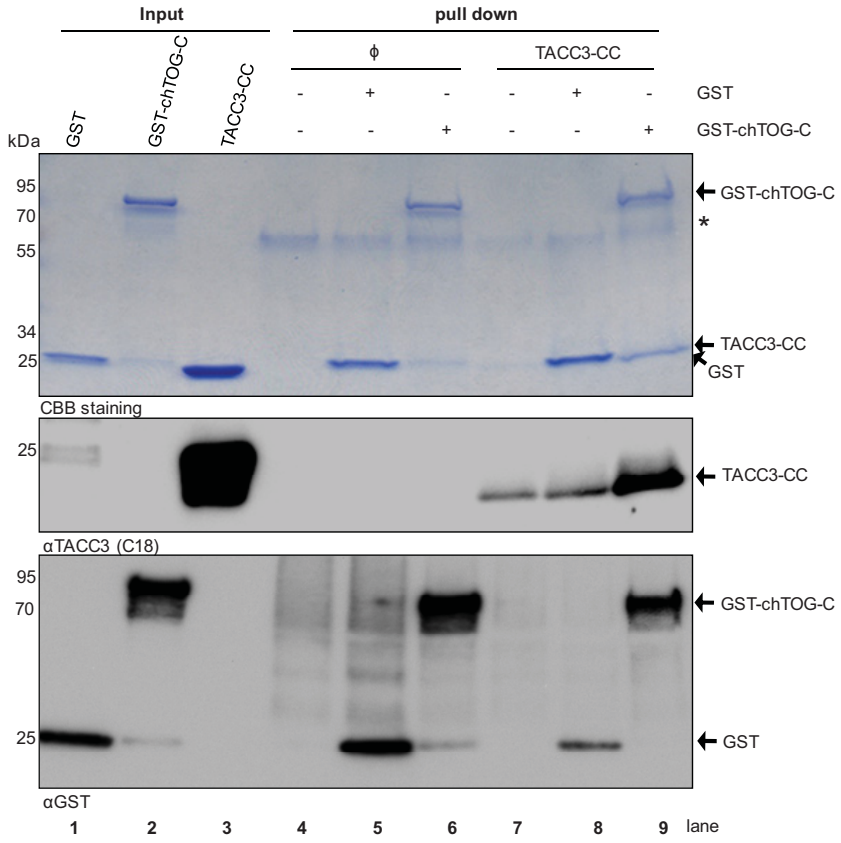

Fig. 26: The C-terminus of chTOG binds to the C-terminal TACC domain of TACC3.
Pull down of TACC3-CC (prey) using GST-chTOG-C as bait. Image displays 4-15% gradient SDS-PAGE analysis followed by CBB staining (upper panel), and immunoblotting (middle and lower panel) antibody (ϕ denotes buffer control, * denotes BSA).

The C-terminal TACC domain of Alp7 (TACC3 homologue in *S. pombe*) has been shown to interact with the C-terminal region of Alp14 (XMAP215 homologue in *S. pombe*) (92). In the literature, similar interaction patterns were suggested for TACC-XMAP215 in all other metazoans (8,34). Therefore, in a second set of experiments, the purified TACC3-CC (prey) *i.e.* the TACC domain was employed and subjected to pull down using GST-chTOG-C as bait. As indicated in Fig. 26, the TACC domain could be detected at a high level upon GST-chTOG-C based pull down (lane 9) as compared to the unspecific binding of the TACC domain to GST-sepharose beads (lane 8). This finding reveals a high binding affinity of the C-terminus of chTOG for the TACC domain. Thus, murine TACC3 interacts with its effector protein chTOG *via* its TACC domain.

5.6.2 The C-terminus of chTOG binds selectively to the CC1 module of the TACC domain

Two separate coiled coil modules (CC1 and CC2) with a different level of amino acid conservation were defined within the TACC domain of murine TACC3 (Fig. 10 and 11). The CC2 to module was identified to be involved in the intramolecular interaction with the SPE-rich seven repeat region of TACC3 (Fig. 22 and 24). Therefore, next we specified the chTOG binding motif within the TACC domain of murine TACC3. For this, two different experimental set ups were planned and performed.

In the first set up, purified chTOG-C was mixed at an equimolar amount (7 nmole of each protein) with purified CC1 and CC2 in different combinations and analyzed on a Superose 6 10/300 column. The peak elution patterns after mixing the proteins were compared with the peak elution pattern of the individual proteins. Thereby, elution fractions (0.5 ml/fraction) were collected and analyzed on SDS-PAGE (4-15% gradient) followed by CBB staining.

As indicated in Fig. 27, CC1 (14.4 kDa), chTOG-C (51.8 kDa), and CC2 (11.6 kDa) appeared in peak fractions corresponding to a molecular size of 300, 160, and 85 kDa respectively. When chTOG-C was mixed with either CC1 (Fig. 27A) or CC2 (Fig. 27B) individually, single peaks of the protein complexes were detected and a left peak shift was

observed in both cases. The peak fractions of chTOG-C/CC1 and chTOG-C/CC2 corresponded to molecular weights of 500 and 183 kDa respectively. The left peak shift was complete for chTOG-C/CC1 and rather partial and moderate for chTOG-C/CC2. These observations revealed a high affinity and selectivity of chTOG-C for binding to the left half (CC1) of the TACC domain as compared to a rather low affinity for the right half (CC2).

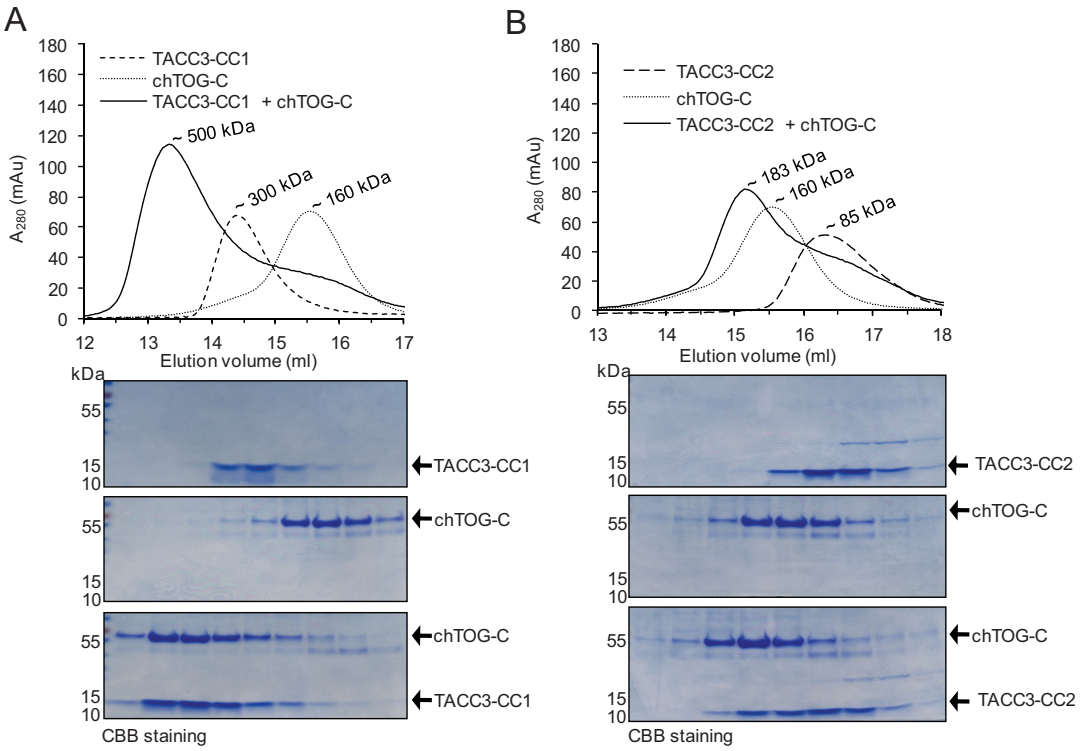

Fig. 27: The C-terminus of chTOG displays a comparatively higher affinity for CC1 when mixed individually with two separate module of the TACC domain, CC1 and CC2.
In both A and B, upper panels display elution profiles (Superose 6 10/300 column). In the lower three panels elution fractions (A, 12.5-17 ml; B, 13.5-18 ml) were analyzed on SDS-PAGE gradient (4-15%) gels followed by CBB staining.

As chTOG-C appeared to bind to both CC1 (strong interaction) and CC2 (weak interaction), a possible state of triple complex formation was assumed in which chTOG-C binds to both CC1 and CC2 together. To address this hypothesis another set of experiments with proper controls were planned and performed. In a first control experiment, the interaction between CC1 and CC2 was tested as described above. After mixing both proteins in an equimolar ratio, a left peak shift was not detected on gel filtration column (Fig. 28A). This indicated that CC1 and CC2 do not form complexes with each other.

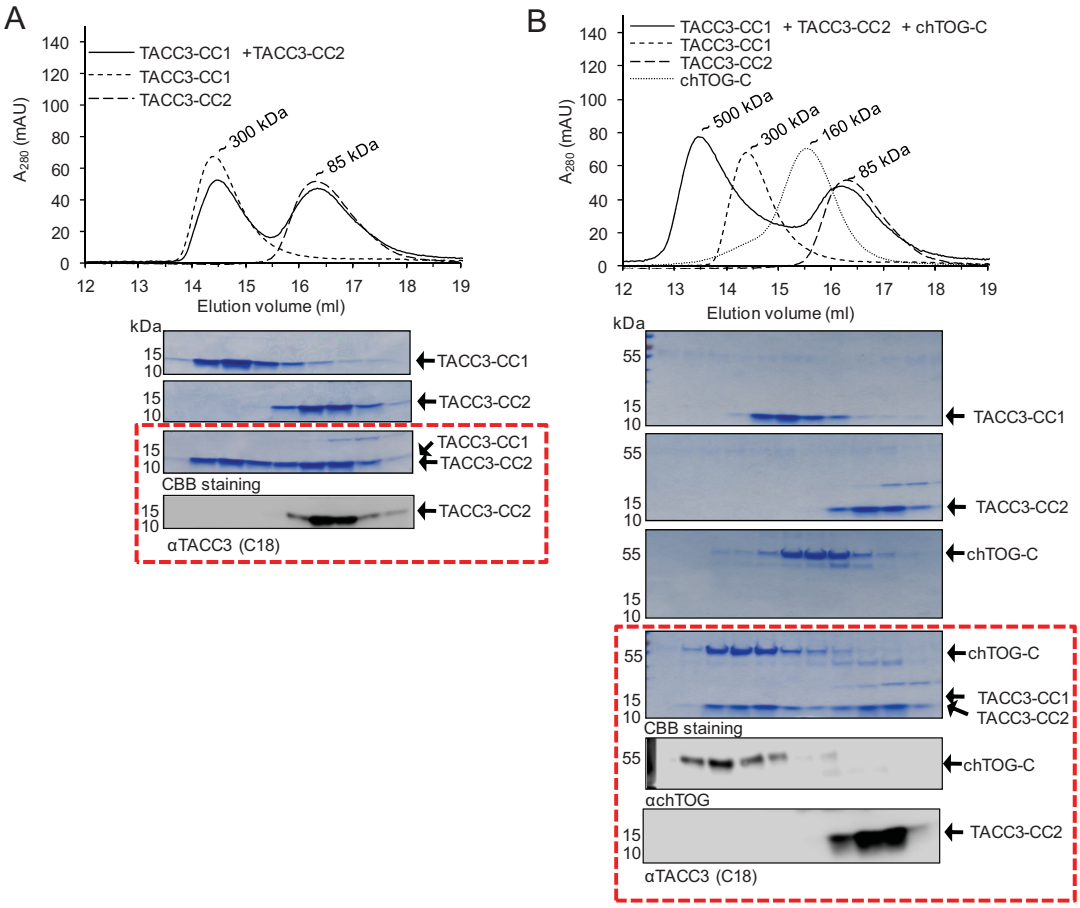

Fig. 28: The chTOG-C specifically interacts with the first half (CC1) but not to the second half (CC2) of the TACC domain.
A, After mixing CC1 with CC2, both proteins elute in their original peak fractions. B, Analysis of an equimolar mixture of CC1, CC2, and chTOG-C for complex formation. The left peak shift of CC1, but not CC2, with chTOG-C indicates a specific interaction between CC1 and chTOG-C. Elution fractions from 13.5-18 ml (A) and 12.5-18 ml (B) were analyzed on SDS-PAGE followed by CBB staining and immunoblotting. Anti-TACC3 (C18) antibody can recognize CC2 but not CC1 region of the TACC domain from murine TACC3. Elution fractions for the mixed protein sample were also analyzed by immunoblotting by use α-TACC3-C18 and α-chTOG antibodies (lower panels in red box).

Lastly, all three proteins (CC1, CC2, and chTOG-C) were mixed together in an equimolar ratio (7 nmole of each) and analyzed on Superose 6 10/300 column followed by SDS-PAGE and CBB staining. As indicated in Fig 28B, and comparable to the result in Fig 28A, the elution peak for the CC1/chTOG-C complex shifted significantly to the left thereby leaving behind CC2 in its original peak. Thus, even when mixing all three proteins together, chTOG-C still showed a clear selectivity in binding to CC1, but not to CC2.

Interestingly the TACC domain could display a parallel or antiparallel structural orientation (Fig. 29). The antiparallel orientation can be only possible when CC1 interacts with CC2. However, on gel filtration CC1 did not show any binding with CC2 (Fig. 28A). Thus, these findings clearly indicate that the TACC domain of murine TACC3 forms a parallel coiled coil structure.

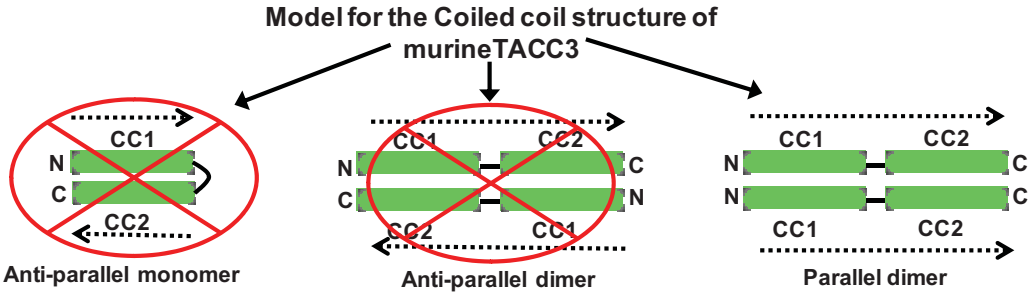

Fig. 29: Possible model for helical orientation in the TACC domain of murine TACC3.

Next, we employed the ITC-method as a complementary approach to address the interaction between CC1, CC2, and chTOG-C. In this experimental series CC1 (400 µM) and CC2 (155 µM) were titrated to chTOG (25 and 15 µM, respectively) and then to buffer (control experiment) for comparison (Fig. 30). When CC1 was titrated to chTOG-C, a clear heat change was observed because of the association (exothermic process) of the two proteins (Fig. 30A) as compared to the control (Fig. 30B). Heat changes reached the saturation level after 11 injections (each consisting of a volume of 15 µl). In contrast, the association between CC2 and chTOG could not be detected in analogous ITC experiment consistent with the finding in Fig. 27 and 28. Taken together, these data suggest that chTOG-C displays a binding pocket for CC1 but not for CC2.

Later, a calculation of the binding affinity between chTOG-C and CC1 was performed employing a nonlinear single binding site curve fitting of the raw data was performed using the MicroCal software. Analyzing the data for the CC1-chTOG-C complex at a minimum chi-square value, the calculated dissociation constant (K_d) was 0.704 µM (±3.39E^5 M^{-1}) with a stoichiometry (N) of 0.831 (±0.0180 sites) and a negative entropy of ΔH=-2218 ±67.82 cal/mol. The low K_d value and the near to one to one stoichiometry value indicate a very strong affinity and 1:1 interaction between chTOG-C and CC1 and hence between chTOG

and TACC3. The obtained stoichiometry also fits well with findings obtained from the gel filtration analysis (Fig. 25 and 27A).

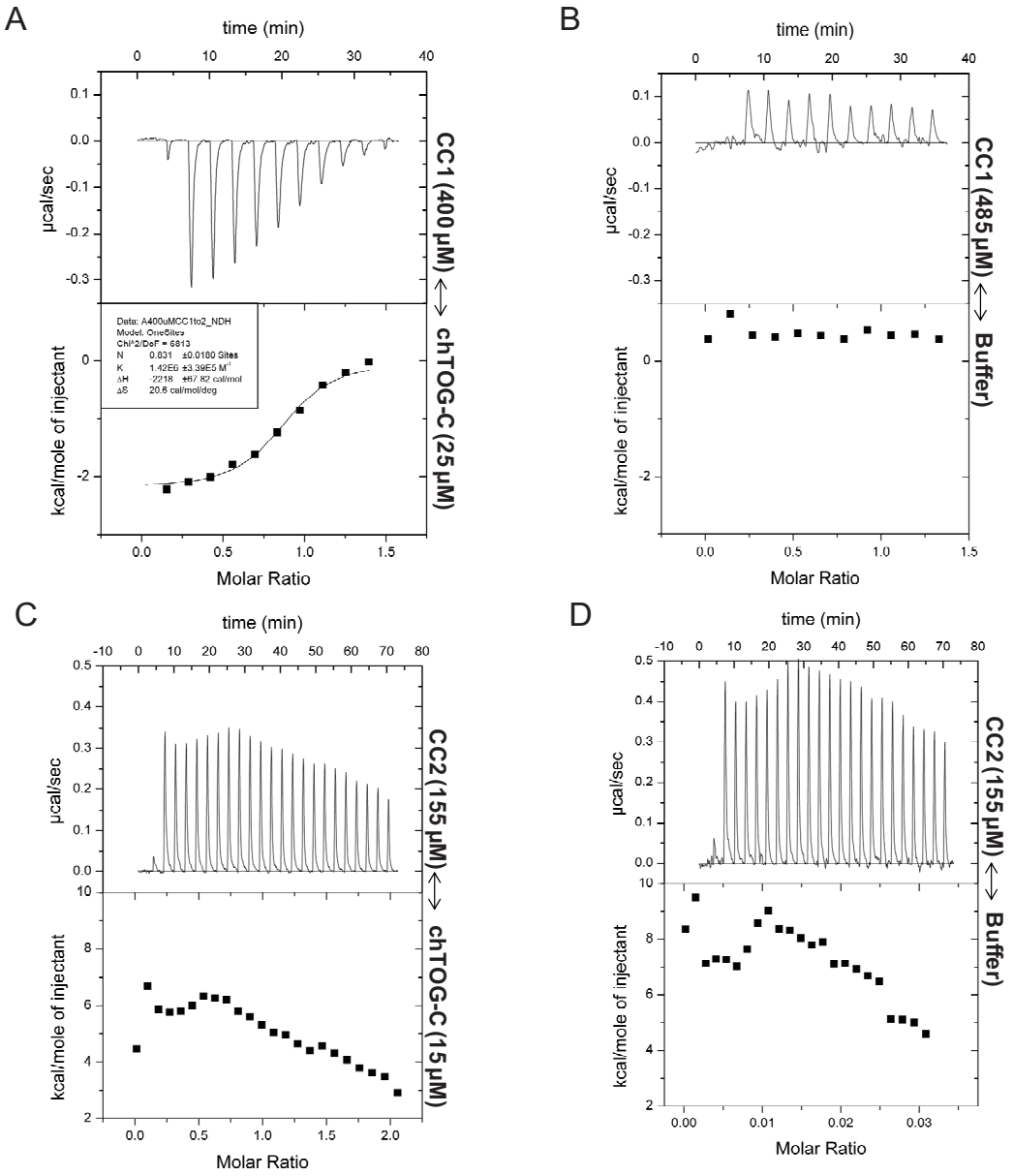

Fig. 30: chTOG displays a high binding affinity to CC1 characterized through a 1:1 binding stoichiometry.
Results from ITC experiment showing changes in heat of association, when CC1 and CC2 titrated to chTOG-C (A and C) and buffer (B and D; for controls).

5.6.3 Binding of chTOG-C to the CC1 module uncouples the intramolecular interaction between the CC2-domain and the seven repeat regions

The CC1 and CC2 modules of the TACC domain were identified to be involved in intermolecular binding to chTOG (section 5.6.2, Fig. 28) and an intramolecular interaction with the seven repeat region (section 5.5.4, Fig. 22), respectively. Therefore, an important next point was to address and understand the relevance of the intramolecular interaction between CC2 and the seven repeat regions in terms of the intermolecular interaction between CC1 and chTOG. Hence, two sets of the experiments were carried out in the following order. In the first set, pulldown assays were performed by using GST-chTOG-C as bait and TACC3 as prey before and after its thrombin cleavage (Fig. 31). In a second set of experiments, gel filtration analysis of the TACC3-chTOG-C complex, that has been subjected to thrombin cleavage was performed.

Pull down assays were performed using 100 µl of GSH-sepharose beads in a final reaction volume of 200 µl, by mixing 5 µM of GST-chTOG or GST alone with 10 µM of TACC3 before and after its thrombin cleavage. Interestingly, as indicated in Fig. 31, GST-chTOG-C was able to pull down the TACC3 (lane 10, blue box) and after thrombin cleavage of TACC3 also the TACC domain (lane 13, red box), but not to the N-terminus containing seven repeat region (TACC3-N7R). This important finding was also confirmed by immunoblotting using antibodies against the N- and C-terminus of murine TACC3 (N18 and C18, respectively).

Next, the results were further confirmed using gel filtration analysis of the TACC3-chTOG-C complex after thrombin cleavage. First, TACC3 protein was mixed with an excess amount of chTOG-C and thereafter subjected to thrombin digestion. Samples were then injected to the Superose 6 10/300 column and the elution pattern was compared with the intramolecular N7R/CC complex obtained after thrombin digestion of the TACC3 (Fig. 32, upper panel).

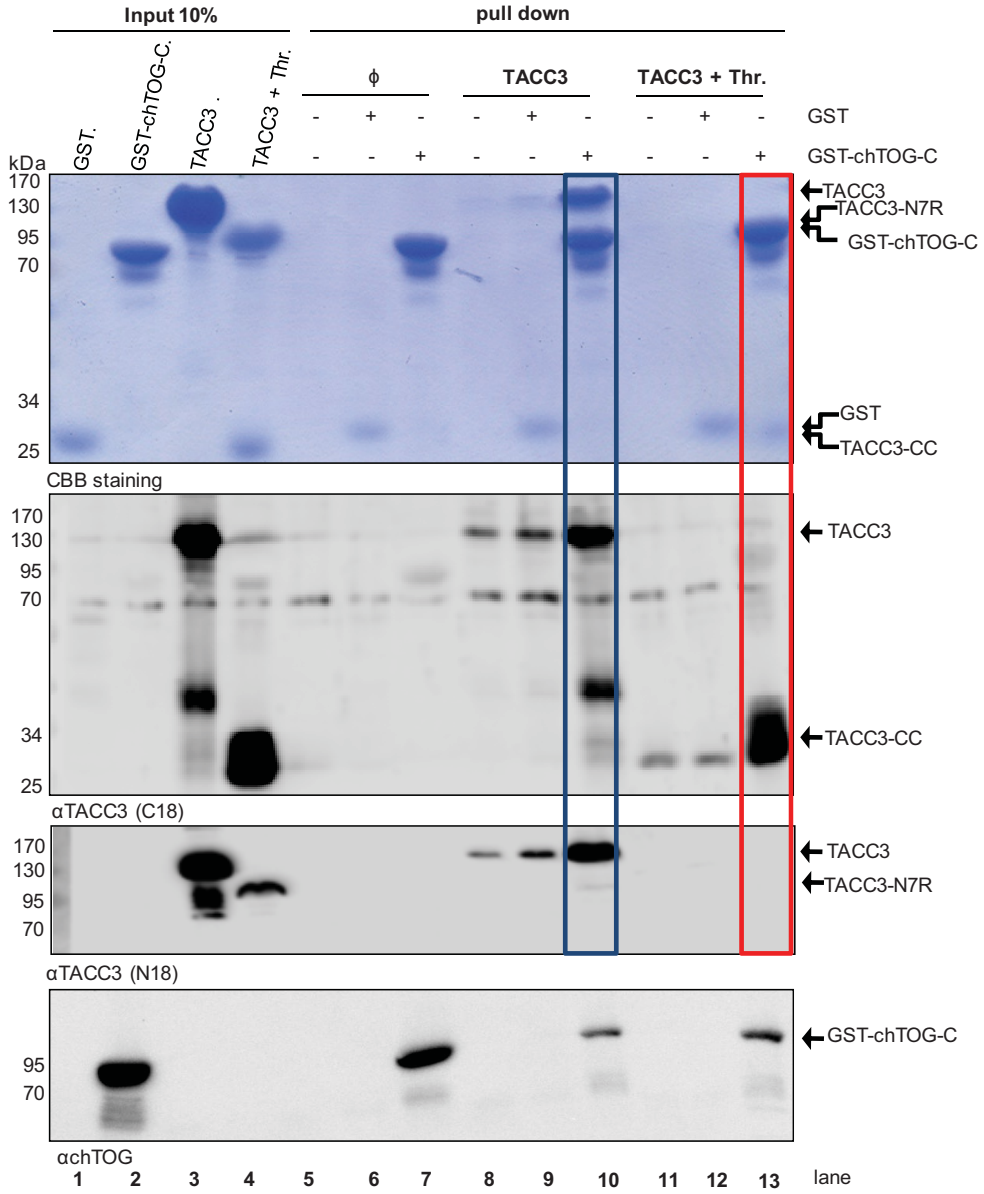

Fig. 31: GST-chTOG-C pulls down the TACC domain but not the repeat region containing N-terminus (N7R) after thrombin cleavage of TACC3.
Blue and red lines indicate the pull down lanes (10 & 13) for TACC3 before and after thrombin cleavage respectively (ϕ indicates the buffer control).

Interestingly, subsequent to thrombin digestion, the preformed TACC3-chTOG-C complex elutes in the peak fractions (~800 kDa) with a left clear peak shift relative to the N7R/CC complex peak (~630 kDa) (Fig. 32). Excess amount of chTOG-C elutes in the original peak (~160 kDa) consistent with Fig. 25. On the SDS-PAGE gel, TACC3-N7R appears to elute in the same fractions in both cases (Fig. 32, red box). In contrast, TACC3-CC

elution shifted together with chTOG-C to fractions left from the peak fraction of the N7R/CC complex (Fig. 32, blue box). Correlating these results with the findings obtained from the pull down assay (Fig. 31), one can conclude that loss of intramolecular interaction between N7R and TACC domain occurs when chTOG binds to the TACC domain of TACC3.

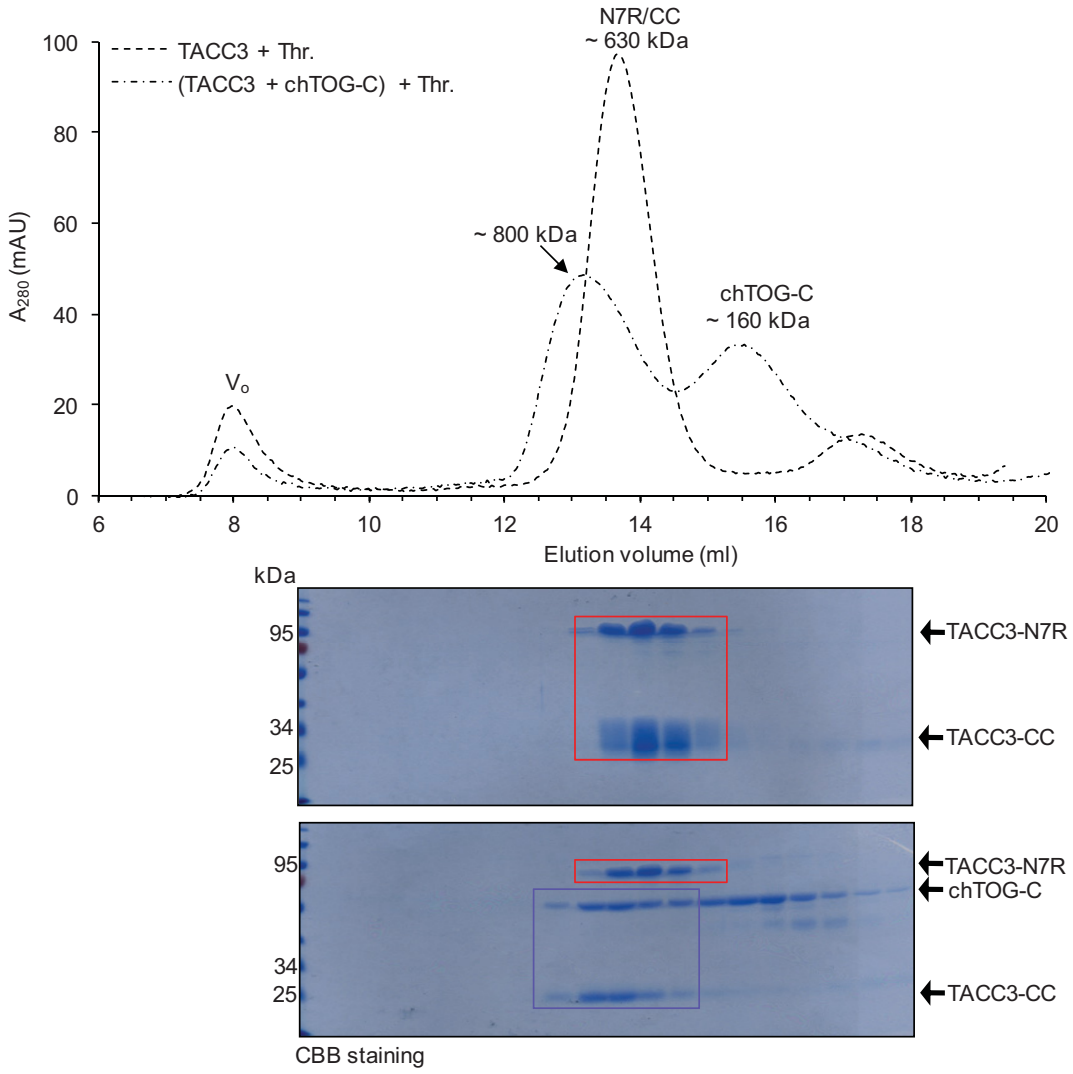

Fig. 32: Binding of the C-terminus of chTOG to the TACC domain precludes the intramolecular interaction of TACC3.
Upper panel displays the elution profiles after thrombin digestion of TACC3 (dashed line) and the TACC3-chTOG-C complex (dashed line with dot). After thrombin cleavage of the TACC3-chTOG-C complex, a peak shift left to the N7R/CC (intramolecular) complex peak was observed (upper panel). Lower two panels display elution fractions from 9-18 ml on the 10% SDS-PAGE followed by CBB staining. The red box indicates the N7R protein alone (in the lower panel) and co-eluting with the TACC domain (in the middle panel). The blue box indicates the left shift of TACC domain co-eluting with chTOG-C. The excess amount of chTOG-C elutes in its original peak fractions.

5.7 Aurora-A phosphorylation of TACC3 is independent from its TACC domain masked and unmasked state

The mitotic and centrosomal protein kinase Aurora-A is an important and specific regulator of the TACC3-chTOG complex (Fig. 6). In particular, phosphorylation of TACC3 by Aurora-A is required for its recruitment to the centrosome (25,30,33,66). Two fragments after thrombin cleavage of recombinant murine TACC3 stay in a complex (Fig. 18) and this state has been named as the TACC domain masked state. The seven repeat region is the critical domain for the intramolecular interaction and thus the masking action (section 5.5.3, Fig. 20). Interestingly, chTOG-C binding to TACC domain precludes the complex formation (section 5.6.3, Fig. 31 and 32). In this regard, Aurora-A has been proposed to be an important factor for unmasking of TACC domain from Xl-TACC3/Maskin (49).

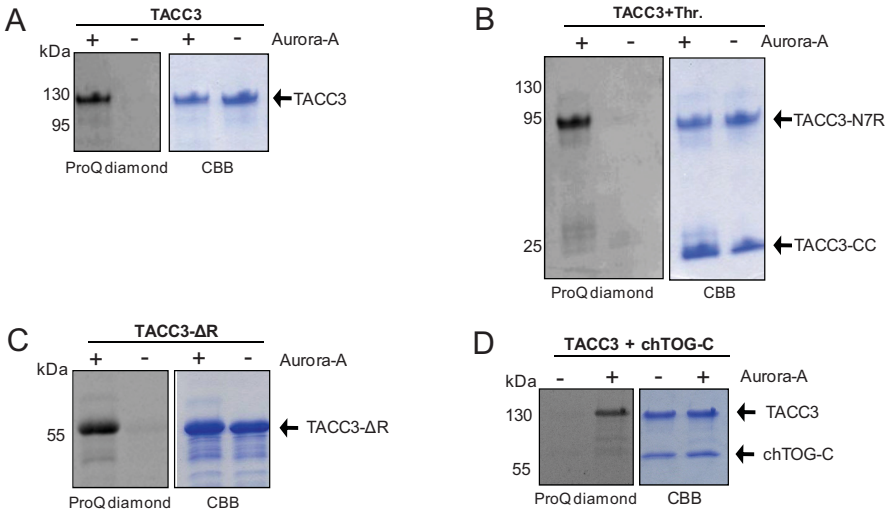

Fig. 33: Aurora-A phosphorylates murine TACC3 independent of its intra- or intermolecular protein binding status.
In vitro Aurora-A mediated phosphorylation of purified murine TACC3 was performed at 30 ˚C and phosphorylation was detected on SDS-PAGE followed by Pro-Q Diamond phosphoprotein staining (left panels) and compared with the total protein loading detected by CBB staining (right panels).

Therefore, to study the impact of the intra- and intermolecular interaction of murine TACC3 on its Aurora-A phosphorylation, *in vitro* kinase assays were performed. GST-fused active Aurora-A (Signal Chem) was mixed with recombinant murine TACC3 in the ratio of 1:2 (0.5 µg enzymes with 1 µg substrate) and reactions were carried out in the presence of

ATP at 30 ˚C for 15 min. Phosphorylated proteins were detected by Pro-Q Diamond phosphostaining within the SDS-PAGE gels (Fig. 33).

As indicated in Fig. 33, the active kinase could phosphorylate TACC3 before and after thrombin cleavage, *i.e.* in the state of an intramolecular interaction, where TACC domain is likely masked. Moreover, deletion of the central repeat region (Fig 33C) or binding of TACC3 to its effector chTOG (Fig. 34D) did not impair Aurora-A phosphorylation of TACC3. All together, these results suggest that Aurora-A phosphorylation of TACC3 is independent of the intra- and intermolecular protein interaction status of TACC3. Consistent with these results, employing the Aurora-A kinase inhibitor VX-680 or λ-phosphatase, it has been shown that the TACC3-chTOG interaction is independent of Aurora-A phosphorylation (80).

5.8 Comprehensive biophysical characterization of purified murine TACC3 and TACC3 variants

The murine TACC3 protein displays a high oligomeric status as examined on the Superose 6 10/300 column (Fig. 18). Although, two fragments after thrombin cleavage of TACC3 stay together by forming a protein complex, but their elution pattern indicates a big change in their conformations and size (Fig. 18). Deletion of the N-terminus conserved region did not impair the elution pattern on gel filtration column (Fig. 19). However, a significant changes in stoke radii (TACC3: 1200 kDa; TACC3-ΔR: 1100 kDa) appear after deletion of the seven repeat region (Fig. 20). Lastly, the TACC domain of TACC3 appears to contain a parallel coiled coil structure (Fig. 29). Thus, based on these previous results, several biophysical methods were employed to characterize the structure and oligomerization of TACC3 in greater detail.

5.8.1 Circular dichroism (CD) spectroscopy

First, the CD spectra of purified murine TACC3 were determined to examine the variation in the amount of secondary structure before and after thrombin cleavage as well as after deletion of the seven repeat regions (TACC3-ΔR). The spectra were scanned in a

wavelength range of 190-260 nm wavelengths with a data pitch 0.2 nm. Spectra from 190-200 nm were removed during data processing because of noise backgrounds whereas 41 data points between 200-241 nm (with a data pitch of 1 nm) were used for further processing and secondary structure calculation by the use of the K2D online program (117).

As indicated in Fig. 34, for all analyzed proteins two minima (θ_{208} and θ_{222}) were obtained which justifies that TACC3 displays mainly α-helical secondary structures. Importantly, the spectrum of TACC3 remains unchanged after its thrombin cleavage. This indicates that *in vitro* thrombin cleavage of TACC3 did not cause any change in the amount and type of secondary structures. Therefore, the right shift of the elution peak of thrombin cleaved TACC3 on gel filtration column (Fig. 18) can be explained either as conformational changes (which cause a change in stock radii) without affecting the secondary structure or as decrease in oligomeric status of protein.

In contrast, the deletion of the seven repeat region causes an upward shift in the spectra at θ_{208} (Fig. 34A). This upward shift at θ_{208} can be interpreted as a loss in the helical content of TACC3 after deletion of the seven repeat region. The calculation of the percentage of α-helical content vs. β-sheet structure after processing of the raw data confirms a significant α-helicity for the TACC3-ΔR mutant (Fig. 34B). This clear loss in the helical content after deletion of the seven repeat region argues for the presence of some α-helices in this region apart from the C-terminal TACC domain of TACC3.

A

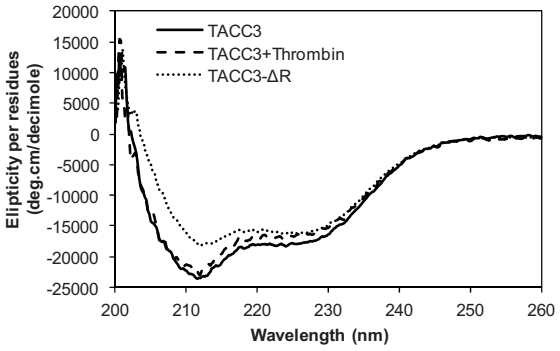

B

Protein	α-Helix (%)	β-Sheet (%)
TACC3	55.51	10.36
TACC3 + Thr.	53.22	10.11
TACC3-ΔR	43.28	14.43

Fig. 34: TACC3 protein is comprised mainly of α-helical secondary structures.
A, The solid and dashed line shows the CD spectra of TACC3 before and after thrombin cleavage, respectively. The dotted line is the spectrum of the TACC3-ΔR mutant. B, amount of secondary structures calculated by the use of the K2D program (117).

5.8.2 Multi angle light scattering (MALS)

The murine TACC3 protein has theoretical polypeptide mass of 70 kDa (Tab. 27). Irrespective of their monomeric mass, during gel filtration chromatography murine TACC3 elutes in a peak fraction corresponding to a molecular weight of ~1200 kDa (Fig. 18) and migrates at a molecular weight of 120 kDa on SDS-PAGE (Fig. 17). Therefore, to determine the actual native molecular mass, MALS experiments were performed in an asymmetric flow field flow fractionation (AF4) mode (129). In this method, narrow band of sample is injected into buffer stream flowing through an elongated chamber and allowed to move freely on a cellulose membrane in the direction of stream. Signals (UV_{280} absorbance, refractive index and amount of scattered light) at outflow position were detected at right angle with time by use of MALS detector. The numerical values for the amount of light scattered at different time point were then used to calculate the molar mass of the molecule. The molar mass at maximum UV_{280} absorbance or refractive index was considered as molecular size of the protein or protein-complex.

A

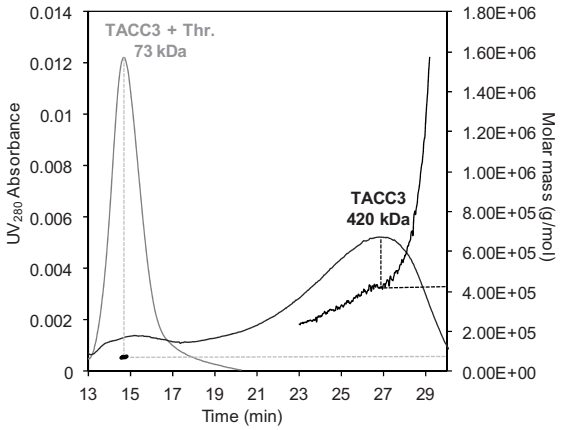

B

	TACC3wt	TACC3 + Thr.
Molar mass moments (g/mol)		
Mn	$4.024e^{+5}$ (12%)	$7.116e^{+4}$ (0.3%)
Mp	$4.204e^{+5}$ (14%)	$7.347e^{+4}$ (0.3%)
Mw	$9.074e^{+5}$ (12%)	$7.133e^{+4}$ (0.3%)
Mz	$6.592e^{+6}$ (20%)	$7.149e^{+4}$ (0.8%)
Polydispersity index		
Mw/Mn	2.255 (16%)	1.002 (0.5%)
Mz/Mn	16.380 (23%)	1.005 (0.8%)

Fig. 35: MALS based determination of the molecular mass and homogeneity of TACC3 before and after thrombin cleavage.
A, MALS-AF4 profiles show the molar mass at the maximum UV absorbance of 280 nm. B, Physical parameter obtained from the MALS experiment. Mn (number-average), Mw (weight average), and Mz (z-average) represents different averages of molecular weight and 'Mp' is peak molecular weight. The value in the brackets indicates the percentage of error. These molar mass averages are calculated from the amount of light scattered data as described in method section (Analyzed and confirmed in collaboration with Dr. Britta Reis and Prof. Dr. Lutz Schmitt)

At the maximum UV_{280} absorbance, TACC3 before and after thrombin cleavage, appears to have molecular size of 420 kDa and 73 kDa, respectively (Fig 35A). The polydispersity index (PDI) for the TACC3 sample was clearly higher than one (PDI>>1; Fig. 35B) which indicates heterogeneous size distribution of the purified TACC3 protein. In contrast, thrombin cleavage of TACC3 caused a transition from polydispersive to monodispersive (PDI=1) size distribution. Constant with the results obtained by gel filtration chromatography (Fig. 18), only one peak (UV_{280}) appeared after the thrombin cleavage of TACC3. This further supports the observation that after thrombin cleavage of TACC3 the N- and C-terminal fragments stay as one protein complex.

5.8.3 Analytical ultracentrifugation sedimentation velocity (AUC-SV)

To further facilitate the determination of the size and shape characteristics of murine TACC3, AUC-SV experiments were performed for TACC3 before and after thrombin cleavage. Raw data were processed and analyzed by the SEDFIT program (version 12.1) by applying the Monte Carlo statistics (Fig. 36). Tab. 28 depicts the statistics from two independent experiments.

Tab. 28: Statistics from the AUC-SV experiments.

Protein		Amount (%)	MW (kDa)	$S_{20,w}$ (S)	f/f0
TACC3	*Species 1*	87.71	108.91 (108.03, 109.87)	3.12 (3.12, 3.12)	2.55 (2.53, 2.57)
	Species 2	12.29	57.40 (57.10, 58.20)	4.72 (4.68, 4.77)	1.10 (1.09, 1.12)
TACC3 (Thrombin cleaved)	*Species 1*	62.30	52.55 (52.17, 52.92)	2.20 (2.19, 2.21)	2.22 (2.21, 2.24)
	Species 2	29.32	61.92 (60.98, 62.86)	1.28 (1.22, 1.27)	4.26 (4.24, 4.29)
	Species 3	8.63	66.09 (63.68, 68.50)	3.78 (3.77, 3.80)	1.51 (1.47, 1.55)

MW, molecular weight; $S_{20,w}$ (S), sedimentation rate at 20 ˚C; f/f0, frictional coefficient. The number in the bracket denotes values obtained from two independent experiments.

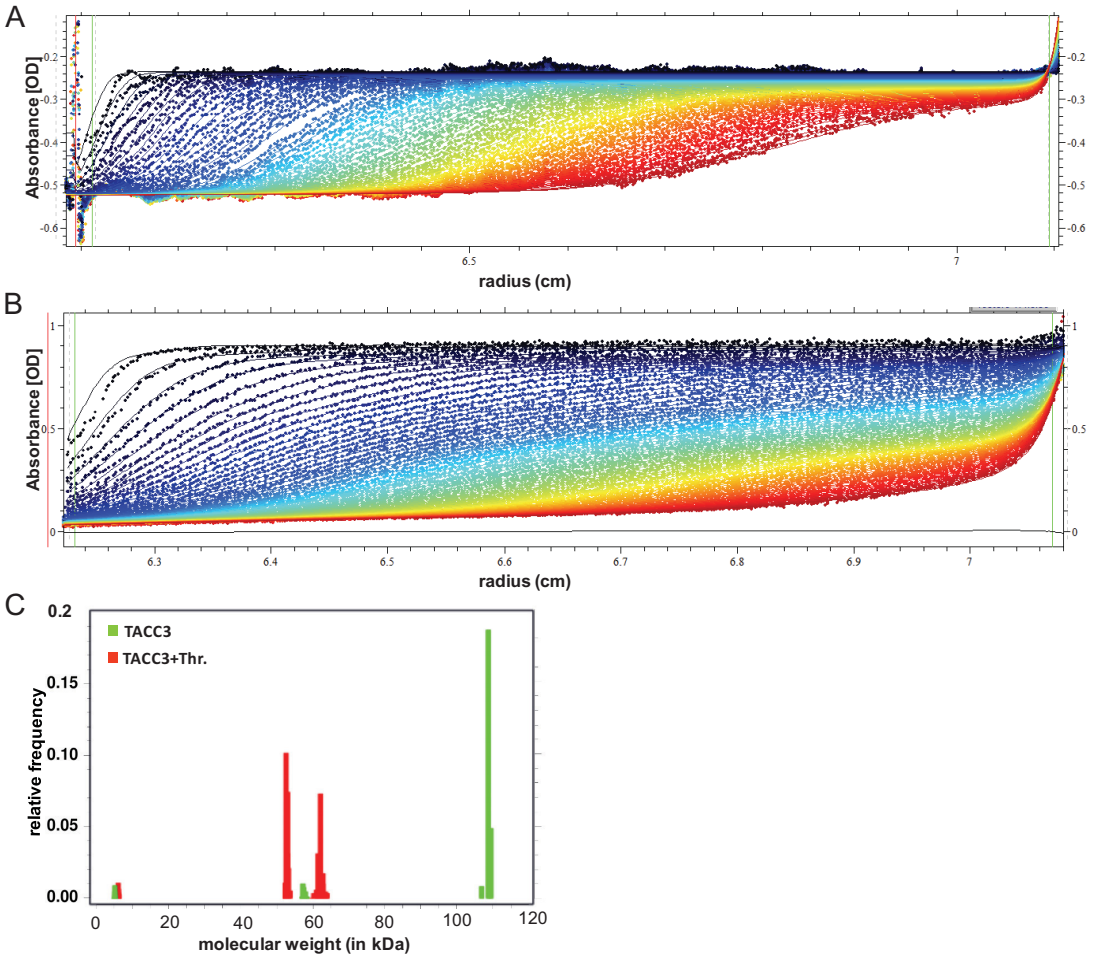

Fig. 36: AUC-SV experiment to explain the size and shape characteristics of TACC3.
AUC-SV scans (raw data) showing sedimentation of TACC3 before (A) and after thrombin digestion (B). The collected absorption (A_{280}) scan data were processed with SEDFIT program and by implementing the Monte Carlo statistics method. C, Plot depicting the molecular weight and the relative frequency of analyzed proteins after processing of the raw data (analyzed and confirmed in collaboration with Dr. Luitgard Nagel-Steger).

As indicated in Fig.36 and summarized in Tab. 29, murine TACC3 appears as one major species (87.71%) with a molecular weight of 108.91 kDa (1.5 times higher than the monomeric mass). However, after thrombin digestion two major species with molecular weights of 52 kDa (62%) and 62 kDa (29%) were observed which can be interpreted as dissociation of their N- and C-termini, two intramolecular interacting fragments, during the run. As observed in ITC experiments (section 5.5.4), the weak affinity between the two fragments could be the reason for the dissociation. Moreover, the theoretical mass for the TACC domain is 25 kDa, which is exactly half of the mass of the dissociating species (52.5 kDa). The theoretical mass for the N-terminal fragment is ~45 kDa which is closer to the mass

of the other dissociating species (61.9 kDa). Based on this calculation it can be concluded that the TACC domain has a dimeric structure. Further to this, the TACC3 protein displays a higher frictional ratio (f/f_0=2.55) and slower sedimentation rate [$S_{20,w}$ (S)=3.12] as compared to thrombin cleaved TACC3. After thrombin digestion the frictional ratio was still higher with a comparatively faster sedimentation of the protein fragments. Such behavior of a protein indicates that it displays three-dimensionally a highly extended shape and structure. Importantly their shape characteristics could be a possible reason for the earlier elution of TACC3 on the gel filtration column (Fig. 18).

5.8.4 Analysis of purified murine TACC3 by Electron Microscopy (EM)

Next, electron microscopy of murine TACC3 following negative staining was performed to visualize the shape and to obtain a low resolution structure. Protein samples were prepared by gel filtration and peak fractions were collected and concentrated up to 1-2 mg/ml for final negative staining (118). Images were collected on a Joel JEM-1400 electron microscope equipped with a LaB_6 filament (130). The particles length and width were measured using the EMAN1 boxer program (131).

As indicated in Fig. 37, under electron microscope after negative staining, TACC3 appeared to display an elongated fiber like structure with variable lengths. The dimension (length and width) of fibers was calculated by using the EMAN1 boxer program resulting in particle length values of ~25 nm to 250 nm and a width variation of between 3-15 nm. Most of the particles appear to have an average length of ~50 nm. Interestingly, similar to the previous finding of 30 nm length for the TACC domain of TACC2 (42), the minimum length observed for the TACC3 fiber was about 25-30 nm and is very similar to the calculated length (30 nm) of the TACC domain consisting of about 200 amino acid residues (42).

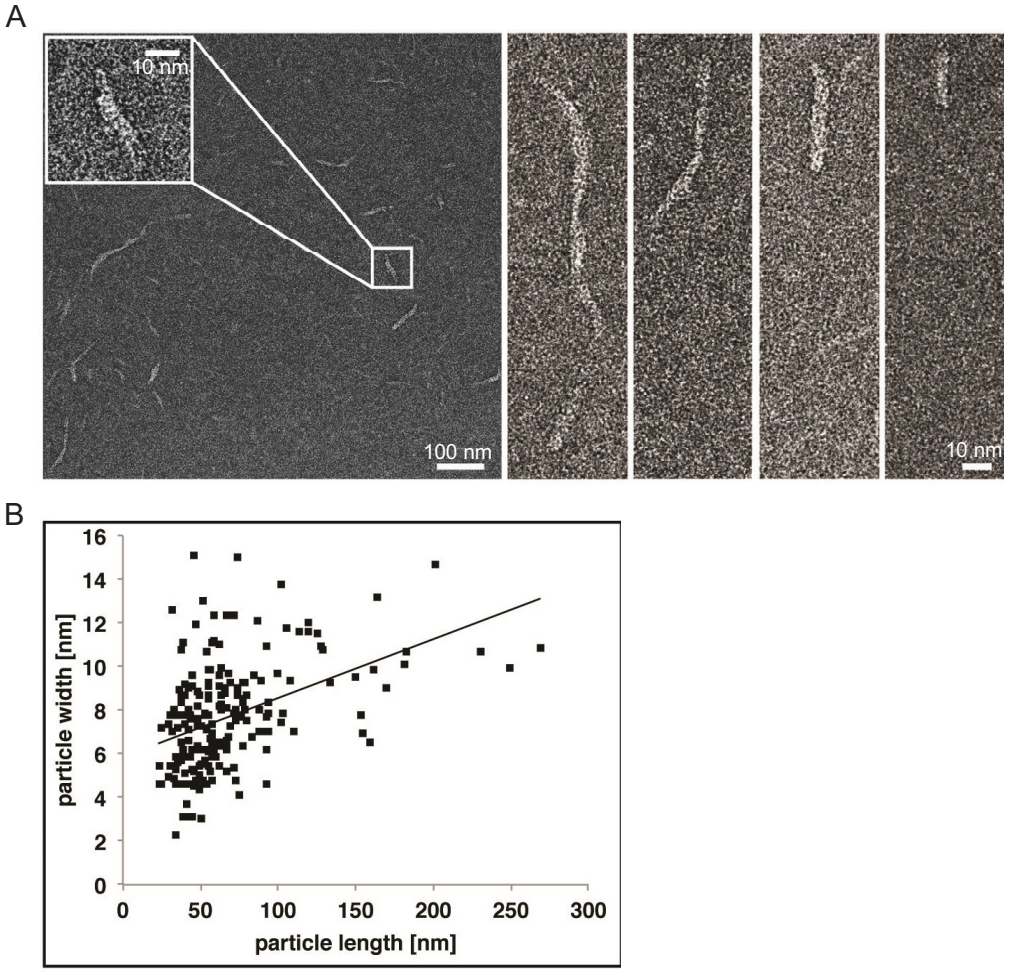

Fig. 37: EM image shows fiber like appearance of TACC3.
TACC3 molecules form fiber like structures (left and middle panel), the middle panel depicts enlarged single TACC3 particles. The left panel depicts the quantitative analysis of particle length and width by use of EMAN1 boxer program (analyzed and confirmed in collaboration with M.Sc. Daniel Prumbaum and Dr. Stefan Raunser)

5.8.5 Isolated CC2-domains form multimeric 2D-sheets like structures at a higher concentration.

In this work, purified CC1 and CC2 proteins were concentrated at a temperature of 4 ˚C. Interestingly, during the concentration process the CC2 molecules deposited on the membrane of the concentrator (Amicon Centricon; 3000 Da) in an ordered manner. After shaking they detached from the membrane wall and appeared floating in solution, where they were clearly visible by eye. An aliquot of this mixture was dropped on glass slides and imaged under a NIKON TE2000 microscope at a 4x-optical zoom (Fig. 38).

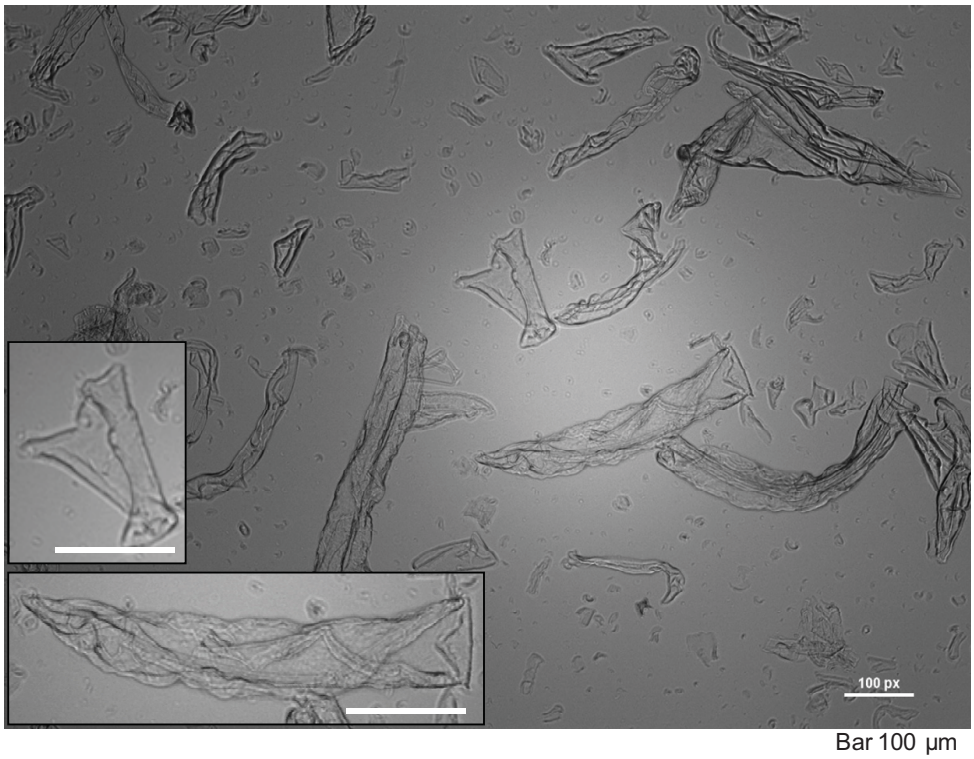

Fig. 38: 2D sheet like polymeric structure of the purified CC2 domain.
Inset displays the enlarged view of 2D sheet like structures. Images were collected under a NIKON TE2000 microscope at 4-fold magnification.

Under the microscope, CC2 did appear to form a random aggregate, but rather folded sheet-like regular polymers (Fig. 38). Similar polymeric structures were also observed by immunoelectron microscopy in HeLa cells overexpressing the GFP-fused TACC domain (42). At this time point the concentration of the CC2 protein was determined to be 150 µM in a Bradford assay. In contrast, the protein solution for CC1 stayed clear even at a quit higher concentration (>400 µM). After combining this result with the fiber like structure formation by TACC3 under electron microscope and previously shown data from immunoelectron microscopy (42), we concluded that the CC2 region is responsible for formation of fiber like or regular polymeric structure after overexpression in eukaryotic cells.

5.8.6 Synopsis of the biophysical characterization of TACC3

In this work, the murine TACC3 protein was extensively studied at the biophysical level. Tab. 29 summarizes the physical properties for TACC3 as determined by different biophysical methods. *In vitro,* this protein displays an abnormal molecular weight and

oligomeric status. On SDS-PAGE gel, TACC3 migrates higher than its actual molecular size of 70 kDa (Fig. 17A). However, after deletion of the SPE-rich seven repeat region, it migrates normally according to its real molecular weight (Fig. 17B). Therefore, the reason for the abnormal migration of TACC3 lies primarily in its central SPE-rich seven repeat region. Analogous to this region of murine TACC3, Hs-TACC3 and Xl-TACC3 isoforms also contain imperfect SPD repeats that might be contributing to their higher migration on SDS-PAGE. Similar migration pattern appeared also during gel filtration where TACC3 and TACC3- ΔR protein elutes in the fraction of ~1200 and ~1100 kDa size, respectively (Fig. 18 and 20).

Tab. 29: Comprehensive physical properties of TACC3

Biophysical method		**TACC3**	**TACC3 + Thr.**		**TACC3-ΔR**
Theoretical size		70.468 kDa	TACC3-N7R, 45.259 kDa; TACC3-CC 25.209 kDa		52.323 kDa
Apparent size on SDS-PAGE gel		~120 kDa	TACC3-N7R ~ 95 kDa TACC3-CC ~ 25 kDa		55 kDa
MALDI-TOF		n.d.	TACC3-CC ~ 25.208 kDa		n.d.
SEC		1200 kDa	630 kDa (intramolecular complex)		1100 kDa
MALS		Mp~420 kDa	Mp~73 kDa		n.d.
AUC-SV		MW~108.9 kDa $S_{20,w}$ (S)~3.12 f/f0~2.55	Species 1 MW~52.5 kDa $S_{20,w}$ (S)~2.20 f/f0~2.22	Species 2 MW~61.9 kDa $S_{20,w}$ (S)~1.28 f/f0~4.26	n.d
CD	α-Helix	~55.51%	~53.22%		~43.28%
	β-Sheet	~10.36%	~10.11%		~14.43%
EM		Elongated fiber of 25-250 nm	n.d.		n.d

n.d., not done; $S_{20,w}$ (S), sedimentation rate at 20 ˚C temperature; f/f0, frictional ratio; SEC, size exclusion chromatography; CD, Circular dichroism D-spectroscopy; EM, electron microscopy

In an alternative method of absolute molecular mass determination by light scattering (MALS), purified TACC3 displays a molecular mass of 420 kDa at the maximum UV_{280} absorbance corresponding to its hexameric size (Fig. 35). However the TACC domain of murine TACC3 appears to have a parallel dimeric coiled coil structure (section 5.8.3). Under electron microscope after negative staining, TACC3 appears to contain fiber like elongated structure (Fig. 37) and similar to this an elongated shape was also predicted from the AUC-SV experiments (Tab. 28) because of slower sedimentation and high frictional ratio.

5.9 Subcellular localization and punctuate-like structures of overexpressed TACC3 and deletion mutants in interphase cells

As an important further step, the subcellular localization and potential aggregation of TACC3 deletion mutant was analyzed in transient transfection studies employing the pcDNA3.1-EGFP vector system and COS7 and HeLa cells. TACC3 (*H. sapiens* and *X. laevis*) and its TACC domain have been shown to localize in the cytoplasm and at the spindle apparatus (8,42,132). Therefore, to analyze the subcellular localization of murine TACC3 variants, pcDNA-3.1-EGFP based constructs (Tab. 24 and Fig. 15) were transiently transfected into COS7 and HeLa cells. After 48 h cells were fixed and stained with α-Tubulin specific antibodies (microtubules) and DAPI (DNA) and analyzed under a NIKON TE2000 microscope at a 40x magnification to visualize EGFP-fused TACC3 and its deletion mutants(Fig. 39 and 40).

As indicated in Fig. 39 and 40, punctuate like structures were typical in interphase cells when transfected with C-terminal EGFP-fused expression constructs for TACC3, TACC3-ΔN, and TACC3-ΔR. In case of TACC3-ΔCC2 and TACC3-ΔCC2, the punctuate structures were less prominent and rather weak. In the case of the TACC3-ΔCC the structures were completely absent. The expression and localization of the EGFP fused TACC3-ΔCC protein was comparable to control EGFP expression. This observation supports the finding of the formation of highly ordered polymeric structures in the cytosol consisting of several layers of a regularly spaced electron-dense matrix when TACC domain of TACC2 was overexpressed in HeLa cells (42). The reasons for the formation of these regular structures are still unknown, however, their formation clearly depends on the presence of the C-terminal TACC domain.

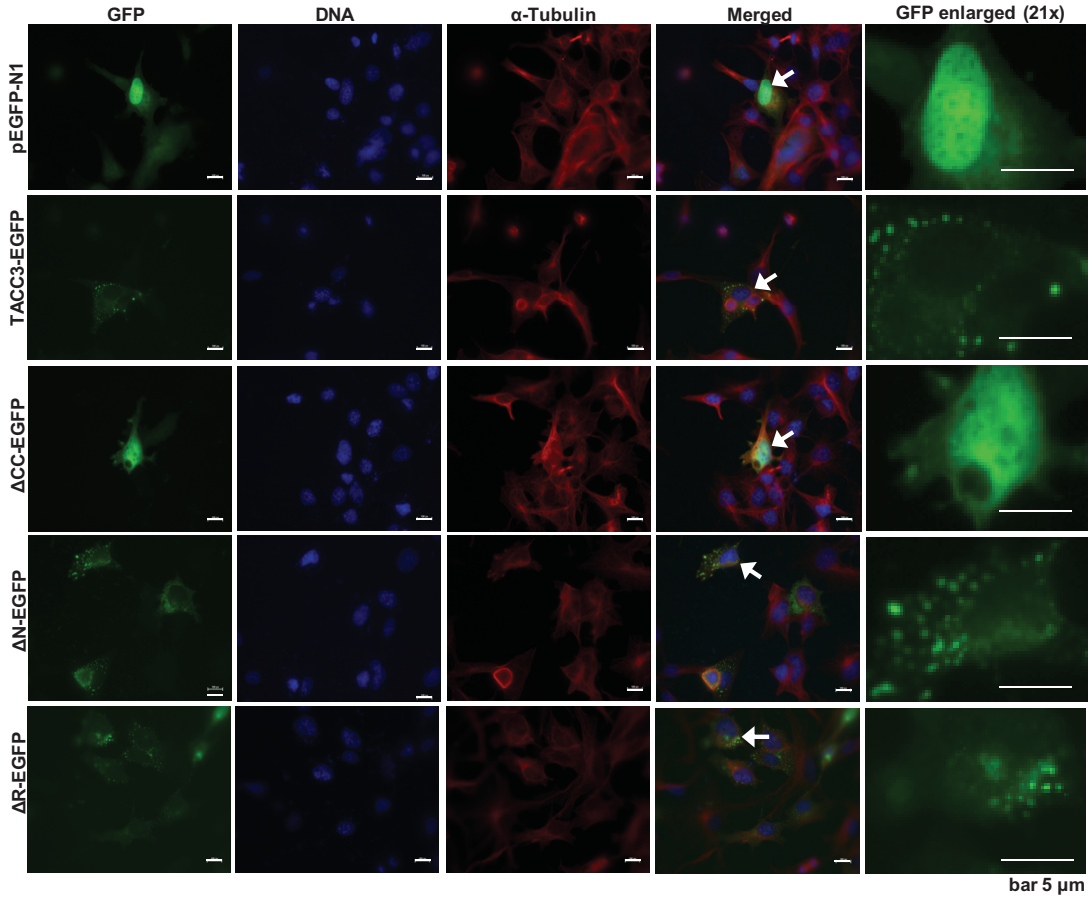

Fig. 39: Subcellular localization of EGFP-fused TACC3 variants during interphase in COS7 cells.
The green color indicates the expression and localization of EGFP and EGFP-fused TACC3 wild type and its variants. Blue and red colors indicate DNA (DAPI) and microtubules (α-tubulin) respectively. Arrows indicate the cell enlarged in the right panels (Images were collected and analyzed with the help of Mr. Madhurendra Singh)

Furthermore, as indicated in Fig. 39, TACC3, TACC3-ΔN, and TACC3-ΔR appeared to localize mainly in the cytoplasm but the TACC3-ΔCC mutant localized in both the cytoplasm as well as in the nucleus. Moreover, similar to TACC3-ΔCC, TACC3-ΔCC1 was also localized in both cytoplasm and nucleus (Fig. 40). In contrast, the localization pattern of the TACC3-ΔCC2 mutants was completely different from other TACC3 variants analyzed. It appeared to localize in a perinuclear manner (Fig. 40). The TACC3-ΔCC1 mutant contains the CC2 module (interacting with the seven repeat region) and the TACC3-ΔCC2 mutant contains the CC1 module (interacting with chTOG). The difference in the localization pattern of these two TACC domain mutants in interphase cells opens the questions whether CC1 and

CC2 take over additional regulatory and/or protein interaction function apart from the mitotic phase.

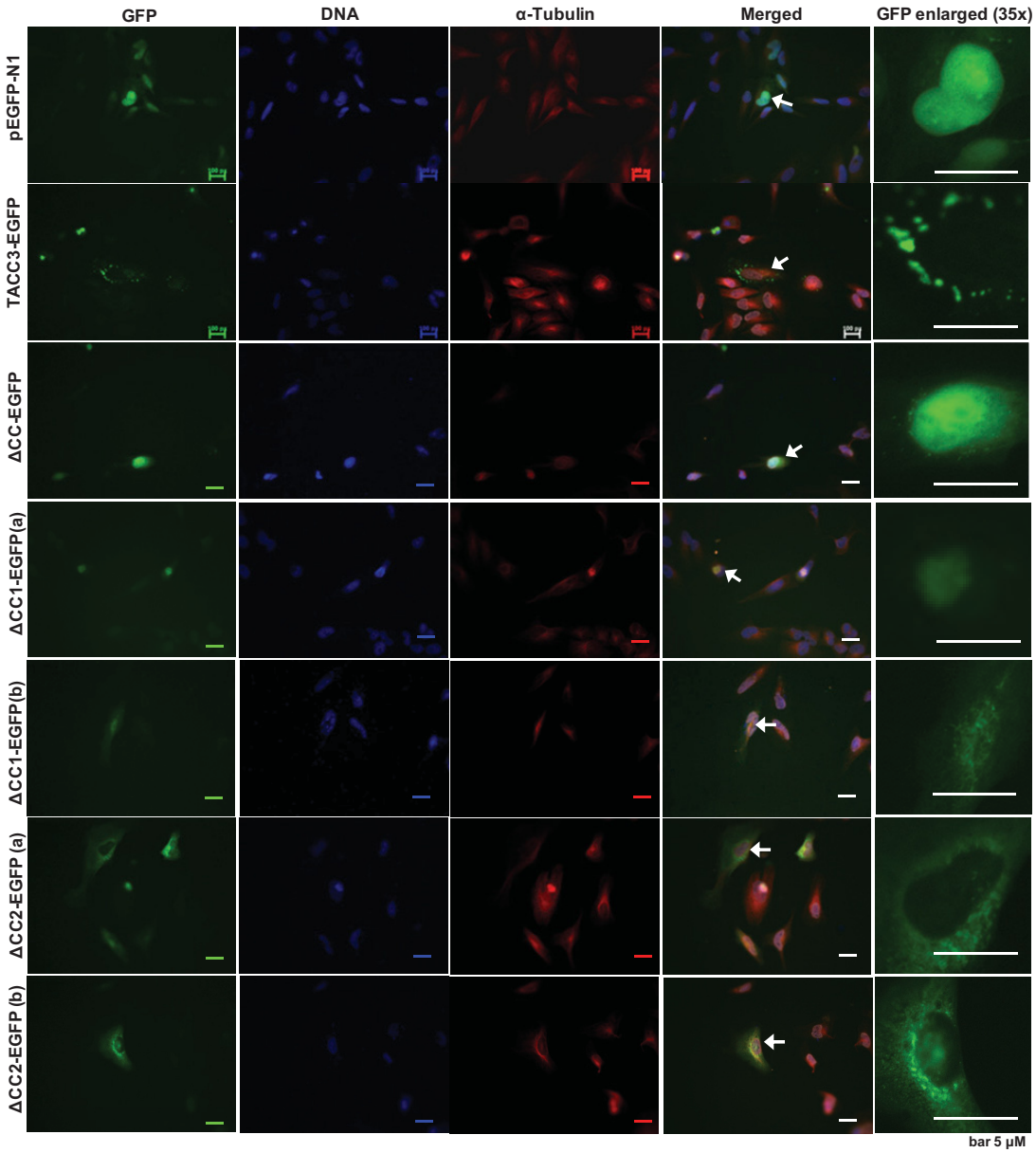

Fig. 40: Subcellular localization of EGFP-fused TACC3 variants during interphase in HeLa cells.

The green color indicates the expression and localization of EGFP and EGFP-fused TACC3 wild type and its variants. Blue and red colors indicate to the DNA (DAPI) and microtubule (α-tubulin) respectively. Arrows indicate the cell enlarged in the right panels (Images were collected and analyzed with the help of M.Sc. Madhurendra Singh)

5.10 Crystallization trials of the TACC3-chTOG-C protein complex, TACC3 deletion mutants, and chTOG-C

One of the main objectives of this work was to determine the crystal structure of TACC3 alone and/or in complex with its effector protein chTOG. Successful crystallization needs a homogeneous protein solution. Therefore, the single peak fractions from gel filtration column were collected and concentrated up to 5-7 mg/ml final protein concentration. Unfortunately, at higher concentration this protein precipitated and formed aggregates. Several thousands of QIAGEN screens in several trials were performed with purified TACC3 before and after thrombin cleavage and for the TACC3-chTOG-C complex (in collaboration with Dr. Astrid Höppner, Crystal and X-Ray Facility, HHU, Düsseldorf). In almost all conditions the protein (complex) precipitated and crystals failed to grow. Later we observed the fiber-like structure of different dimensions (Fig. 37) and a polydisperse or heterogeneous nature (Fig. 35) for the wild type TACC3 protein. Thus, this could have been literally the reason behind the unsuccessful crystallization trials for TACC3 alone and in complex with chTOG.

In order to identify a small stable domain of TACC3 with a homogeneous nature, partial protease digestion experiments with trypsin and chymotrypsin were performed. Trypsin and chymotrypsin were mixed with purified TACC3 in different ratios (1:1000, 1:500 and 1:100). The time dependent reaction was performed at 37˚C reactions and initiated by adding the enzyme and stopped by adding 2x Laemmli buffer followed by heat denaturation (90˚C). Samples were analyzed on 8.5% SDS-PAGE gels followed by CBB staining for the digested fragments.

As indicated in Fig. 41, purified TACC3 displays a clear resistance to digestion at lower concentration of trypsin (1:1000 and 1:500). However, at increased concentrations several fragments were obtained along with a small amount of the full-length protein. Similarly, TACC3 also resists the digestion by chymotrypsin even at its higher concentration of chymotrypsin (1:100, data not shown). The resistance to protease digestion could be possibly explained with the fiber-like structure of the purified TACC3 as observed by EM (Fig. 37).

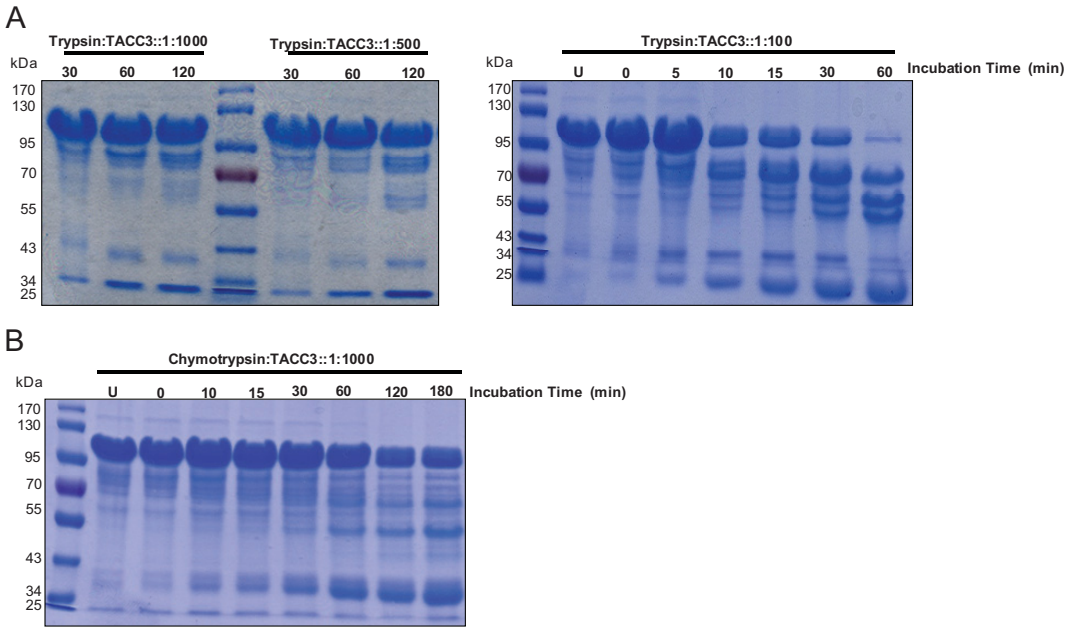

Fig. 41: Partial protease digestion of purified TACC3.
Murine TACC3 exhibits a relative resistance to trypsin (A) and chymotrypsin digestion. The ratios of the enzyme to the TACC3 protein in the reaction mixtures are indicated.

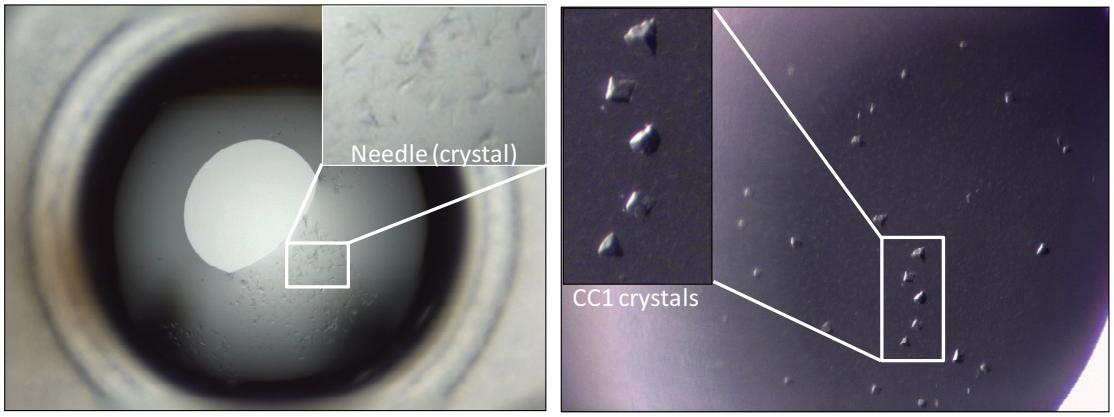

Fig. 42: Crystals of the CC1 module of the TACC domain.
Right panel displays the needle of CC1 crystal obtained during screening and right panel shows the big crystals of CC1 protein grown under the condition of salt with 30% ethanol. Inset shows the enlarged view of the growing crystals.

As a next step, different domains of TACC3 were subcloned and purified (Fig. 15 and 17). The isolated CC1 module of the TACC domain of TACC3 was found to be most stable, soluble and homogeneous and it showed a high affinity to the C-terminus of the microtubule polymerase chTOG (Fig. 27A). Therefore, new crystallization trials for the CC1-domain and

C-terminal domain of chTOG were performed. In almost all conditions, chTOG-C precipitated and crystals did not appear. Interestingly, three different crystallization conditions were identified for CC1, which appeared to form crystal needle (Fig. 42). After several trials of condition optimization, the quality and size of the crystals improved and CC1 appeared to form crystals with bipyramidal geometry under crystallization conditions of salt with 30% ethanol. However, the crystals were still fragile and sensitive to ethanol evaporation during picking up on a cryogenic loop. Therefore, further trials using the microbatch method under oil (prevents ethanol evaporation) is ongoing for obtaining stable crystals.

6 Discussion

The centrosomal TACC protein family member TACC3 is a multi-domain protein. TACC3 in complex with the microtubule polymerase XMAP215/chTOG regulates spindle microtubule assembly and its stability and dynamics during mitosis in a Aurora-A kinase dependent manner (8,25,33,42,133). The TACC domain of TACC3 and the C-terminus of XMAP215/chTOG mediates the interaction of both proteins. The TACC domain of Xl-TACC3 has been proposed to form a masked and unmasking may be required for its function at the spindle pole (49).

In the present work, TACC3, its deletion mutants and isolated domains were studied to identify the critical region of the TACC domain for binding to the C-terminus of the microtubule polymerase chTOG. Furthermore, the mechanism of masking of the TACC-domain of murine TACC3 by its N-terminal region and its further unmasking by intermolecular interaction have been investigated at molecular level.

TACC family members from different representative species have been elaborately studied in the last few years and also identified as an important regulatory molecules for spindle microtubule dynamics (30,34). TACC3 is associated with tumor development and was recognized as a new antineoplastic drug target (68). Therefore, in this work an attempt has been made to characterize various biophysical parameters of TACC3 to get insight into structural details of the molecule. Moreover, attempts have been made to crystallize full length TACC3 and small variants (alone and in complex with the C-terminus of chTOG) for X-ray structure determination. Needles (crystals) for the first half (CC1 region) of the TACC domain have been successfully obtained and their further crystal quality and condition optimization is currently ongoing.

Discussion

6.1 An overview of structural and functional characteristics of evolutionary conserved TACC family proteins

The TACC family members are identified by their conserved C-terminal CC-domain comprised of about 200 amino acids (34,41,42). In higher eukaryotes, TACC family members are evolved with longer N-terminal domain with very few helices or β-sheet like folded structure(s) (41,42,51). In contrast, TAC1 from *C. elegans* does not have a N-terminal domain and consists mainly of the TACC domain (24,41). The vertebrates evolved with three isoforms of TACC family proteins called TACC1, TACC2 and TACC3 (42,45,46). The TACC3 protein has a separate branch of evolution than TACC1 and TACC2 (41). However, very less information is available about the specific role of these three isoforms explaining their evolution in vertebrates.

About hundred residues from the N-terminus are conserved only in TACC3 isoforms and so far no interacting partner for this region is known (41). One regulatory Aurora-A phosphorylation site (S33 in Xl-TACC3 and S34 in higher vertebrate TACC3) is present in this conserved region (27,41). Several proteins like Msps/XMAP215 family members, FOG1, ARNT, MBD2, and hGCN5L2 have been identified to interact solely with the TACC domain thereby regulating various cellular processes (56,57,67,134-136). Interaction of the TACC domain with Msps/XMAP215 family members and the functions upon binding is found to be conserved during evolution (8,41,42). Furthermore, RNA processing elements (LSM7 and SmG), one adaptor protein TRAP, and the transcription regulator GAS41 were found to interact with the longer N-terminal region of the human TACC1 isoform (25,34,137,138). The transcription regulator GAS41 also interacts with TACC2 (138). Nevertheless, the actual role(s) of these interactions in an *in-vivo* setting are still unknown. In the N-terminal conserved region of human TACC3, several point mutations have been identified from breast cancer patients samples, but the significance of such mutations in tumor development is currently unknown (71).

Beside the rather conserved N- and C-termini of murine TACC3, the central region displays the semiconserved repeat region and two Aurora-A phosphorylation sites which are required for centrosomal localization of TACC3 and further in spindle microtubule dynamics

and stability during mitosis (27,33,34,60,66,70). The function of the repeat region was unknown prior to this work. In murine TACC3, the seven SPE-rich repeats are involved in an intramolecular interaction with the TACC domain thereby playing a critical role in TACC domain masking. Interestingly, each repeat contains one PXXP motif which mirrors a well characterized SH3-domain binding motif (Fig. 43) (119). However, SH3-domain containing interacting partners for TACC3 has not been described yet.

Although, the primary structure and function for TACC domain remained conserved during evolution, the TACC domains of mammalian TACC3 are different from TACC1 and TACC2 isoforms and from isoforms of other vertebrates in terms of the coiled coil pattern. As indicated in Fig. 43, the TACC domain of mammalian TACC3 isoforms is further subdivided by a coiled coil breaking peptide region (low COILS score region) into two modules called CC1 and CC2 (57).

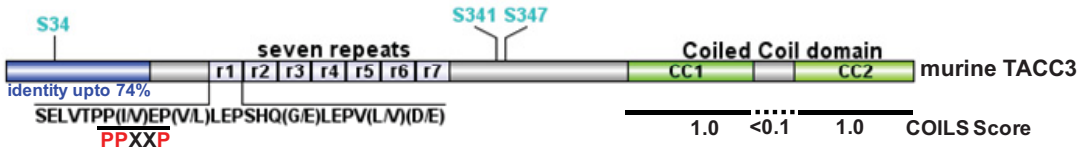

Fig. 43: Primary structure of murine TACC3.
The highly conserved TACC domain is present at the very C-terminus. The COILS program scan identifies a low score region at the center of the TACC domain which divides it into two separate modules, namely CC1 and CC2. About 100s of amino acid residues from N-terminus (blue) are also conserved in vertebrate TACC3 isoforms. The highly variable central region contains a serine (S), prolin (P), and glutamate (E)-rich seven repeat region (r1-7), each consisting of 24 amino acid residues. Each repeat contains a "PPXXP" motif. S34, S341 and S347 indicate the three different Aurora-A phosphorylation sites.

The amino acid residues in the CC2 module and coiled coil breaking motif are highly conserved in all TACC family members while the residues in the CC1 module are comparatively less conserved (Fig. 11). The highly conserved CC2 module of murine TACC3 is involved in an intramolecular interaction with the SPE-rich seven repeat region. This intramolecular interaction plays an important role in TACC domain masking through the longer N-terminal region of murine TACC3. A similar masking action has been also proposed for Xl-TACC3, as other vertebrate TACC family members contains analogous SPD-imperfect repeat in their longer N-terminal region (34,60). Therefore, based on this work it is proposed that an identical mechanism of masking of the TACC domain exist for the rest of the

vertebrate TACC3 proteins. In contrast, it is evident from this work that the TACC domain alone is unstable as it forms point-like structures when over-expressed and also purified protein precipitates even at very low concentration (42). Therefore, providing stability to the TACC domain could be a potential reason behind the masking action by the N-terminal domains. Intramolecularly, the less conserved CC1 module of the TACC domain interacts with the C-terminus of the microtubule polymerase chTOG (Fig. 28 and 30), and this interaction and function downstream remains conserved during evolution (8,34,41). In contrast, only one protein is known so far that binds to the rather conserved CC2 molecule, FOG1, a transcriptional co-repressor of GATA1 (134).

As mentioned earlier vertebrates evolved with three TACC family proteins of which the third member displays a separate evolutionary branch (41). The reason(s) behind the separate evolutionary branch for TACC3 isoforms are missing. Conservation of hundred residues from the N-terminus in all TACC3 isoforms and evolution of the low COILS score region or coiled coil braking motif in TACC domain of mammalian TACC3 makes it distinct from TACC1 and TACC2 isoforms and indicates clearly TACC3 isoform specific function. This hypothesis can be also be supported by the finding, that TACC3 knockout mice are embryonic lethal (10,13), however, TACC2 knockout mice have no obvious phenotype (139).

During mitosis subcellular localization of TACC3 depends on its phosphorylation by Aurora A kinase (25,33,76,140,141). In D-TACC, only one Aurora-A phosphorylation site (S863) is known, while in vertebrate TACC3 isoforms three sites have been identified (S33, S620 and S626 in Xl-TACC3; S34, S552 and S558 in Hs-TACC3; S34, S341 and S347 in Mm-TACC3) (32,33,66). Phosphorylation by Aurora A at S863 (D-TACC), S620 (Xenopus Maskin/TACC3), and S558 (human TACC3) is crucial and sufficient for their centrosome recruitment (27,32,33,141). In contrast, phosphorylation at S620 and S626 in Xl-TACC3 is important for Clathrin heavy chain binding and CHC-dependent spindle microtubule stability and dynamics (27,142). To date, the role of phosphorylation of the first serine residue (S33 in Xl-TACC3 and S34 in mammalian TACC3) by Aurora A are not well understood (27).

6.2 Biophysical properties of the TACC3 protein

All TACC family members have coiled coil α-helical regions at their C-terminus, while the N-terminal region contains few helices or β-sheet-like secondary structures (34,41,42,135). Structure(s) for any TACC family members or their domain is not available in the protein data bank (PDB). Current evidence suggests that the coiled coil structures can be present in the form of a dimer/trimer with a parallel/antiparallel fashion (143,144). In agreement with this, gel filtration, light scattering, and electron microscopy data suggest a higher oligomeric status for murine TACC3. On the other hand, AUC-SV experiments designates the dimeric elongated structure of the TACC domain of murine TACC3 (134). Besides this, intra-domain interaction studies using deletion mutants gave a clue for a parallel orientation of the TACC domain (Fig. 29).

Under the electron microscope, purified murine TACC3 protein displayed a fiber-like elongated structure of different dimensions (lengths and diameter). The smallest fibers had a length of about ~25-30 nm and this length is matching with the theoretical length for the TACC domain comprised of 200s amino acid residues (42). TACC3 forms unusual punctuates-like structures in a TACC-domain dependent manner, when transiently transfection and overexpression in COS7 and HeLa cells (Fig. 39 and 40). Similarly, Gergely et al also observed punctuate like structure and highly ordered polymers with regular spacing of 30 nm when GFP-fusion construct of TACC domain of TACC2 was overexpressed in HeLa cells (42). The overexpressed TACC3-ΔCC mutant did not appear to form any punctuate-like structures. Furthermore, deletion of the CC1 module of the TACC domain inhibited the punctuate-like structures formation in comparison to wild-type TACC3 while after deletion of the CC2 module, smaller and fewer point-like structures were still detectable in HeLa cells (Fig. 40). Moreover, purified CC2 domain from murine TACC3 shows the similar behavior at higher concentrations *i.e.* it forms 2-D sheet-like structures (Fig. 38), whereas purified CC1 domain was soluble even at higher (>5 mg/ml). Therefore, the punctuate-like structure formation in eukaryotic cells is dependent on the presence of the full length TACC domain of TACC3.

Lastly, on SDS-PAGE gels the denatured form of TACC3 always migrated abnormally higher than its actual size [(Mm-TACC3 (70 kDa) migrates like 120 kDa; Hs-TACC3 (90 kDa) migrates like 140 kDa)] (71). The acidic pI (~4.5) of the protein has been reasoned to be responsible for this abnormal migration behaviour. Interestingly, after deletion of the SPE-rich central repeat region, murine TACC3 migrates normally although still having an acidic pI~4.9 (Fig. 17). Therefore, the actual causes for such abnormal behavior are present in the SPE-rich seven repeat region and possibly in the polyproline stretches.

6.3 Masking and unmasking of the TACC domain through intra- and intermolecular protein interactions

Cell-based assays have been performed to analyze the expression and localization of TACC family members (34). In interphase, TACC3 protein localizes in the cytosol and during mitosis, Aurora-A regulates their localization to the centrosome and spindle microtubule (33,42). It was postulated that, the TACC domain of Xl-TACC3 is masked by its N-terminus, which then gets unmasked upon Aurora-A phosphorylation prior to centrosomal localization and function (49). Deletion mutant based interaction studies suggested that in murine TACC3 the SPE-rich seven repeat region interacts with the CC2 module and thus the N-terminal region indeed masking the TACC domain (Fig. 44). However, in contrast to the proposed “unmasking” role of Aurora-A (49), competitive protein-protein interaction demonstrated that chTOG binding to CC1 is sufficient to releases the intramolecular interaction between the CC2-domain and seven repeat region of murine TACC3 (Fig. 31 and 32). Consistent with a lack of an “unmasking” role of Aurora-A is lastly the observation, that Aurora-A phosphorylation of murine TACC3 is independent from its intra- or intermolecular binding (masked/unmasked) states (Fig. 33).

Altogether, the finding of this work suggest that TACC domain gets masked by its longer N-terminal region which is mediated through intramolecular interaction between the SPE rich seven repeat region and the CC2 module (Fig. 44). Microtubule polymerase chTOG binding to CC1 elicits conformational changes in the CC-domain that induces the release of intramolecular interaction and precludes the masking effect by the N-terminal region. Although this concept goes against the previous postulate of the unmasking through Aurora-A

phosphorylation(49), nevertheless, it gives a direct proof and principle for TACC3-chTOG interaction and regulation. Aurora-A phosphorylation of TACC3 or the TACC3-chTOG complex is responsible for their directional recruitment to the centrosome (66). This work, however, does not strike out a potential *in vivo* co-operative action of both chTOG binding to CC1 and Aurora A phosphorylation of TACC3 in the course of unmasking of the CC-domain.

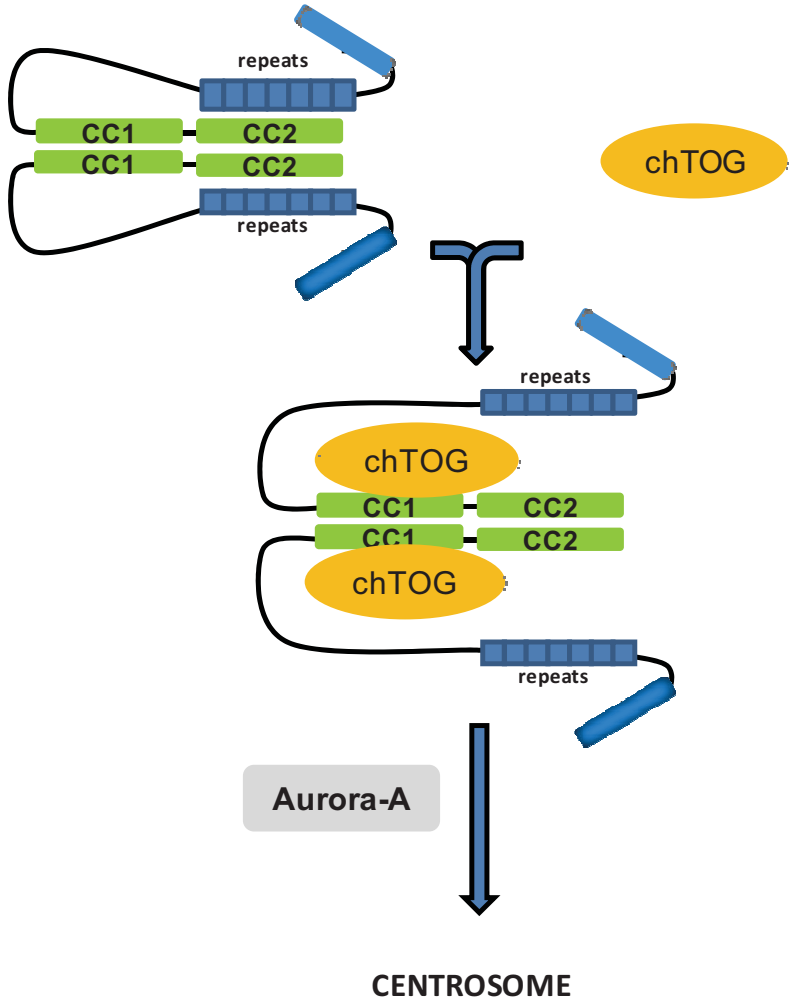

Fig. 44: Model for the masking and unmasking of the TACC domain and recruitment of the TACC3-chTOG complex to the centrosome.
The intramolecular interaction between seven repeat region and CC2 mediates the masking of the TACC domain. chTOG binding to CC1 precludes the intramolecular interaction and releases the masking effect on the TACC domain. Finally, Aurora A phosphorylation of TACC3 or the TACC3-chTOG complex triggers recruitment to the centrosome.

6.4 Molecular insight into TACC3 action and regulation of mitosis

To date the cellular role of TACC family members in mitosis, particularly in spindle microtubule dynamics, have been well described. Alp7 (*S. Pombe*), TACC (*D. discoideum*) and TAC1 (*C. elegans*) are the simplest members of this family which are known to interact with the XMAP215 ortholog Alp14, CP224, and Zyg9 respectively (24,51,92). D-TACC (*D. melanogaster*) along with the three vertebrate isoforms TACC1, TACC2 and TACC3 are the representative members of this family in higher eukaryotes (42,46). All of them are known to interact with their XMAP215 homologues via their conserved TACC domain and regulate spindle microtubule stability and dynamics (8,34). The TACC family members in higher eukaryotes are different from the simplest eukaryotes with having a longer N-terminal domain and a role of this domain has been shown in this work to mask the TACC domain (34,49).

The expression patterns of the three mammalian TACC protein isoforms (TACC1, TACC2, and TACC3) have been extensively studied. In contrast to the rather postmitotic expression of TACC1 and TACC2, TACC3 is found in high level in particularly in regenerating and proliferating tissues, hematopoietic cells, epithelial cells, testis and ovary (13,58,70). High TACC3 expression levels are very prominent in embryonic developmental stages. Consistent with this, TACC3 knockout mice are embryonically lethal, a phenotype accompanied by reduced cell numbers due to mitotic defects and apoptosis (13). A study based on the generation of several conditional, null and hypomorphic TACC3 mouse mutants demonstrated that TACC3 is essential for the proper cell division of sclerotomal mesenchymal cells during formation of the axial skeleton (10). Cellular depletion of TACC3 in murine NIH3T3 cells results into $p21^{WAF}$ mediated cell cycle arrest in the G_1 and G_2 phase (11). Consistent with this, TACC3 knockdown in human MCF7 cells triggers cell cycle arrest through induction of premature senescence (69). Comparable with other cell cycle regulatory proteins, TACC3 expression is also increased and decreased in a cyclic manner during cell cycle progression. Minimal expression of TACC3 has been observed during interphase, while in G_2/M phase TACC3 reaches highest level before it again returns to basal amounts by the end of the cell cycle (13). Taken together, these reports altogether summarize the critical role of TACC3 in cell division during the mitotic phase of the cell cycle.

Discussion

The information available about sub-cellular localization of TACC proteins during interphase of the cell cycle is rather scanty. Experiments based on human TACC protein isoforms and Xl-TACC3 indicate their nuclear localization (42,91). During interphase, all three human TACC isoforms localize in the cytosol and then are found in particular during mitosis at the centrosome with a slightly different distribution pattern (33,42,132,133,145). This observation together with N-terminal conservation of 100s amino acid residues only in TACC3 isoforms pinpoints to the non-overlapping function(s) of all three TACC protein isoforms in human and other vertebrates (34). TACC3 isoforms localizes to the centrosome and along spindle microtubules in an Aurora-A phosphorylation dependent manner (25,31,33,76,91). Thereby being crucial for microtubule dynamics (polymerization and depolymerization), TACC3 is essential for spindle dependent chromosome alignment and mitotic survival (8,29,34).

In transient cell transfection studies using HeLa and COS7 cells, Mm-TACC3 appears to form punctuate-like structures in TACC domain-dependent manner in interphase cells (Fig. 39 and 40). Similar structures have also been observed for the TACC domain of Hs-TACC2 in HeLa cells (42). Deletion of the CC1 or CC2 modules of the TACC domain of Mm-TACC3 inhibits the punctuate structure formation as compared to wild type TACC3-GFP. During mitosis, the TACC domain alone is sufficient to colocalize with chTOG at the centrosome and spindle microtubules (42,132). This arise possibly the question for the role of the longer N-terminal region besides the masking action on the TACC domain. In this regard, this work explicitly describes the role of the N-terminal region of Mm-TACC3 in intramolecular interaction and TACC domain masking which is possibly required for TACC domain stability before the TACC-chTOG complex formation.

In a first subcellular localization study in HeLa cells during the metaphase stage employing GFP-fusion proteins (data not shown), both TACC3-ΔCC1 and TACC3-ΔCC2 deletion mutants were found to localize at the centrosome and along the spindle. However, the TACC3 wild-type protein and the TACC3-ΔCC2 mutant both localized at the centrosomes and along spindle microtubules, while TACC3-ΔCC1 mutant was predominantly found at the centrosomes and rather weekly at spindle microtubules. Moreover, the GFP fused TACC3-ΔCC mutant (lacking the TACC domain) was also examined and the localization pattern was found to be similar to the TACC3-ΔCC1 mutant. The result was surprising, given a former

report that the GFP-fused TACC domain of Xl-TACC3 was capable to localize *per se* to the centrosome, where as the GST-fused N-terminal domain of Xl-TACC3 failed to do so (132). Similar to the wild-type protein TACC3-ΔCC, TACC3-ΔCC1, and TACC3-ΔCC2 all mutants still contain the three Aurora-A phosphorylation sites which regulate both directional recruitment of TACC3 to the centrosome as well as binding to the Clathrin heavy chain (CHC). Therefore, a possible phosphorylation of the GFP-fused TACC3-ΔCC mutant and its further binding to CHC may explain its centrosomal recruitment independent of the TACC domain. Thus, it will be important to analyze the localization of GFP-fused phosphoinhibitory and phosphomimetic (3A and 3E) mutants of TACC3-ΔCC during mitosis.

The interaction of TACC3 with the processive microtubule polymerase XMAP215/chTOG is well described (23,92). This function upon complex formation has been implemented in the regulation of spindle microtubule stability and dynamics during mitosis (8,27,33,49,66,132). However the role of the adapter protein TACC3 in TACC3-chTOG complex and in spindle microtubule stability and dynamics is not fully understood. The N-terminus of XMAP215/chTOG proteins contains two to five TOG domains. TOG domains bind to αβ-tubulin heterodimers and add them to the plus end of spindle microtubules in the GTP bound form (20,73,75). The C-terminus of microtubule polymerase chTOG interacts with the CC1 module and unmasks the TACC domain of murine TACC3 (Fig. 28 and 30). Thus, TACC3 may simply act as an adaptor protein for chTOG thereby forming a microtubule stabilizing factor as suggested previously (8). Aurora-A phosphorylation TACC3 then recruits this microtubule stabilizing factor to the centrosome (Fig. 6), where it forms a complex with CHC and counteracts the microtubule destabilizing activity of the kinesin XKCM1/MCAK (27,33,146,147). Another study based on the use of XMAP215 deletion mutants in *Xenopus laevis* egg extracts supports thereby the role of the N- and C-terminus of XMAP215 in microtubule polymerization (rescue) and depolymerization (catestrophe) respectively (75). Therefore, one possible and crucial role of TACC3 could be in the engagement or scavenging of the catestrophe promoting C-terminal domain of chTOG thereby promoting rescue events through the N-terminal domain of chTOG.

The Clathrin triskelion is a vesicle trafficking protein complex (148), that plays a critical role during mitosis especially in spindle microtubule stability at the centrosome (Fig. 6) (26-28,30,81,82). It also interacts with TACC3 in an Aurora-A phosphorylation dependent

manner (27,81). Binding of CHC to TACC3 depends on its Aurora-A phosphorylation at the S552 and S558 residues in human TACC3 (S620 and S626 in Xl-TACC3) (27,146). Whereas, phosphorylation of S558 of Hs-TACC3 (S626 of Xl-TACC3 or S347 of Mm-TACC3) regulates their centrosomal localization (33). The domain proximal to the N-terminus of CHC binds directly to the Aurora-A phosphorylation sites near to the TACC domain of TACC3 (28,146). The C-terminus of CHC is known to interact with Clathrin light chain (CLC) in order to form the triskelion complex (149). Thus, the role of the TACC3-CHC interaction has been proposed in cross linking and stabilization of spindle microtubule bundles at the centrosome (28). In contrast, unphosphorylated TACC3 form has been shown along the spindle microtubules and at their plus ends (33). Further studies of phosphomimetic mutants of TACC3 and the inhibition and silencing of Aurora-A kinase function revealed that TACC3 mislocalizes from both the centrosome and the spindle microtubules (33,66). These observations collectively call for the presence of an unknown protein phosphatase (PP), that dephophorylates TACC3 after Aurora-A phosphorylation for the subsequent spindle microtubule localization of TACC3.

In *D. melanogaster*, role of the Mars protein has been implicated in linking of centrosomes to spindle microtubules and in proper spindle organization during the rapid mitotic cycles in early embryogenesis (150). Interestingly Mars directly interacts with protein phosphatase 1 (PP1) and thereby mediates the controlled dephophorylation of D-TACC (151). Tousled-Like Kinase (TLK) functions in parallel to Mars and their balance activity is required for cells to progress correctly through mitosis, thus ensuring chromosomal fidelity (152). In vertebrates, HURP (hepatoma up-regulated protein) is a Mars related protein and constitute a part of the Ran-dependent complex involved in spindle formation (150,153,154). It controls spindle stability and dynamics to achieve an efficient kinetochore capture, timely chromosomal congression and proper interkinetochore tension during mitosis (150,155). Also, HURP gets phosphorylated and stabilized by the mitotic kinase Aurora-A, and was proposed to possess a transforming function during mitosis (156,157). However, a probable role of HURP in controlled dephosphorylation of TACC3 is not determined yet.

As discussed before, similar to various other cell cycle regulatory proteins, the level of TACC3 in cells is tightly regulated throughout the cell cycle (11,13,33). Followed by interphase and/or during the G_2/M-phase TACC3 level are dramatically upregulated and

decline rapidly to a minimal level by the end of division (13). Importantly, the pattern of TACC3 level remains in line to that of several cell cycle marker proteins like cyclin B1, Cdh1, and Cdc20 (35,158,159). All these proteins are known to be degraded during mitotic exit *via* the proteasomal degradation pathway (35,159). Therefore, proteasomal degradation of TACC3 protein has also been proposed during mitotic exit. In HeLa cells, TACC3 has been shown to interact with Cdh1 which facilitates the degradation of several mitotic proteins thereby activating the E3 ubiquitin ligase APC/C. It was observed that Cdh1 promotes ubiquitination of TACC3 and its further degradation in cells during mitotic exit (35). Overall, one can assume that degradation of TACC3 "releases" the catastrophe promoting domain of XMAP215/chTOG, thereby catalyzing the required depolymerization of spindle microtubules during mitotic exit.

6.5 TACC3 interaction network and regulation of cellular processes

To date, several attempts from different model organisms describe a direct or indirect interaction of the TACC family members with proteins involved in the microtubule dynamics, and in the regulation of transcription and translation. As listed in Tab. 30, a list of proteins known to interact with TACC family members in higher eukaryotes (*D. melanogaster* and vertebrates) and the regulation of various cellular processes are briefly described.

Tab. 30: Interacting partners of TACC family members in higher eukaryotes

TACC Family members	Interacting Partners	Regulation of cellular process after interaction	Ref.
TACC (*Drosophila melanogaster*)	Msps	Microtubule dynamics	(23)
	Aurora-A kinase	TACC-Msps activation	(32)
	Cnn (centrosomin)	Recruitment of TACC/Msps complex and γ-tubulin to centrosomes	(160)
	Mars	Attachment of centrosomes to mitotic spindle	(150)
Maskin (*Xenopus laevis*)	XMAP215	Microtubule anchorage at centrosome	(33,49)
	Aurora-A kinase	Centrosome dependent microtubule assembly	(33,91)
		Control of sequential protein synthesis during oocyte maturation	(161)
	Importin-β	Nuclear localization	(91)
	CPEB and eLF-4E	Translation regulation	(62)
TACC3	chTOG/CKAP5	Spindle pole organization	From this

(*Mus Musculus*)	Aurora-A kinase	Cell cycle regulation and spindle pole organization	work
	FOG1	FOG1 localization and transcription regulation	(56)
	ARNT	n.d. (proposed function: transcription regulation)	(58)
	DOCK7	Interkinetic nuclear migration and cortical neurogenesis	(84)
	Cep120	Interkinetic nuclear migration and neocortex development	(83)
TACC1 (*Homo sapiens*)	chTOG/CKAP5	n.d. (proposed function: mRNA translation, cell division in conjugation with spindle pole organization)	(25)
	Aurora-A kinase	n.d. (proposed role in centrosomal localization and spindle pole organization during anaphase and telophase)	(25)
	Aurora-B kinase	n.d. (possible role in cytokinesis)	(162)
	TDRD7 (tudor)	n.d.	(25)
	LSM7 and SNRPG	n.d. (proposed role in mRNA processing and homeostasis)	(137)
	YEATS4	n.d. (proposed role in transcriptional regulation)	(138)
TACC2 (*Homo sapiens*)	chTOG/CKAP5	n.d. (proposed function in microtubule dynamics)	(163)
	YEATS4	n.d. (proposed role in transcriptional regulation)	(47)
	TTK	n.d. (proposed role in mitotic spindle maintenance)	(164)
TACC3 (*Homo sapiens*)	chTOG/CKAP5	Spindle pole organization	(8)
	Aurora-A kinase	Cell cycle regulation and spindle pole organization	(25,66,140)
	NDEL1	Centrosomal maturation and mitotic entry	(165)
	CLTC	Centrosomal localization	(27,146)
	Notch4/Int3 and CDC10/Ankyrin repeat	Regulation of notch signaling	(166)
	TSC2	Maintenance of nuclear envelope structure and control of cell division	(61)
	DOCK7	Interkinetic nuclear migration and cortical neurogenesis	(84)

Ref., References; n.d., not described

Several proteins are known to interact with the TACC domain of TACC family members (Fig. 45), however only few proteins have been found to interact with the highly variable N-terminal region (34). Independent from the conserved interaction with

XMAP215/chTOG, the TACC domain of murine and human TACC3 isoforms has been described to interact with FOG-1, ARNT and MBD2 proteins thereby potentially regulating transcription processes (56-58,67,134,135).

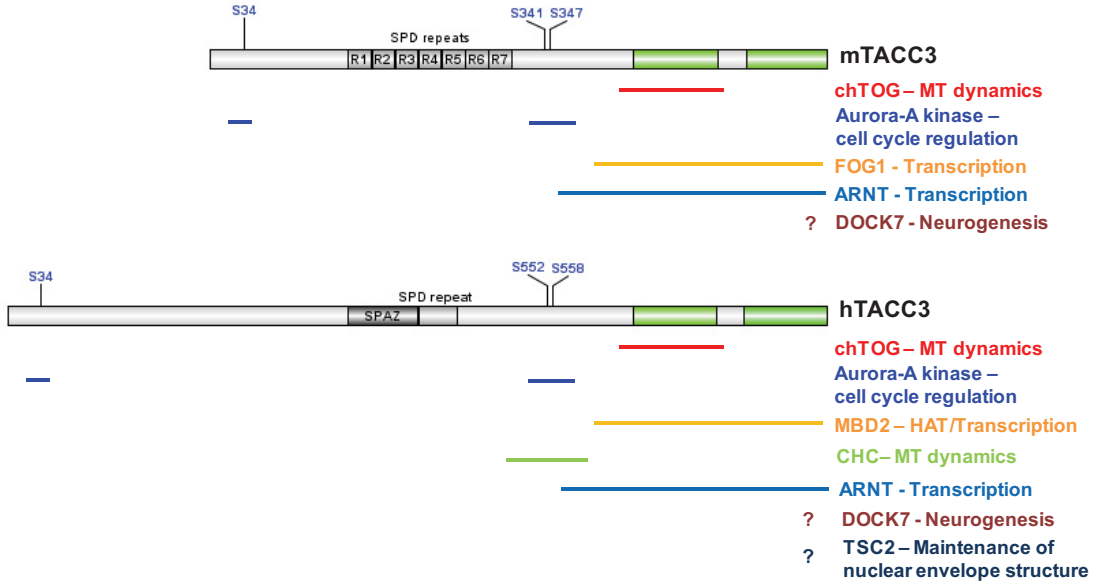

Fig. 45: Proteins known or proposed to interact with different domains of human and murine TACC3.
Most of the partner proteins bind to the CC-domain (green) of TACC3. The DOCK7 and TSC2 binding domain in TACC3 is currently unknown.

Recently, three new TACC3 interacting partners (CHC, TSC2 and DOCK7) of TACC3 have been described. CHC was found to interact with pTACC3 and the role upon interaction has been implicated in the stability of centrosomal spindle microtubule bundles (30,82,146). Interaction of TSC2 with TACC3 regulates the maintenance of nuclear envelop structure during cell division (61). DOCK7 (Dedicator of cytokinesis 7), a member of the DOCK180 protein family, is the latest described interaction partner of TACC3. DOCK7 binding to TACC3 regulates the interkinetic nuclear migration and cortical neurogenesis in human and mouse brain development (84). Lastly, the TACC domain from TACC1 and TACC2 isoforms interacts to another transcriptional regulator, hGCN5L2 however its function upon interaction is unknown (64). Thus, the interacting network of TACC family members is currently in growing stage. This raises an interest to find out the new interacting partner and multifunctional roles of TACC family members in various cellular processes.

6.6 Pathobiological relevance of TACC3 function and dysfunction

Initially all three TACC genes have been identified from human breast cancer patient samples and later on found to be physically linked with corresponding FGFR regions on three different chromosomes (41,45,46). The FGFR loci of these chromosomes are linked to the development of cancer and many other pathological conditions in human (167). Interestingly, human and mouse TACC3 demonstrated that the gene is upregulated in various cancer types. Thereby it alters the controlled cell growth and differentiation processes (12,25,45,56,85,87,168-170). Along with FGFR3, MMSET and $p21^{WAF}$, the TACC3 expression has been correlated with the multiple myeloma phenotype (89). Single amino acid variants of TACC3 have been identified from various human cancer patients sample screening (71,85,171). Expression of TACC3 and its upstream regulator Aurora-A has shown to be deregulated in thyroid cancer tissues (172,173). Recently, in brain tumor glioblastoma multiforme, a small subset (3.1%) of a transforming in frame fusion of FGFR and TACC genes and their involvement in a lethal form of tumor development has been reported (88). A single nucleotide polymorphism in the TACC3 gene (4p16 human chromosomal locus) has been identified in a Chinese population being associated with a increased risk of bladder cancer (90).

Alterations in microtubule dynamics and associated protein function disrupt the mitotic cell division process (34,42,174). Abnormal TACC3 expression and therefore function leads to enhanced centrosomal abnormalities, activation of apoptotic and senescence programs, and loss of anchorage-independent growth (13,42,69,135,175). *In vitro* TACC3 depletion induces the multipolar spindle formation and causes mitotic arrest followed by apoptosis. These evidences collectively suggest that TACC3 is a transforming but also therapeutically susceptible component of the spindle apparatus. Therefore it could be a promising therapeutic target for anti-mitotic and cancer chemotherapy. Interestingly, magnetic resonance imaging (MRI) based study has been implicated that, conditional loss of TACC3 *in vivo* in tumors caused there massive regression and apoptosis as recently shown in a model of mouse thymic lymphoma (68).

6.7 Conclusions and perspectives

Based upon current and previous knowledge, here a sequential model is proposed for the role of TACC3 in spindle microtubule stability and dynamics (Fig. 46). The G_2/M-phase is characterized by a huge change in microtubule arrangement and upregulation of the TACC3 expression level (13). This work stay grounded to explain the events of the spindle assembly factor TACC3 prior to its centrosomal recruitment. Immediately after *de novo* synthesis in the cell, murine TACC3 stays in a masked state and seems to be required for the stability of the TACC domain. The masking action is caused by intramolecular interaction between the central SPE-rich seven repeats and the CC2 module of the TACC domain. Furthermore, this work also identified the CC1 module as a chTOG interacting motif, with this interaction precluding the intramolecular interaction of TACC3 and thus unmasking the TACC domain. Our data indicate that Aurora-A phosphorylation of TACC3 is independent of intra- and intermolecular interaction status. TACC3 interacts with the C-terminus of chTOG, which has been shown to be involved in microtubule depolymerizing activity (75,92). The N-terminus of chTOG binds directly to microtubules and catalyze their polymerization (9,20,73,174). Considering all together, it seems that binding of the TACC domain to chTOG "engages or captures" its "catastrophe" promoting domain (75). This interaction also leads to the inactivation of XKCM1/MCAK depolymerizing activity (33,147).

As an important regulatory step, Aurora-A phosphorylation of TACC3 recruits the TACC3-chTOG complex to the centrosome, where it catalyzes spindle microtubules nucleation and elongation (32,33). The Mars-PP1 complex in *D. melanogaster* catalyzes the controlled dephosphorylation of D-TACC (151). This suggests a similar role for its vertebrate homologue, the HURP protein that is also a target of the mitotic kinase Aurora-A (150,156). This dephosphorylation event potentially leads to recruitment of TACC3-XMAP215/chTOG complex to the plus end of microtubule and along spindle microtubules. At the plus end of spindle microtubules, the complex upholds the rescue or polymerization process. All these events seem to be tightly regulated by Aurora-A kinase. At the time of the mitotic exit or during anaphase, Cdh1 interacts with TACC3 and endorses its ubiquitination and proteasomal degradation. Therefore, this releases the catestrophe promoting C-terminal domain chTOG thereby switching the balance towards depolymerization events of spindle microtubules.

Thus, TACC3 regulates spindle microtubule stability and their dynamics (rescue and catastrophe) during mitosis.

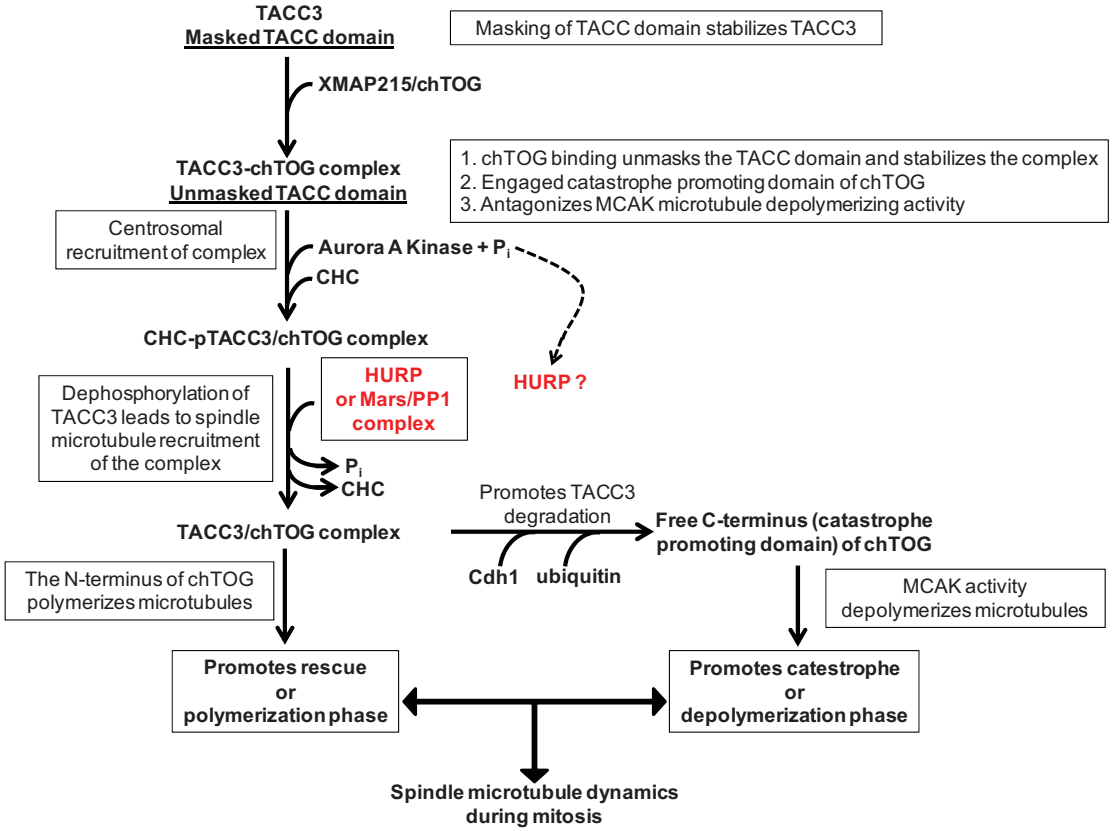

Fig. 46: Schematic model for the role of TACC3 in spindle microtubule dynamics during mitosis.

The literature reveals an importance of Aurora-A dependent regulatory mechanisms and action of TACC3-chTOG complex during mitosis. The proteins along the Aurora-A kinase-TACC3-chTOG axis have been shown to be involved in the development of many tumor types (65,68). This work clearly shows that the CC1 module of murine TACC3 acts as a minimal binding domain for chTOG. Therefore, subcellular localization studies on CC1 and CC2 deletion mutants of human and murine TACC3 in mammalian cells will provide further insight about the unmasking mechanism and the interaction and colocalization with chTOG and the localization pattern of the TACC3-chTOG protein complex at the mitotic spindle apparatus. Additional studies on HURP, a Mars related protein, in context to TACC3 dephosphorylation will provide a new dimension to the current understanding of the spindle microtubule dynamics process.

Discussion

This work fruitfully characterized murine TACC3 at the biochemical and biophysical level. Intramolecular interaction or TACC domain masking in murine TACC3 was identified *in vitro* by subjecting purified TACC3 and the TACC3-ΔN and TACC3-ΔR mutants to thrombin cleavage at the internal thrombin site. Here, the CC2 module and the seven repeat region mediated the intramolecular interaction while the CC1 module of the TACC domain showed a strong intermolecular interaction with the C-terminus of chTOG. Therefore, thrombin cleavage and further *in vitro* analysis of the purified TACC3-ΔCC1 and TACC3-ΔCC2 mutants will provide a further proof for intramolecular interaction.

Lastly and importantly, this work has crystallized for the first time the minimal stable CC1 domain of murine TACC3. Therefore, the X-ray structure determination of CC1 alone and in complex with its interacting domain from chTOG will provide the required atomic level details for potentially designing an antimitotic drug targeting TACC3-chTOG interaction as basis for a novel antineoplastic approach.

7 Summary

The centrosomal protein TACC3 belongs to the TACC (Transforming Acidic Coiled Coil) family of mitotic spindle-associated proteins, which display a highly conserved C-terminal coiled coil (TACC) and protein interaction domain and a rather functionally uncharacterized N-terminus. TACC3 is critical in particular for embryonic development and stem cell proliferation, a phenotype that became evident upon TACC3 gene inactivation in the mouse.

TACC3 is highly expressed in a cell cycle-dependent manner during the G_2/M phase where its centrosomal localization depends on its phosphorylation mediated by the mitotic kinase Aurora-A. Functionally, TACC3 forms a complex with the microtubule polymerase chTOG (colonic and hepatic Tumor Overexpressed Gene) thereby regulating spindle microtubule stability and dynamics and hence correct chromosomal segregation. It was proposed that the TACC domain of the *X. laevis* TACC3 homologue is being "masked" by an unknown molecular mechanism and that phosphorylation by Aurora-A kinase may "unmask" the C-terminus possibly required for binding to XMAP215, the chTOG homologue of *X. laevis*. However, despite this, the modus and directionality of this protein interaction that is mediated through the TACC domain of TACC3 and the C-terminus of chTOG/XMAP215 were largely uncharacterized at the molecular level at the beginning of this work.

Therefore, GST-fused murine TACC3 deletion mutants and single fragments as well as the C-terminal part of murine chTOG were overexpressed in *E. coli*, purified, and thereafter subjected to an in-depth analysis regarding their molecular interaction, Aurora-A mediated phosphorylation, and lastly subcellular localization employing various biochemical, biophysical, and cell imaging-based methods, the latter following transient transfection of GFP-fused constructs. In particular, the following major questions were addressed:

(I) Does the N-terminus of TACC3 mask the C-terminal TACC domain *via* an intramolecular interaction? Which domain of TACC3 is involved in such an intramolecular interaction?

(II) How does the TACC domain interact with the C-terminus of chTOG? Which part of the TACC domain is involved in this intermolecular interaction? Does the interaction of chTOG with the TACC domain interfere with an intramolecular interaction and thus TACC domain masking?

(III) Is Aurora-A-mediated phosphorylation of TACC3 dependent from its intramolecular ("masked") or intermolecular (chTOG-bound) interaction state?

(IV) What structural insight can be gained from the biophysical analysis of TACC3?

Subjecting murine TACC3 to an in-depth *in silico* comparison within the vertebrate and mammalian TACC family revealed that TACC3 contains (i) a conserved N-terminal domain of approximately 100 amino acids, (ii) a central serine/prolin-rich repeat region, and (iii) a

Summary

TACC domain consisting of two previously not described coiled coil modules, CC1 and CC2, separated by a breaking peptide region. CC2 displays thereby a clearly higher conservation than CC1.

Based on these findings and addressing the first point, it is shown in protein-protein interaction studies using complementary methods (pulldown, gel filtration analysis, ITC) that the central repeat region undergoes a specific intramolecular interaction with the CC2 module of the TACC domain of TACC3 thereby likely mediating the previously proposed masking function. In contrast, the CC1 module within the TACC domain binds selectivily to the C-terminus of chTOG and thereby precludes the intramolecular interaction between CC2 and the central repeat region. With this, intramolecular "masking" of the TACC domain may regulate its stability prior to chTOG binding. Interestingly, in *in vitro* kinase assays, TACC3 was efficiently phosphorylated by Aurora-A independent of its intra- or intermolecular interaction status thereby suggesting that, in contrast to its critical function in centrosomal recruitment of TACC3 or the TACC3-chTOG complex, Aurora-A does not play a decisive role in the "unmasking" action of the TACC domain prior to chTOG binding. Thus, these findings overall establish a novel role of the TACC domain of TACC3 where CC1 and CC2 as two functionally diverse modules which direct and determine TACC3-chTOG protein complex formation probably prior to its Aurora-A regulated centrosomal localization.

Purified murine TACC3 was characterized at a biophysical and structural level. Employing various methods, including gel filtration, multi angle light scattering (MALS), analytical ultracentrifugation (AUC), and electron microscopy (EM) clearly revealed an elongated, fiber-like oligomeric structure of full length TACC3 with the coiled coil-containing TACC domain displaying a parallel α-helical orientation throughout the CC1 and CC2 modules. Interestingly, the oligomeric/multimeric nature of TACC3 could be confirmed by transient transfection studies of TACC3-GFP fusion proteins in eukaryotic cells. The occurrence of punctuate-like structures in interphase cells was thereby dependent on the presence of the TACC domain and clearly reduced when either one of the CC modules was deleted. In first crystallization attempts crystals for the CC1 module could be successfully generated which are now being optimized and subjected to molecular structure determination.

The clinical relevance of human TACC3 alterations becomes increasingly evident. Various alterations in TACC3 gene expression have been linked to cancer development and several TACC3 point mutations have been identified in primary human tumors. Recently, a Fibroblast Growth Factor Receptor 3-TACC3 gene fusion with transforming activity has been reported in glioblastoma patients. Thus, future work will focus on the molecular elucidation of the mechanistic impact of cancer associated structural TACC3 alterations on TACC3-chTOG interaction and function and ultimately chromosomal segregation and stability. In particular, blocking the molecular CC1-chTOG binding interface may represent a candidate anti-neoplastic approach against TACC3 and chTOG overexpressed in tumors.

8 Zusammenfassung

Das zentrosomale Protein TACC3 ist ein Mitglied der TACC (*Transforming Acidic Coiled Coil*) Proteinfamilie, deren Mitglieder am mitotischen Spindelapparat lokalisieren und sich strukturell durch eine hochkonservierte, C-terminale *coiled coil*-Proteininteraktionsdomäne (TACC-Domäne) auszeichnen. Der N-Terminus der TACC-Proteine ist hingegen funktionell unverstanden und wenig charakterisiert. TACC3 nimmt eine essentielle Rolle insbesondere in der Embryonalentwicklung und Stammzellproliferation ein, was durch die embryonale Letalität TACC3-defizienter Mauslinien deutlich wurde.

TACC3 wird in seiner Expression zellzyklusabhängig reguliert und hierbei in hohen Mengen während den G_2/M-Phasen vorgefunden. Aurora-A-Kinase-vermittelte Phosphorylierung von TACC3 reguliert hierbei dessen subzelluläre Lokalisation und zentrosomale Rekrutierung. Funktionell geht TACC3 einen Komplex mit der Mikrotubulipolymerase chTOG (colonic and hepatic Tumor Overexpressed Gene) ein und reguliert dadurch die Stabilität und Dynamik von Spindelfasern und somit eine gleichmässige chromosomale Segregation während der Zellteilung. Literaturbefunde liesen vermuten, dass die TACC-Domäne des TACC3-Homologs aus *X. laevis* durch einen unbekannten Mechanismus in einem „maskierten“ Zustand vorliegt. Es wurde hierbei angenommen, dass Aurora-A-Phosphorylierung von Xl-TACC3 einen „demaskierenden“ Effekt auf die TACC-Domäne ausübt und somit deren Bindung an XMAP215, dem chTOG-Homolog aus *X. laevis*, ermöglicht. Die Interaktion der TACC-Domäne von TACC3 mit dem C-Terminus von chTOG/XMAP215 und deren Regulation waren jedoch zu Beginn dieser Arbeit auf molekularer Ebene unverstanden.

Daher wurden GST-Fusionsproteine von Deletionsmutanten und -Fragmenten von murinem TACC3 sowie der C-Terminus von murinem chTOG nach Überexpression in *E. coli* und nachfolgender Aufreinigung einer eingehenden molekularen Charakterisierung unterzogen (intra- und intermolelulare Komplexbildung und Interaktionsanalyse, Phosphorylierung durch Aurora-A-Kinase, subzelluläre Lokalisation). Hierbei wurden verschiedene biochemische und biophysikalische Methoden sowie bildgebende Verfahren, letztere nach transienter Transfektion von GFP-Fusionskonstrukten, eingesetzt, um im Besonderen die folgenden Fragen zu klären:

(I) „Maskiert” der N-Terminus von TACC3 die C-terminale TACC-Domäne durch eine intramolekulare Interaktion?

(II) Wie interagiert die TACC-Domäne mit dem C-Terminus von chTOG? Welcher Teil der TACC-Domäne ist beteiligt an dieser intermolekularen Bindung? Interferiert die Interaktion zwischen chTOG und der TACC-Domäne mit deren intramolekularen „Maskierung“?

(III) Beeinflusst der intramolekulare („maskierte“) oder intermolekulare (chTOG-gebundene) Status von TACC3 dessen Aurora-A-vermittelte Phosphorylierung?

(IV) Welche strukturellen Erkenntnisse über murines TACC3 lassen sich mit Hilfe biophysikalischer Methoden gewinnen?

Ein eingehender *in silico*-basierter Vergleich von murinem TACC3 mit TACC-Proteinen aus Vertebraten und Säugetieren zeigte, dass TACC3 (i) einen konservierten, N-terminalen Bereich von ungefähr 100 Aminosäuren aufweist, (ii) eine zentrale Domäne bestehend aus sieben serin- und prolinreichen Wiederholungen (SPR-Domäne) zeigt, und (iii) durch eine C-terminale TACC-Domäne bestehend aus zwei *coiled coil*-reichen Modulen, CC1 und CC2, charakterisiert ist. CC2 ist hierbei deutlich stärker konserviert als CC1.

Proteininteraktionsstudien mittels komplementärer Methoden (Pulldown, Gelfiltration, ITC) zeigten, dass die SPR-Domäne eine spezifische Bindung mit dem CC2-Modul eingeht und anscheinend die intramolekulare Interaktion mit der TACC-Domäne und somit deren „Maskierung“ vermittelt. Im Gegensatz hierzu bindet CC1 intermolekular selektiv an den C-Terminus von chTOG, mit der Folge, dass die intramolekulare SPR-CC2-Interaktion aufgehoben wird. Möglicherweise reguliert die intramolekulare Maskierung der TACC-Domäne deren Stabilität bevor chTOG bindet. Interessanterweise konnte TACC3 in *in vitro* Kinaseassays unabhängig von seinem intra- oder intermolekularem Proteinbindungsstatus effizient durch Aurora-A Kinase phosphoryliert werden. Aurora-A scheint daher keine entscheidende Rolle in der „Demaskierung“ der TACC-Domäne (und in der TACC3-chTOG Interaktion) zu spielen, im Gegensatz zur wichtigen, regulierenden Funktion in der zentrosomalem Rekrutierung von TACC3 bzw. des TACC3-chTOG-Komplexes. Insgesamt definieren diese Befunde CC1 und CC2 als zwei funktionell diverse Module innerhalb der TACC-Domäne von TACC3, die die Bildung des TACC3-chTOG Komplexes regulieren und vermitteln, bevor dieser Aurora-A-abhängig an die Zentrosomen rekrutiert wird.

Aufgereinigtes murines TACC3 wurde des Weiteren auf biophysikalischer und struktureller Ebene eingehend charakterisiert. Der Einsatz verschiedener Methoden, wie Gelfiltration, *multi angle light scattering* (MALS), analytische Ultrazentrifugation (AUC), und Elektronenmikroskopie (EM) ließ erkennen, dass murines TACC3 eine elongierte, faserartige oligomere Struktur aufweist. Hierbei zeigt die TACC-Domäne mit ihren beiden Modulen CC1 und CC2 eine parallele α-helikale Orientierung. Hinweise auf eine oligomere/multimere Natur von TACC3 konnten auch *in vivo* in transienten Transfektionsstudien eukaryonter Zellen mit Hilfe von TACC3-GFP-Fusionsproteinen gewonnen werden. Hierbei war das Auftreten von punktähnlichen Strukturen/Aggregaten klar abhängig von der Anwesenheit der C-terminalen TACC-Domäne und hierbei deutlich reduziert, wenn eines der beiden CC-Module deletiert wurde. In ersten

Zusammenfassung

Kristallisationsexperimenten konnten Kristalle für das CC1-Modul erhalten werden, deren Qualität derzeit optimiert wird mit dem Ziel der molekularen Strukturaufklärung.

Die klinische Relevanz humaner TACC3-Veränderungen zeichnet sich mehr und mehr ab. TACC3 Genexpressionsveränderungen sind assoziiert mit Krebsentwicklung, wobei verschiedene TACC3-Punktmutationen in humanen Primärtumoren identifiziert werden konnten. Des Weiteren konnte kürzlich eine Fibroblast Growth Factor Receptor (FGFG) 3 – TACC3 Gentranslokation, deren Produkt als Fusionsprotein transformierend wirkt, in Glioblastoma-Patienten beschrieben werden. Einerseits ist bisher ungeklärt, inwieweit sich diese tumorassoziierten, strukturellen TACC3-Veränderungen molekular auf die TACC3-chTOG-Interaktion und -Funktion und somit auf die chromosomale Segregation und Stabilität auswirken. Andererseits stellen TACC3 und chTOG, im Besonderen der CC1-chTOG-Komplex, mögliche antineoplastische Zielstrukturen dar.

References

1. Nasmyth, K. (2002) Segregating Sister Genomes: The Molecular Biology of Chromosome Separation, Science **297**, 559-565

2. Kops, G. J. P. L., Weaver, B. A. A., and Cleveland, D. W. (2005) On the road to cancer: aneuploidy and the mitotic checkpoint, Nat Rev Cancer **5**, 773-785

3. http://www.nobelprize.org. (2001) The Nobel Prize in Physiology or Medicine 2001 Leland H. Hartwell, Tim Hunt, Sir Paul Nurse.

4. Satyanarayana, A., and Kaldis, P. (2009) Mammalian cell-cycle regulation: several Cdks, numerous cyclins and diverse compensatory mechanisms, Oncogene **28**, 2925-2939

5. Alberts, B., Johnson, A., and Lewis, J. (2002) Molecular Biology of the Cell, 4th edition ed., Garland Science, New York

6. Lodish H, B. A., Zipursky SL, et al. . (2008) Molecular Cell Biology, 6th ed., W. H. Freeman, New York

7. Gergely, F. (2002) Centrosomal TACCtics, BioEssays **24**, 915-925

8. Gergely, F., Draviam, V. M., and Raff, J. W. (2003) The ch-TOG/XMAP215 protein is essential for spindle pole organization in human somatic cells, Genes & Development **17**, 336-341

9. Cassimeris, L., and Morabito, J. (2004) TOGp, the Human Homolog of XMAP215/Dis1, Is Required for Centrosome Integrity, Spindle Pole Organization, and Bipolar Spindle Assembly, Molecular Biology of the Cell **15**, 1580-1590

10. Yao, R., Natsume, Y., and Noda, T. (2007) TACC3 is required for the proper mitosis of sclerotome mesenchymal cells during formation of the axial skeleton, Cancer Science **98**, 555-562

11. Schneider, L., Essmann, F., Kletke, A., Rio, P., Hanenberg, H., Schulze-Osthoff, K., Nurnberg, B., and Piekorz, R. P. (2007) TACC3 depletion sensitizes to paclitaxel-induced cell death and overrides p21WAF-mediated cell cycle arrest, Oncogene **27**, 116-125

12. Sadek, C. M., Pelto-Huikko, M., Tujague, M., Steffensen, K. R., Wennerholm, M., and Gustafsson, J. Å. (2003) TACC3 expression is tightly regulated during early differentiation, Gene Expression Patterns **3**, 203-211

13. Piekorz, R. P., Hoffmeyer, A., Duntsch, C. D., McKay, C., Nakajima, H., Sexl, V., Snyder, L., Rehg, J., and Ihle, J. N. (2002) The centrosomal protein TACC3 is

essential for hematopoietic stem cell function and genetically interfaces with p53-regulated apoptosis, EMBO J **21**, 653-664

14. Azimzadeh, J., and Bornens, M. (2005) The Centrosome in Evolution. in Centrosomes in Development and Disease, Wiley-VCH Verlag GmbH & Co. KGaA. pp 93-122

15. Meraldi, P., and Nigg, E. A. (2002) The centrosome cycle, FEBS Letters **521**, 9-13

16. Bornens, M. (2002) Centrosome composition and microtubule anchoring mechanisms, Current Opinion in Cell Biology **14**, 25-34

17. Crasta, K., and Surana, U. (2006) Disjunction of conjoined twins: Cdk1, Cdh1 and separation of centrosomes, Cell Division **1**, 12

18. Mitchison, T., and Kirschner, M. (1984) Dynamic instability of microtubule growth, Nature **312**, 237-242

19. Desai, A., and Mitchison, T. J. (1997) Microtubule Polymerization Dynamics, Annual Review of Cell and Developmental Biology **13**, 83-117

20. Brouhard, G. J., Stear, J. H., Noetzel, T. L., Al-Bassam, J., Kinoshita, K., Harrison, S. C., Howard, J., and Hyman, A. A. (2008) XMAP215 Is a Processive Microtubule Polymerase, Cell **132**, 79-88

21. Brittle, A. L., and Ohkura, H. (2005) Centrosome Maturation: Aurora Lights the Way to the Poles, Current Biology **15**, R880-R882

22. Walczak, C. E., Gan, E. C., Desai, A., Mitchison, T. J., and Kline-Smith, S. L. (2002) The Microtubule-Destabilizing Kinesin XKCM1 Is Required for Chromosome Positioning during Spindle Assembly, Current biology : CB **12**, 1885-1889

23. Lee, M. J., Gergely, F., Jeffers, K., Peak-Chew, S. Y., and Raff, J. W. (2001) Msps/XMAP215 interacts with the centrosomal protein D-TACC to regulate microtubule behaviour, Nat Cell Biol **3**, 643-649

24. Bellanger, J.-M., and Gönczy, P. (2003) TAC-1 and ZYG-9 Form a Complex that Promotes Microtubule Assembly in C. elegans Embryos, Current Biology **13**, 1488-1498

25. Conte, N., Delaval, B., Ginestier, C., Ferrand, A., Isnardon, D., Larroque, C., Prigent, C., Seraphin, B., Jacquemier, J., and Birnbaum, D. (2003) TACC1-chTOG-Aurora A protein complex in breast cancer, Oncogene **22**, 8102-8116

26. Royle, S. J., Bright, N. A., and Lagnado, L. (2005) Clathrin is required for the function of the mitotic spindle, Nature **434**, 1152-1157

References

27. Fu, W., Tao, W., Zheng, P., Fu, J., Bian, M., Jiang, Q., Clarke, P. R., and Zhang, C. (2010) Clathrin recruits phosphorylated TACC3 to spindle poles for bipolar spindle assembly and chromosome alignment, Journal of Cell Science **123**, 3645-3651

28. Royle, S. J. (2012) The role of clathrin in mitotic spindle organisation, Journal of Cell Science **125**, 19-28

29. Booth, D. G., Hood, F. E., Prior, I. A., and Royle, S. J. (2011) A TACC3/ch-TOG/clathrin complex stabilises kinetochore fibres by inter-microtubule bridging, EMBO J **30**, 906-919

30. Hood, F. E., and Royle, S. J. (2011) Pulling it together: The mitotic function of TACC3, BioArchitecture **1**, 105-109

31. Hirota, T., Kunitoku, N., Sasayama, T., Marumoto, T., Zhang, D., Nitta, M., Hatakeyama, K., and Saya, H. (2003) Aurora-A and an Interacting Activator, the LIM Protein Ajuba, Are Required for Mitotic Commitment in Human Cells, Cell **114**, 585-598

32. Barros, T. P., Kinoshita, K., Hyman, A. A., and Raff, J. W. (2005) Aurora A activates D-TACC–Msps complexes exclusively at centrosomes to stabilize centrosomal microtubules, The Journal of Cell Biology **170**, 1039-1046

33. Kinoshita, K., Noetzel, T. L., Pelletier, L., Mechtler, K., Drechsel, D. N., Schwager, A., Lee, M., Raff, J. W., and Hyman, A. A. (2005) Aurora A phosphorylation of TACC3/maskin is required for centrosome-dependent microtubule assembly in mitosis, The Journal of Cell Biology **170**, 1047-1055

34. Peset, I., and Vernos, I. (2008) The TACC proteins: TACC-ling microtubule dynamics and centrosome function, Trends in Cell Biology **18**, 379-388

35. Jeng, J.-C., Lin, Y.-M., Lin, C.-H., and Shih, H.-M. (2009) Cdh1 controls the stability of TACC3, Cell Cycle **8**, 3537-3544

36. Doxsey, S., McCollum, D., and Theurkauf, W. (2005) CENTROSOMES IN CELLULAR REGULATION, Annual Review of Cell and Developmental Biology **21**, 411-434

37. Nigg, E. A., and Raff, J. W. (2009) Centrioles, Centrosomes, and Cilia in Health and Disease, Cell **139**, 663-678

38. Jakobsen, L., Vanselow, K., Skogs, M., Toyoda, Y., Lundberg, E., Poser, I., Falkenby, L. G., Bennetzen, M., Westendorf, J., Nigg, E. A., Uhlen, M., Hyman, A. A., and Andersen, J. S. (2011) Novel asymmetrically localizing components of human centrosomes identified by complementary proteomics methods, EMBO J **30**, 1520-1535

References

39. Andersen, J. S., Wilkinson, C. J., Mayor, T., Mortensen, P., Nigg, E. A., and Mann, M. (2003) Proteomic characterization of the human centrosome by protein correlation profiling, Nature **426**, 570-574

40. Nogales-Cadenas, R., Abascal, F., Díez-Pérez, J., Carazo, J. M., and Pascual-Montano, A. (2009) CentrosomeDB: a human centrosomal proteins database, Nucleic Acids Research **37**, D175-D180

41. Still, I., Vettaikkorumakankauv, A., DiMatteo, A., and Liang, P. (2004) Structure-function evolution of the Transforming acidic coiled coil genes revealed by analysis of phylogenetically diverse organisms, BMC Evolutionary Biology **4**, 16

42. Gergely, F., Karlsson, C., Still, I., Cowell, J., Kilmartin, J., and Raff, J. W. (2000) The TACC domain identifies a family of centrosomal proteins that can interact with microtubules, Proceedings of the National Academy of Sciences **97**, 14352-14357

43. Chen, X. P., Yin, H., and Huffaker, T. C. (1998) The Yeast Spindle Pole Body Component Spc72p Interacts with Stu2p and Is Required for Proper Microtubule Assembly, The Journal of Cell Biology **141**, 1169-1179

44. Sato, M., Koonrugsa, N., Toda, T., Vardy, L., Tournier, S., and Millar, J. B. A. (2003) Deletion of Mia1/Alp7 activates Mad2-dependent spindle assembly checkpoint in fission yeast, Nat Cell Biol **5**, 764-766

45. Still, I. H., Vince, P., and Cowell, J. K. (1999) The Third Member of the Transforming Acidic Coiled Coil-Containing Gene Family, TACC3, Maps in 4p16, Close to Translocation Breakpoints in Multiple Myeloma, and Is Upregulated in Various Cancer Cell Lines, Genomics **58**, 165-170

46. Ivan H Still, M. H., Pauline Vince, Alan Wolfman and John K Cowell. (1999) Cloning of TACC1, an embryonically expressed, potentially transforming coiled coil containing gene, from the 8p11 breast cancer amplicon, Oncogene **18**, 4032-4038

47. Lauffart, B., Gangisetty, O., and Still, I. H. (2003) Molecular cloning, genomic structure and interactions of the putative breast tumor suppressor TACC2, Genomics **81**, 192-201

48. Klein, S. L., Strausberg, R. L., Wagner, L., Pontius, J., Clifton, S. W., and Richardson, P. (2002) Genetic and genomic tools for Xenopus research: The NIH Xenopus initiative, Developmental Dynamics **225**, 384-391

49. Albee, A. J., and Wiese, C. (2008) Xenopus TACC3/Maskin Is Not Required for Microtubule Stability but Is Required for Anchoring Microtubules at the Centrosome, Molecular Biology of the Cell **19**, 3347-3356

50. Steadman, B. T., Schmidt, P. H., Shanks, R. A., Lapierre, L. A., and Goldenring, J. R. (2002) Transforming Acidic Coiled-coil-containing Protein 4 Interacts with

Centrosomal AKAP350 and the Mitotic Spindle Apparatus, Journal of Biological Chemistry **277**, 30165-30176

51. Samereier, M., Baumann, O., Meyer, I., and Gräf, R. (2011) Analysis of Dictyostelium TACC reveals differential interactions with CP224 and unusual dynamics of Dictyostelium microtubules, Cell. Mol. Life Sci. **68**, 275-287

52. Neuber, A., Franke, J., Wittstruck, A., Schlenstedt, G., Sommer, T., and Stade, K. (2008) Nuclear Export Receptor Xpo1/Crm1 Is Physically and Functionally Linked to the Spindle Pole Body in Budding Yeast, Molecular and Cellular Biology **28**, 5348-5358

53. Boulton, S. J., Martin, J. S., Polanowska, J., Hill, D. E., Gartner, A., and Vidal, M. (2004) BRCA1/BARD1 Orthologs Required for DNA Repair in Caenorhabditis elegans, Current Biology **14**, 33-39

54. Walhout, A. J. M., Sordella, R., Lu, X., Hartley, J. L., Temple, G. F., Brasch, M. A., Thierry-Mieg, N., and Vidal, M. (2000) Protein Interaction Mapping in C. elegans Using Proteins Involved in Vulval Development, Science **287**, 116-122

55. Wang, H.-Y., Wang, I. F., Bose, J., and Shen, C. K. J. (2004) Structural diversity and functional implications of the eukaryotic TDP gene family, Genomics **83**, 130-139

56. Garriga-Canut, M., and Orkin, S. H. (2004) Transforming Acidic Coiled-coil Protein 3 (TACC3) Controls Friend of GATA-1 (FOG-1) Subcellular Localization and Regulates the Association between GATA-1 and FOG-1 during Hematopoiesis, Journal of Biological Chemistry **279**, 23597-23605

57. Partch, C. L., and Gardner, K. H. (2011) Coactivators necessary for transcriptional output of the hypoxia inducible factor, HIF, are directly recruited by ARNT PAS-B, Proceedings of the National Academy of Sciences **108**, 7739-7744

58. Sadek, C. M., Jalaguier, S., Feeney, E. P., Aitola, M., Damdimopoulos, A. E., Pelto-Huikko, M., and Gustafsson, J.-Å. (2000) Isolation and characterization of AINT: a novel ARNT interacting protein expressed during murine embryonic development, Mechanisms of Development **97**, 13-26

59. Nathalie Conte, E. C.-J., Bénédicte Delaval, José Adélaïde, Christophe Ginestier, Jeannine Geneix, Daniel Isnardon, Jocelyne Jacquemier and Daniel Birnbaum. (2002) Carcinogenesis and translational controls: TACC1 is down-regulated in human cancers and associates with mRNA regulators, Oncogene **21**, 5619-5630

60. Brenda Lauffart, S. J. H., Jason E Tasch, John K Cowell, Ivan H Still. (2002) Interaction of the transforming acidic coiled-coil 1 (TACC1) protein with ch-TOG and GAS41/NuBI1 suggests multiple TACC1-containing protein complexes in human cells. , Biochemical Journal **363**, 195-200

References

61. Gómez-Baldó, L., Schmidt, S., Maxwell, C. A., Bonifaci, N., Gabaldón, T., Vidalain, P.-O., Senapedis, W., Kletke, A., Rosing, M., Barnekow, A., Rottapel, R., Capellá, G., Vidal, M., Astrinidis, A., Piekorz, R. P., and Pujana, M. A. (2010) TACC3-TSC2 maintains nuclear envelope structure and controls cell division, Cell Cycle **9**, 1143-1155

62. Stebbins-Boaz, B., Cao, Q., de Moor, C. H., Mendez, R., and Richter, J. D. (1999) Maskin Is a CPEB-Associated Factor that Transiently Interacts with eIF-4E, Molecular Cell **4**, 1017-1027

63. Richter, J. D. (2007) CPEB: a life in translation, Trends in Biochemical Sciences **32**, 279-285

64. Gangisetty, O., Lauffart, B., Sondarva, G. V., Chelsea, D. M., and Still, I. H. (2004) The transforming acidic coiled coil proteins interact with nuclear histone acetyltransferases, Oncogene **23**, 2559-2563

65. Crane, R., Gadea, B., Littlepage, L., Wu, H., and Ruderman, J. V. (2004) Aurora A, Meiosis and Mitosis, Biology of the Cell **96**, 215-229

66. LeRoy, P. J., Hunter, J. J., Hoar, K. M., Burke, K. E., Shinde, V., Ruan, J., Bowman, D., Galvin, K., and Ecsedy, J. A. (2007) Localization of Human TACC3 to Mitotic Spindles Is Mediated by Phosphorylation on Ser558 by Aurora A: A Novel Pharmacodynamic Method for Measuring Aurora A Activity, Cancer Research **67**, 5362-5370

67. Angrisano, T., Lembo, F., Pero, R., Natale, F., Fusco, A., Avvedimento, V. E., Bruni, C. B., and Chiariotti, L. (2005) TACC3 mediates the association of MBD2 with histone acetyltransferases and relieves transcriptional repression of methylated promoters, Nucleic Acids Research **34**, 364-372

68. Yao, R., Natsume, Y., Saiki, Y., Shioya, H., Takeuchi, K., Yamori, T., Toki, H., Aoki, I., Saga, T., and Noda, T. (2012) Disruption of Tacc3 function leads to in vivo tumor regression, Oncogene **31**, 135-148

69. Schmidt, S., Schneider, L., Essmann, F., Cirstea, I. C., Kuck, F., Kletke, A., Janicke, R. U., Wiek, C., Hanenberg, H., Ahmadian, M. R., Schulze-Osthoff, K., Nurnberg, B., and Piekorz, R. P. (2010) The centrosomal protein TACC3 controls paclitaxel sensitivity by modulating a premature senescence program, Oncogene **29**, 6184-6192

70. Hao, Z., Stoler, M. H., Sen, B., Shore, A., Westbrook, A., Flickinger, C. J., Herr, J. C., and Coonrod, S. A. (2002) TACC3 expression and localization in the murine egg and ovary, Molecular Reproduction and Development **63**, 291-299

71. Eslinger MR, L. B., Still IH. (2010) TACC3 (transforming, acidic coiled-coil containing protein 3), Atlas of Genetics and Cytogenetics in Oncology and Haematology

References

72. Gard, D. L., and Kirschner, M. W. (1987) A microtubule-associated protein from Xenopus eggs that specifically promotes assembly at the plus-end, The Journal of Cell Biology **105**, 2203-2215

73. Al-Bassam, J., Larsen, N. A., Hyman, A. A., and Harrison, S. C. (2007) Crystal Structure of a TOG Domain: Conserved Features of XMAP215/Dis1-Family TOG Domains and Implications for Tubulin Binding, Structure (London, England : 1993) **15**, 355-362

74. Kinoshita, K., Habermann, B., and Hyman, A. A. (2002) XMAP215: a key component of the dynamic microtubule cytoskeleton, Trends in Cell Biology **12**, 267-273

75. Popov, A. V., Pozniakovsky, A., Arnal, I., Antony, C., Ashford, A. J., Kinoshita, K., Tournebize, R., Hyman, A. A., and Karsenti, E. (2001) XMAP215 regulates microtubule dynamics through two distinct domains, EMBO J **20**, 397-410

76. Fu, J., Bian, M., Jiang, Q., and Zhang, C. (2007) Roles of Aurora Kinases in Mitosis and Tumorigenesis, Molecular Cancer Research **5**, 1-10

77. Tsai, M.-Y., Wiese, C., Cao, K., Martin, O., Donovan, P., Ruderman, J., Prigent, C., and Zheng, Y. (2003) A Ran signalling pathway mediated by the mitotic kinase Aurora A in spindle assembly, Nat Cell Biol **5**, 242-248

78. Ananthalaksmy K Vettaikkorumakankauv, B. L., Omkaram, Gangisetty, M. A. C., Lesley Ann Hawthorne, John K Cowell, Ivan H, and Still6. (2008) The TACC proteins are coregulators of the Retinoid X Receptor β Cancer Therapy **6**, 805

79. Schmidt, S., Essmann, F., Cirstea, I. C., Kuck, F., Thakur, H. C., Singh, M., Kletke, A., Jänicke, R. U., Wiek, C., Hanenberg, H., Ahmadian, M. R., Schulze-Osthoff, K., Nürnberg, B., and Piekorz, R. P. (2010) The centrosome and mitotic spindle apparatus in cancer and senescence, Cell Cycle **9**, 4469-4473

80. Lin, C. H., Hu, C. K., and Shih, H. M. (2010) Clathrin heavy chain mediates TACC3 targeting to mitotic spindles to ensure spindle stability, J Cell Biol **189**, 1097-1105

81. Fu, W., Jiang, Q., and Zhang, C. (2011) Novel functions of endocytic player clathrin in mitosis, Cell Res **21**, 1655-1661

82. Foraker, A. B., Camus, S. M., Evans, T. M., Majeed, S. R., Chen, C.-Y., Taner, S. B., Corrêa, I. R., Doxsey, S. J., and Brodsky, F. M. (2012) Clathrin promotes centrosome integrity in early mitosis through stabilization of centrosomal ch-TOG, The Journal of Cell Biology **198**, 591-605

83. Xie, Z., Moy, L. Y., Sanada, K., Zhou, Y., Buchman, J. J., and Tsai, L.-H. (2007) Cep120 and TACCs Control Interkinetic Nuclear Migration and the Neural Progenitor Pool, Neuron **56**, 79-93

References

84. Yang, Y. T., Wang, C. L., and Van Aelst, L. (2012) DOCK7 interacts with TACC3 to regulate interkinetic nuclear migration and cortical neurogenesis, Nat Neurosci **15**, 1201-1210

85. Lauffart, B., Vaughan, M., Eddy, R., Chervinsky, D., DiCioccio, R., Black, J., and Still, I. (2005) Aberrations of TACC1 and TACC3 are associated with ovarian cancer, BMC Women's Health **5**, 8

86. Sylvain L'Espérance, I. P., Magdalena Bachvarova, Marie Plante, Nancy Patten, Lin Wu, Bernard Têtu, Dimcho Bachvarov. (2006) Gene expression profiling of paired ovarian tumors obtained prior to and following adjuvant chemotherapy: Molecular signatures of chemoresistant tumors, International Journal of Oncology **29**, 5-24

87. Jung, C. K., Jung, J. H., Park, G. S., Lee, A., Kang, C. S., and Lee, K. Y. (2006) Expression of transforming acidic coiled-coil containing protein 3 is a novel independent prognostic marker in non-small cell lung cancer, Pathology International **56**, 503-509

88. Singh, D., Chan, J. M., Zoppoli, P., Niola, F., Sullivan, R., Castano, A., Liu, E. M., Reichel, J., Porrati, P., Pellegatta, S., Qiu, K., Gao, Z., Ceccarelli, M., Riccardi, R., Brat, D. J., Guha, A., Aldape, K., Golfinos, J. G., Zagzag, D., Mikkelsen, T., Finocchiaro, G., Lasorella, A., Rabadan, R., and Iavarone, A. (2012) Transforming Fusions of FGFR and TACC Genes in Human Glioblastoma, Science **337**, 1231-1235

89. Stewart, J. P., Thompson, A., Santra, M., Barlogie, B., Lappin, T. R. J., and Shaughnessy, J. (2004) Correlation of TACC3, FGFR3, MMSET and p21 expression with the t(4;14)(p16·3;q32) in multiple myeloma, British Journal of Haematology **126**, 72-76

90. Ma, Z., Hu, Q., Chen, Z., Tao, S., Macnamara, L., Kim, S. T., Tian, L., Xu, K., Ding, Q., Zheng, S. L., Sun, J., Xia, G., and Xu, J. (2012) Systematic evaluation of bladder cancer risk-associated single-nucleotide polymorphisms in a Chinese population, Mol Carcinog **18**, 21932

91. Albee, A. J., Tao, W., and Wiese, C. (2006) Phosphorylation of Maskin by Aurora-A Is Regulated by RanGTP and Importin β, Journal of Biological Chemistry **281**, 38293-38301

92. Sato, M., Vardy, L., Angel Garcia, M., Koonrugsa, N., and Toda, T. (2004) Interdependency of Fission Yeast Alp14/TOG and Coiled Coil Protein Alp7 in Microtubule Localization and Bipolar Spindle Formation, Molecular Biology of the Cell **15**, 1609-1622

93. Russo, E. (2003) Special Report: The birth of biotechnology, Nature **421**, 456-457

94. François, B. (1999) Recombinant protein expression in Escherichia coli, Current Opinion in Biotechnology **10**, 411-421

References

95. Fotadar, U., Zaveloff, P., and Terracio, L. (2005) Growth of Escherichia coli at elevated temperatures, Journal of Basic Microbiology **45**, 403-404

96. Novick, A. (1955) Growth of Bacteria, Annual Review of Microbiology **9**, 97-110

97. Thompson, J. D., Gibson, T. J., and Higgins, D. G. (2002) Multiple Sequence Alignment Using ClustalW and ClustalX. in Current Protocols in Bioinformatics, John Wiley & Sons, Inc. pp

98. Waterhouse, A. M., Procter, J. B., Martin, D. M. A., Clamp, M., and Barton, G. J. (2009) Jalview Version 2—a multiple sequence alignment editor and analysis workbench, Bioinformatics **25**, 1189-1191

99. Lupas, A., Van Dyke, M., and Stock, J. (1991) Predicting Coiled Coils from Protein Sequences, Science **252**, 1162-1164

100. Gasteiger, E., Gattiker, A., Hoogland, C., Ivanyi, I., Appel, R. D., and Bairoch, A. (2003) ExPASy: the proteomics server for in-depth protein knowledge and analysis, Nucleic Acids Research **31**, 3784-3788

101. Ren, J., Wen, L., Gao, X., Jin, C., Xue, Y., and Yao, X. (2009) DOG 1.0: illustrator of protein domain structures, Cell Res **19**, 271-273

102. Sambrook, J., and Russel, D. W. (2001) Molecular Cloning: A Laboratory Manual 3rd Ed. Cold Spring Harbor Laboratory Press, Cold Spring Harbor, NY

103. Bergmans, H. E. N., Van Die, I. M., and Hoekstra, W. P. M. (1981) Transformation in Escherichia coli: stages in the process, Journal of Bacteriology **146**, 564-570

104. Yoshida, N., and Sato, M. (2009) Plasmid uptake by bacteria: a comparison of methods and efficiencies, Applied Microbiology and Biotechnology **83**, 791-798

105. Voytas, D. (2001) Agarose Gel Electrophoresis. in Current Protocols in Immunology, John Wiley & Sons, Inc. pp

106. Kuslich, C. D., Chui, B., and Yamashiro, C. T. (2008) Overview of PCR. in Current Protocols Essential Laboratory Techniques, John Wiley & Sons, Inc. pp

107. Bimboim, H. C., and Doly, J. (1979) A rapid alkaline extraction procedure for screening recombinant plasmid DNA, Nucleic Acids Research **7**, 1513-1523

108. Kresge, N., Simoni, R. D., and Hill, R. L. (2006) SDS-PAGE to Determine the Molecular Weight of Proteins: the Work of Klaus Weber and Mary Osborn, Journal of Biological Chemistry **281**, e19

References

109. Weber, K., and Osborn, M. (1969) The Reliability of Molecular Weight Determinations by Dodecyl Sulfate-Polyacrylamide Gel Electrophoresis, Journal of Biological Chemistry **244**, 4406-4412

110. Jerker, P. (1992) Immobilized metal ion affinity chromatography, Protein Expression and Purification **3**, 263-281

111. Block, H., Maertens, B., Spriestersbach, A., Brinker, N., Kubicek, J., Fabis, R., Labahn, J., and Schäfer, F. (2009) Reprint of: Immobilized-Metal Affinity Chromatography (IMAC): A Review, Protein Expression and Purification **463**, 439-473

112. Harper, S., and Speicher, D. W. (2001) Expression and Purification of GST Fusion Proteins. in Current Protocols in Protein Science, John Wiley & Sons, Inc. pp

113. Aatsinki, J. T., and Rajaniemi, H. J. (2005) An alternative use of basic pGEX vectors for producing both N- and C-terminal fusion proteins for production and affinity purification of antibodies, Protein Expression and Purification **40**, 287-291

114. Jaiswal, M., Gremer, L., Dvorsky, R., Haeusler, L. C., Cirstea, I. C., Uhlenbrock, K., and Ahmadian, M. R. (2011) Mechanistic Insights into Specificity, Activity, and Regulatory Elements of the Regulator of G-protein Signaling (RGS)-containing Rho-specific Guanine Nucleotide Exchange Factors (GEFs) p115, PDZ-RhoGEF (PRG), and Leukemia-associated RhoGEF (LARG), Journal of Biological Chemistry **286**, 18202-18212

115. Marion M, B. (1976) A rapid and sensitive method for the quantitation of microgram quantities of protein utilizing the principle of protein-dye binding, Analytical Biochemistry **72**, 248-254

116. Stoscheck, C. (1990) Quantification of protein., Methods Enzymol. **182**, 50-68

117. Kelly, S. M., Jess, T. J., and Price, N. C. (2005) How to study proteins by circular dichroism, Biochimica et Biophysica Acta (BBA) - Proteins & Proteomics **1751**, 119-139

118. Ohi, M., Li, Y., Cheng, Y., and Walz, T. (2004) Negative staining and image classification — powerful tools in modern electron microscopy, Biological Procedures Online **6**, 23-34

119. Kay, B. K., Williamson, M. P., and Sudol, M. (2000) The importance of being proline: the interaction of proline-rich motifs in signaling proteins with their cognate domains, The FASEB Journal **14**, 231-241

120. Andrade, M. A., and Bork, P. (1995) HEAT repeats in the Huntington's disease protein, Nat Genet **11**, 115-116

References

121. Groves, M. R., Hanlon, N., Turowski, P., Hemmings, B. A., and Barford, D. (1999) The Structure of the Protein Phosphatase 2A PR65/A Subunit Reveals the Conformation of Its 15 Tandemly Repeated HEAT Motifs, Cell **96**, 99-110

122. Huber, A. H., Nelson, W. J., and Weis, W. I. (1997) Three-Dimensional Structure of the Armadillo Repeat Region of β-Catenin, Cell **90**, 871-882

123. Michaely, P., Tomchick, D. R., Machius, M., and Anderson, R. G. W. (2002) Crystal structure of a 12 ANK repeat stack from human ankyrinR, EMBO J **21**, 6387-6396

124. Das, A. K., Cohen, P. T. W., and Barford, D. (1998) The structure of the tetratricopeptide repeats of protein phosphatase 5: implications for TPR-mediated protein-protein interactions, EMBO J **17**, 1192-1199

125. Kippert, F., and Gerloff, D. L. (2009) Highly Sensitive Detection of Individual HEAT and ARM Repeats with HHpred and COACH, PLoS ONE **4**, e7148

126. Chang, J.-Y. (1985) Thrombin specificity, European Journal of Biochemistry **151**, 217-224

127. Artimo, P., Jonnalagedda, M., Arnold, K., Baratin, D., Csardi, G., de Castro, E., Duvaud, S., Flegel, V., Fortier, A., Gasteiger, E., Grosdidier, A., Hernandez, C., Ioannidis, V., Kuznetsov, D., Liechti, R., Moretti, S., Mostaguir, K., Redaschi, N., Rossier, G., Xenarios, I., and Stockinger, H. (2012) ExPASy: SIB bioinformatics resource portal, Nucleic Acids Research **40**, W597-W603

128. Al-Bassam, J., and Chang, F. (2011) Regulation of microtubule dynamics by TOG-domain proteins XMAP215/Dis1 and CLASP, Trends in Cell Biology **21**, 604-614

129. Silveira, J. R., Hughson, A. G., and Caughey, B. (2006) Fractionation of Prion Protein Aggregates by Asymmetrical Flow Field-Flow Fractionation. in Methods in Enzymology (Indu, K., and Ronald, W. eds.), Academic Press. pp 21-33

130. Müller, M., Mazur, A., Behrmann, E., Diensthuber, R., Radke, M., Qu, Z., Littwitz, C., Raunser, S., Schoenenberger, C.-A., Manstein, D., and Mannherz, H. (2012) Functional characterization of the human α-cardiac actin mutations Y166C and M305L involved in hypertrophic cardiomyopathy, Cell. Mol. Life Sci. **69**, 3457-3479

131. Ludtke, S. J., Baldwin, P. R., and Chiu, W. (1999) EMAN: Semiautomated Software for High-Resolution Single-Particle Reconstructions, Journal of Structural Biology **128**, 82-97

132. Peset, I., Seiler, J., Sardon, T., Bejarano, L. A., Rybina, S., and Vernos, I. (2005) Function and regulation of Maskin, a TACC family protein, in microtubule growth during mitosis, The Journal of Cell Biology **170**, 1057-1066

133. O'Brien, L. L., Albee, A. J., Liu, L., Tao, W., Dobrzyn, P., Lizarraga, S. B., and Wiese, C. (2005) The Xenopus TACC Homologue, Maskin, Functions in Mitotic Spindle Assembly, Molecular Biology of the Cell **16**, 2836-2847

134. Simpson, R. J., Yi Lee, S. H., Bartle, N., Sum, E. Y., Visvader, J. E., Matthews, J. M., Mackay, J. P., and Crossley, M. (2004) A classic zinc finger from friend of GATA mediates an interaction with the coiled-coil of transforming acidic coiled-coil 3, J Biol Chem **279**, 39789-39797

135. Lappin, T. R., Mullan, R. N., Stewart, J. P., Morgan, N. A., Thompson, A., and Maxwell, A. P. (2002) AINT/ERIC/TACC: An Expanding Family of Proteins with C-terminal Coiled Coil Domains, Leukemia & Lymphoma **43**, 1455-1459

136. Aitola, M., Sadek, C. M., Gustafsson, J. A., and Pelto-Huikko, M. (2003) Aint/Tacc3 is highly expressed in proliferating mouse tissues during development, spermatogenesis, and oogenesis, J Histochem Cytochem **51**, 455-469

137. Conte, N., Charafe-Jauffret, E., Delaval, B., Adélaïde, J., Ginestier, C., Geneix, J., Isnardon, D., Jacquemier, J., and Birnbaum, D. (2002) Carcinogenesis and translational controls: TACC1 is down-regulated in human cancers and associates with mRNA regulators, Oncogene **21**, 5619-5630

138. Lauffart, B., Howell, S. J., Tasch, J. E., Ccwell, J. K., and Still, I. (2002) Interaction of the transforming acidic coiled-coil 1 (TACC1) protein with ch-TOG and GAS41/NuBI1 suggests multiple TACC1-containing protein complexes in human cells, Biochemical Journal, 195-200

139. Schuendeln, M. M., Piekorz, R. P., Wichmann, C., Lee, Y., McKinnon, P. J., Boyd, K., Takahashi, Y., and Ihle, J. N. (2004) The Centrosomal, Putative Tumor Suppressor Protein TACC2 Is Dispensable for Normal Development, and Deficiency Does Not Lead to Cancer, Molecular and Cellular Biology **24**, 6403-6409

140. Tien, A. C., Lin, M. H., Su, L. J., Hong, Y. R., Cheng, T. S., Lee, Y. C., Lin, W. J., Still, I. H., and Huang, C. Y. (2004) Identification of the substrates and interaction proteins of aurora kinases from a protein-protein interaction model, Mol Cell Proteomics **3**, 93-104

141. Giet, R., McLean, D., Descamps, S., Lee, M. J., Raff, J. W., Prigent, C., and Glover, D. M. (2002) Drosophila Aurora A kinase is required to localize D-TACC to centrosomes and to regulate astral microtubules, The Journal of Cell Biology **156**, 437-451

142. Cheeseman, L. P., Booth, D. G., Hood, F. E., Prior, I. A., and Royle, S. J. (2011) Aurora A kinase activity is required for localization of TACC3/ch-TOG/clathrin inter-microtubule bridges, Commun Integr Biol **4**, 409-412

143. Crick, F. (1953) The packing of [alpha]-helices: simple coiled-coils, Acta Crystallographica **6**, 689-697

References

144. Mason, J. M., and Arndt, K. M. (2004) Coiled Coil Domains: Stability, Specificity, and Biological Implications, ChemBioChem **5**, 170-176

145. Gergely, F., Kidd, D., Jeffers, K., Wakefield, J. G., and Raff, J. W. (2000) D-TACC: a novel centrosomal protein required for normal spindle function in the early Drosophila embryo, EMBO J **19**, 241-252

146. Lin, C.-H., Hu, C.-K., and Shih, H.-M. (2010) Clathrin heavy chain mediates TACC3 targeting to mitotic spindles to ensure spindle stability, The Journal of Cell Biology **189**, 1097-1105

147. Tournebize, R., Popov, A., Kinoshita, K., Ashford, A. J., Rybina, S., Pozniakovsky, A., Mayer, T. U., Walczak, C. E., Karsenti, E., and Hyman, A. A. (2000) Control of microtubule dynamics by the antagonistic activities of XMAP215 and XKCM1 in Xenopus egg extracts, Nat Cell Biol **2**, 13-19

148. Pearse, B. M. (1976) Clathrin: a unique protein associated with intracellular transfer of membrane by coated vesicles, Proceedings of the National Academy of Sciences **73**, 1255-1259

149. Wakeham, D. E., Chen, C.-Y., Greene, B., Hwang, P. K., and Brodsky, F. M. (2003) Clathrin self-assembly involves coordinated weak interactions favorable for cellular regulation, EMBO J **22**, 4980-4990

150. Zhang, G., Breuer, M., Förster, A., Egger-Adam, D., and Wodarz, A. (2009) Mars, a Drosophila protein related to vertebrate HURP, is required for the attachment of centrosomes to the mitotic spindle during syncytial nuclear divisions, Journal of Cell Science **122**, 535-545

151. Tan, S., Lyulcheva, E., Dean, J., and Bennett, D. (2008) Mars promotes dTACC dephosphorylation on mitotic spindles to ensure spindle stability, The Journal of Cell Biology **182**, 27-33

152. Li, H.-H., Chiang, C.-S., Huang, H.-Y., and Liaw, G.-J. (2009) mars and tousled-like kinase act in parallel to ensure chromosome fidelity in Drosophila, Journal of Biomedical Science **16**, 51

153. Koffa, M. D., Casanova, C. M., Santarella, R., Köcher, T., Wilm, M., and Mattaj, I. W. (2006) HURP Is Part of a Ran-Dependent Complex Involved in Spindle Formation, Current Biology **16**, 743-754

154. Silljé, H. H. W., Nagel, S., Körner, R., and Nigg, E. A. (2006) HURP Is a Ran-Importin β-Regulated Protein that Stabilizes Kinetochore Microtubules in the Vicinity of Chromosomes, Current Biology **16**, 731-742

155. Wong, J., and Fang, G. (2006) HURP controls spindle dynamics to promote proper interkinetochore tension and efficient kinetochore capture, The Journal of Cell Biology **173**, 879-891

References

156. Wong, J., Lerrigo, R., Jang, C.-Y., and Fang, G. (2008) Aurora A Regulates the Activity of HURP by Controlling the Accessibility of Its Microtubule-binding Domain, Molecular Biology of the Cell **19**, 2083-2091

157. Yu, C.-T. R., Hsu, J.-M., Lee, Y.-C. G., Tsou, A.-P., Chou, C.-K., and Huang, C.-Y. F. (2005) Phosphorylation and Stabilization of HURP by Aurora-A: Implication of HURP as a Transforming Target of Aurora-A, Molecular and Cellular Biology **25**, 5789-5800

158. Hwang, A., Maity, A., McKenna, W. G., and Muschel, R. J. (1995) Cell Cycle-dependent Regulation of the Cyclin B1 Promoter, Journal of Biological Chemistry **270**, 28419-28424

159. Foster, Scott A., and Morgan, David O. (2012) The APC/C Subunit Mnd2/Apc15 Promotes Cdc20 Autoubiquitination and Spindle Assembly Checkpoint Inactivation, Molecular Cell **47**, 921-932

160. Zhang, J., and Megraw, T. L. (2007) Proper Recruitment of γ-Tubulin and D-TACC/Msps to Embryonic Drosophila Centrosomes Requires Centrosomin Motif 1, Molecular Biology of the Cell **18**, 4037-4049

161. Pascreau, G., Delcros, J.-G., Cremet, J.-Y., Prigent, C., and Arlot-Bonnemains, Y. (2005) Phosphorylation of Maskin by Aurora-A Participates in the Control of Sequential Protein Synthesis during Xenopus laevis Oocyte Maturation, Journal of Biological Chemistry **280**, 13415-13423

162. Delaval, B., Ferrand, A., Conte, N., Larroque, C., Hernandez-Verdun, D., Prigent, C., and Birnbaum, D. (2004) Aurora B -TACC1 protein complex in cytokinesis, Oncogene **23**, 4516-4522

163. Hutchins, J. R. A., Toyoda, Y., Hegemann, B., Poser, I., Hériché, J.-K., Sykora, M. M., Augsburg, M., Hudecz, O., Buschhorn, B. A., Bulkescher, J., Conrad, C., Comartin, D., Schleiffer, A., Sarov, M., Pozniakovsky, A., Slabicki, M. M., Schloissnig, S., Steinmacher, I., Leuschner, M., Ssykor, A., Lawo, S., Pelletier, L., Stark, H., Nasmyth, K., Ellenberg, J., Durbin, R., Buchholz, F., Mechtler, K., Hyman, A. A., and Peters, J.-M. (2010) Systematic Analysis of Human Protein Complexes Identifies Chromosome Segregation Proteins, Science **328**, 593-599

164. Dou, Z., Ding, X., Zereshki, A., Zhang, Y., Zhang, J., Wang, F., Sun, J., Huang, H., and Yao, X. (2004) TTK kinase is essential for the centrosomal localization of TACC2, FEBS Letters **572**, 51-56

165. Mori, D., Yano, Y., Toyo-oka, K., Yoshida, N., Yamada, M., Muramatsu, M., Zhang, D., Saya, H., Toyoshima, Y. Y., Kinoshita, K., Wynshaw-Boris, A., and Hirotsune, S. (2007) NDEL1 phosphorylation by Aurora-A kinase is essential for centrosomal maturation, separation, and TACC3 recruitment, Mol Cell Biol **27**, 352-367

References

166. Bargo, S., Raafat, A., McCurdy, D., Amirjazil, I., Shu, Y., Traicoff, J., Plant, J., Vonderhaar, B. K., and Callahan, R. (2010) Transforming acidic coiled-coil protein-3 (Tacc3) acts as a negative regulator of Notch signaling through binding to CDC10/Ankyrin repeats, Biochem Biophys Res Commun **400**, 606-612

167. Turner, N., and Grose, R. (2010) Fibroblast growth factor signalling: from development to cancer, Nat Rev Cancer **10**, 116-129

168. Raouf, A., and Seth, A. (2002) Discovery of osteoblast-associated genes using cDNA microarrays, Bone **30**, 463-471

169. Peters, D. G., Kudla, D. M., Deloia, J. A., Chu, T. J., Fairfull, L., Edwards, R. P., and Ferrell, R. E. (2005) Comparative gene expression analysis of ovarian carcinoma and normal ovarian epithelium by serial analysis of gene expression, Cancer Epidemiol Biomarkers Prev **14**, 1717-1723

170. L'Esperance, S., Popa, I., Bachvarova, M., Plante, M., Patten, N., Wu, L., Tetu, B., and Bachvarov, D. (2006) Gene expression profiling of paired ovarian tumors obtained prior to and following adjuvant chemotherapy: molecular signatures of chemoresistant tumors, Int J Oncol **29**, 5-24

171. Eslinger, M. R. (2006) Molecular Analysis of TACC3 in ovarian cancer. in M.Sc. thesis

172. Ulisse, S., Baldini, E., Toller, M., Delcros, J. G., Gueho, A., Curcio, F., De Antoni, E., Giacomelli, L., Ambesi-Impiombato, F. S., Bocchini, S., D'Armiento, M., and Arlot-Bonnemains, Y. (2007) Transforming acidic coiled-coil 3 and Aurora-A interact in human thyrocytes and their expression is deregulated in thyroid cancer tissues, Endocr Relat Cancer **14**, 827-837

173. Arlot-Bonnemains, Y., Baldini, E., Martin, B., Delcros, J. G., Toller, M., Curcio, F., Ambesi-Impiombato, F. S., D'Armiento, M., and Ulisse, S. (2008) Effects of the Aurora kinase inhibitor VX-680 on anaplastic thyroid cancer-derived cell lines, Endocr Relat Cancer **15**, 559-568

174. Cassimeris, L., Becker, B., and Carney, B. (2009) TOGp regulates microtubule assembly and density during mitosis and contributes to chromosome directional instability, Cell Motil Cytoskeleton **66**, 535-545

175. Cappell, K. M., Sinnott, R., Taus, P., Maxfield, K., Scarbrough, M., and Whitehurst, A. W. (2012) Multiple cancer testes antigens function to support tumor cell mitotic fidelity, Mol Cell Biol **6**, 6

Eidesstattliche Erklärung

Hiermit erkläre ich an Eides statt, dass ich die hier vorgelegte Dissertation eigenständig und ohne unerlaubte Hilfe angefertigt habe. Es wurden keinerlei andere Quellen und Hilfsmittel, außer den angegebenen, benutzt. Zitate aus anderen Arbeiten wurden kenntlich gemacht. Diese Dissertation wurde in der vorgelegten oder einer ähnlichen Form noch bei keiner anderen Institution eingereicht und es wurden bisher keine erfolglosen Promotionsversuche von mir unternommen.

Düsseldorf, im November 2012

Curriculum Vitae

Personal information

Family Name:	Thakur
First Name:	Harish Chandra
Nationality:	Indian
Date of Birth:	February 04, 1984
Sex:	Male

Educational qualifications:

2009-2012: Ph.D. Fellow, Institute for Biochemistry and Molecular Biology II Heinrich-Heine-University, Duesseldorf, Germany.

2007-2009: M.Sc. (Life Sciences), School of Life Sciences, Jawaharlal Nehru University, New Delhi, India.

2003-2007: B.Sc. (Agriculture), Institute of Agricultural Sciences, Banaras Hindu University, Varanasi, India.

1998-2000: Higher Secondary School Examination, Bihar Intermediate Education Council, Patna, India.

1998: Secondary School Examination, Bihar School Examination Board, Patna, India.

Publications:

1. **Thakur HC.**, Singh M., Nagel-Steger L., Prumbaum D., Fansa EK., Gremer L., Abts A., Willbold D., Schmitt L., Raunser S., Ahmadian MR., Piekorz RP. Two functionally diverse modules of the TACC domain of the centrosomal adaptor protein TACC3 determine interaction with the microtubule polymerase chTOG (*Manuscript under preparation for submission to J. Biol. Chem.*).

2. Schmidt S., Essmann F., Cirstea IC., Kuck F., **Thakur HC.**, Singh M., Kletke A., Jänicke RU., Wiek. C., Hanenberg H., Ahmadian MR., Schulze-Osthoff K., Nürnberg B., Piekorz RP. (2010). The centrosome and mitotic spindle apparatus in cancer and senescence. **Cell Cycle** 9, 4469-4473.

Scholarships, prizes and awards:

1. **2009–2012; PhD Scholarship:** NRW Research School Biostruct, Heinrich-Heine-University, Düsseldorf, Germany.

2. **2008–Joint CSIR-UGC (Center for Scientific and Industrial Research-University Grant Commission) award of Junior Research Fellowship (JRF) and National Eligibility for Lectureship (NET):** held on 21 Dec 2008, conducted by Human Resource Development Ministry, Govt. of India.

3. **2008–GATE-Life Science (Graduate Aptitude Test in Engineering)**, **Percentile score-99.05, All India Rank 124, GATE score-507:** Standardized test conducted by Indian Institute of Science, Bangalore, India, for graduate studies in life sciences and biomedical engineering.

4. **2007–2009; Recipient of Merit cum Means fellowship:** from Jawaharlal Nehru University New Delhi, during M.Sc (Life Science) studies.

5. **2004–2007; Awardees of state level fellowship:** from District Welfare Society, Madhubani, India: during B.Sc. (Ag.) studies.

Presentations at conferences (Oral/Poster):

1. **2nd-6th October, 2011: EMBO conference series, "Centrosome & Spindle Pole bodies Meeting" Barcelona, Spain**. 'Biophysical and biochemical characterization of the centrosomal protein TACC3'.

2. **12th–15th September, 2011: BioStruct Master Class 2011**, NRW research school BioStruct, HHU, Düsseldorf. 'Biochemical, biophysical and functional characterization of the centrosomal protein TACC3'.

3. **6th–9th September, 2010: BioStruct Master Class 2010**, NRW research school BioStruct, HHU, Düsseldorf. 'Purification and characterization of the centrosomal protein TACC3'.

Abstracts:

1. **Harish C. Thakur**, Luitgard Nagel-Steger, Madhurendra Singh, Lothar Gremer, Britta Tschapek, Stephan Schmidt, Stefan Raunser, Dieter Willbold, Lutz Schmitt, Mohammad R. Ahmadian, Roland P. Piekorz. 'Biophysical, biochemical, and functional characterization of the centrosomal protein TACC3'. 8th Centrosome and Spindle Pole Body EMBO Conference, October, 2011, Barcelona, Spain.

2. **Harish C. Thakur**, Luitgard Nagel-Steger, Madhurendra Singh, Lothar Gremer, Britta Tschapek, Stephan Schmidt, Stefan Raunser, Dieter Willbold, Lutz Schmitt, Mohammad R. Ahmadian, Roland P. Piekorz. 'Biophysical, biochemical, and functional characterization of the centrosomal protein TACC3'. Master Class 2011, NRW Research School Biostruct, HHU, Duesseldorf, Germany.

3. **Harish C. Thakur**, Lothar Gremer, Britta Tschapek, Stephan Schmidt, Lutz Schmitt, Mohammad R. Ahmadian, Roland P. Piekorz. 'Purification and characterization of the centrosomal protein TACC3'. Master Class 2010, NRW Research School Biostruct, HHU, Düsseldorf, Germany.

Curriculum Vitae

Training Courses/Workshops:

1. **25th–29th June, 2012:** 'NMR-Spectroscopy of biological macromolecules in liquid and solid state', Heinrich-Heine-University, Forschungszentrum Jülich, Germany.

2. **29th August –2nd September, 2011:** 'Fluorescence Spectroscopy and Microscopy: basics of fluorescence', Heinrich-Heine-University, Düsseldorf.

3. **Summer Semester 2011:** 'Structural Bioinformatics and Molecular Modelling Course', Institut für Pharmazeutische und Medizinische Chemie, Heinrich-Heine-University, Düsseldorf.

4. **26th–30th April, 2010:** 'Conducting Molecular Dynamics Simulations with the AMBER11 Modelling suite' held at NRW Research School BioStruct, Heinrich-Heine-University, Düsseldorf.

5. **2nd–6th November, 2009:** 'Fluorescence-based spectroscopic and calorimetric applications in the analysis of bio-molecular interactions', AG Ahmadian, Institute for Biochemistry and Molecular Biology II Heinrich-Heine-University, Düsseldorf.

Workshops on Transferable Skills:

1. **14th October, 2011:** QIAGEN Production unit and Research Lab Visit, Organized by NRW Research School Biostruct, HHU, Düsseldorf, in cooperation with QIAGEN, N.V, Hilden.

2. **03rd–04th March, 2011:** 'Presenting Science2 – convincing debating & discussing', iGRAD, Heinrich-Heine-University Düsseldorf.

3. **07th–08th October, 2010:** 'Optimizing writing strategies for publishing in English', iGRAD, Heinrich-Heine-University, Düsseldorf.

4. **27th July, 2010:** Participated in Schrödinger workshop 'From structural biology to drug discovery and virtual screening' NRW Research School BioStruct, Heinrich-Heine-University Düsseldorf.

5. **19th–20th March, 2010:** 'Cross-cultural communication- How to act successfully in an international environment', iGRAD, Heinrich-Heine-University, Düsseldorf.

6. **11th–12th December, 2009:** 'Fundamentals of Project Management', iGRAD, Heinrich-Heine-University, Düsseldorf.

7. **30th November, 2009:** Biostruct Minisymposium on "Structural biology of amyloidogenic proteins", NRW Research School Biostruct, Heinrich-Heine-University, Düsseldorf.

8. **16th-17th November, 2009:** 'Presenting Science1 - Comprehensive, Competent and Convincing', iGRAD, Heinrich-Heine-University, Düsseldorf.

Acknowledgements

This dissertation was written after three years of laboratory work. The work started in October 2009 and ended by the end of year 2012. In this time frame, several people contributed to this work in innumerable ways, and I am grateful to all of them. First and foremost, I am deeply indebted of my topic supervisor and mentor Dr. Roland Piekorz, Institute for Biochemistry and Molecular Biology II, for his ever interesting discussions, precious advices, directional guidance, useful critics, and motivational support. His thoughtful ideas, constructive critics, excellent scientific writing skill and his precious time aided considerably in the completion of the study and finalizing the work into this thesis.

My greater appreciation goes to my PhD supervisor PD. Dr. Reza Ahmadian, Institute for Biochemistry and Molecular Biology II, for his expedient advices and availing the facility for protein production and purification. I am grateful of my supplementary supervisor Prof. Dr. Lutz Schmitt, Chairman of the Institute of Biochemistry I, Mathematics and Natural Sciences Faculty, Heinrich-Heine-University, Düsseldorf for his significant inputs during the follow-up meetings and providing the facility of light scattering experiments. I am obliged of Prof. Dr. Jürgen Scheller, Chairman of the Institute for Biochemistry and Molecular Biology II, at the Med. faculty, Heinrich-Heine-University, Düsseldorf, for providing the space and facilities.

I give my heartfelt thanks to the Graduate School BioStruct at Heinrich-Heine-University, Düsseldorf, for giving me an opportunity to work as a PhD fellow. I express my gratitude to Ministry for Innovation Science and Research, NRW, Germany and Gründerstiftung of the Heinrich-Heine-University for providing financial support for this research.

My research required the support of many academies, I am grateful to all of the people at these institutions who not only provided access to the facility under their care but also valuable discussions about the experiments. In particular, I would like to thank these individuals: Prof. Dr. Dieter Willbold, Chairman of the Institute of Physical Biology, Mathematics and Natural Sciences Faculty, Heinrich-Heine-University, Düsseldorf for

providing the facility of Analytical ultracentrifugation and CD spectroscopy; Dr. Luitgard Nagel-Steger, Institute of Physical Biology, Heinrich-Heine-University, Düsseldorf for her assistance in Analytical ultracentrifugation experiments; Dr. Stefan Raunser and Daniel Prumbaum, Max-Planck-Institute of Molecular Physiology, Dortmund, for availing Electron Microscope facility and imaging; Dr. Astrid Höppner, Crystal and X-ray facility center, Heinrich-Heine-University, for crystal screening and optimization; Dr. Sabine Metzger, BMFZ, Heinrich-Heine-University, for supporting in mass spectroscopy analysis.

I am grateful to all of my colleagues who have provided their assistance. In particular, I would like to thank Madhurendra Singh for his generous helping hand in cloning and cLSM imaging; Eyad Fansa for his support and advices in ITC protein-protein interaction measurements; Dr. Lother Gremer, Institute of Physical Biology, Heinrich-Heine-University, Düsseldorf for his valuable guidance in planning the experiments; Dr. Stephan Schmidt, Dr. Fabian Kuck, Dr. Katja Pexa, Carola Barth, Hakima Ezzahoini, Fereshteh Kamrani, Zeynep Tokyürek, Ilse Meyer for their kind co-operation. My special thanks go to Petra Opree Jeremic, secretary of the institute for assisting me in administrative work. I would like to acknowledge all other members of the institute for their mutual efforts and support.

I would like to extend my deepest gratitude to my family in Düsseldorf: my Daddy Nick, Mama Erika, Mama Karin, Mama Rita, Uncle Jürgen Lutz, Aunt Hanne and Julia for their blessings, emotional support, and considering me as part of their family. They always have provided unwavering love and encouragement. Thank you for believing in me.

Last, but not least, my honest indebtedness goes to my wife Dr. Shailaja Mahajan-Thakur for her love, understanding, encouragement, inspiration and standing beside me throughout the critical time. I was continually amazed by our fruitful discussions and her willingness to proof read pages of my dissertation. My loving parents (Maa and Babu Ji), brothers and sisters receive my utmost gratitude for their dedication, consistent support during my primary and undergraduate studies, and social learning. I could not have done it without you. Thank you for being there for me from the very beginning of life that provided the foundation for this work.